# THE DIRECTIONAL FACTOR AS A KEY DETERMINANT OF CHATTER-FREE ROBOTIC MILLING IN LIGHT ALLOYS

by
ALİ KARACA

Submitted to the Graduate School of Engineering and Natural Sciences
in Partial Fulfilment of
the Requirements for the Degree of Master of Science

Sabancı University
July 2025

## ABSTRACT

THE DIRECTIONAL FACTOR AS A KEY DETERMINANT OF CHATTER-FREE ROBOTIC MILLING IN LIGHT ALLOYS

ALİ KARACA

Manufacturing Engineering, MSc. Thesis, 2025

Thesis Supervisor: Prof Dr. ERHAN BUDAK

Keywords: Robotic machining, low-frequency chatter, mean directional factor (MDF)

Robotic machining can be a cost-effective alternative to conventional CNC systems, especially for processing large or complex workpieces. However, the inherently low stiffness and posture-dependent dynamics of industrial robots results in them being highly susceptible to chatter, especially at low frequencies. Thus, this thesis focuses on the identification of low-frequency chatter in robotic milling, emphasizing the role of structural dynamics and the mean directional factor (MDF) in chatter formation. This is novel because there are some studies that attribute low-frequency chatter to mode-coupling in literature. To study the effect of MDF in a controlled environment, a custom flexure-based fixture was designed to mimic the dominant low-frequency mode typically observed in robotic arms. This fixture offers a single-mode-dominant system, which provides repeatable testing and clear interpretation of dynamic behaviour. Modal analysis was carried out using finite element modelling (FEM) and validated through experimental modal analysis (EMA). High correlation between simulation and test results confirmed the accuracy of the simplified model. The system was finally tested under machining conditions, validating theoretical predictions related to mean directional factors (MDF) and demonstrating that slotting operations can effectively reduce chatter. The results confirm that positive MDF values are associated with stable cutting, while negative MDF values lead to low-frequency self-excitation. This study offers a practical framework for enhancing stability in robotic milling and contributes to the development of chatter-resistant robotic systems for high-speed machining.

# ÖZET


HAFİF ALAŞIMLARIN ROBOTLU FREZELENMESİNDE TIRLAMANIN ÖNLENMESİNDE YÖNELME FAKTÖRÜNÜN TEMEL ROLÜ

ALİ KARACA

Üretim Mühendisliği, Yüksek Lisans Tezi, 2025

Tez Danışmanı: Prof. Dr. ERHAN BUDAK

Anahtar Kelimeler: Robotlu talaşlı imalat, düşük frekanslı tırlama, ortalama yönelme faktörü (MDF)

Robotlu talaşlı imalat, özellikle büyük veya karmaşık iş parçalarının işlenmesinde konvansiyonel CNC sistemlerine kıyasla maliyet açısından etkin bir alternatif olabilir. Ancak, endüstriyel robotların doğası gereği düşük rijitlikleri ve konuma bağlı değişken dinamik davranışları, bu sistemleri özellikle düşük frekanslı tırlamaya karşı oldukça hassas hale getirir. Bu nedenle, bu tez çalışması robotlu frezeleme işlemlerinde düşük frekanslı tırlamanın belirlenmesine odaklanmakta ve bu bağlamda yapısal dinamikler ile ortalama yönelme faktörünün (MDF) bu tırlamaların oluşumundaki rolünü vurgulamaktadır. Literatürde bu tür tırlamalar çoğunlukla mod bağlaşımı ile açıklanırken, bu çalışma farklı bir yaklaşım sunmaktadır. MDF'nin etkisini incelemek amacıyla, endüstriyel robotlarda gözlemlenen baskın düşük frekanslı modu taklit eden özel bir esnek fikstür tasarlanmıştır. Bu fikstür, tek mod baskınlığına sahip bir sistem sunarak tekrarlanabilir deneylerin yapılmasına ve dinamik davranışın net bir şekilde yorumlanmasına olanak sağlamaktadır. Modal analiz, sonlu elemanlar yöntemi (FEM) ile gerçekleştirilmiş ve deneysel modal analiz (EMA) ile doğrulanmıştır. Simülasyon ve deneyler arasındaki yüksek korelasyon, modelin doğruluğunu ortaya koymuştur. Sistem, robotlu frezeleme koşullarında test edilerek MDF'ye dayalı teorik öngörüler doğrulanmış ve kanal frezeleme işlemlerinin tırlamayı azaltabileceği görülmüştür. Pozitif MDF değerleri kararlı kesme ile ilişkilendirilirken, negatif değerlerin düşük frekanslı tırlamaya neden olduğu tespit edilmiştir. Bu çalışma, robotlu frezeleme süreçlerinde kararlılığı artırmak için uygulanabilir bir yöntem sunmakta ve yüksek hızlı işleme için tırlamaya dirençli robot sistemlerinin geliştirilmesine katkı sağlamaktadır.

# TABLE OF CONTENTS

## LIST OF FIGURES

## LIST OF TABLES

# 1. INTRODUCTION

## 1.1 Background: Robotic Milling

In recent years, robotic milling has gained traction as a versatile alternative to conventional computer numerical control (CNC) machining, particularly in applications requiring large workspaces, complex geometries, or flexible manufacturing systems. Its adoption is especially prominent in industries such as aerospace, shipbuilding, and energy, where the ability to process large or irregular components with adaptable positioning is critical. Serial industrial robots, typically designed for pick-and-place, welding, or assembly tasks, are being increasingly repurposed for machining operations due to their cost-effectiveness and multi-axis capability (Dombovari,2025), (Hazarika,2018), (Valente,2019).

Before robotic arms were considered for milling, Parallel Kinematic Machines (PKMs) had already been explored and implemented in high-performance machining scenarios (Paccot,1996). Developed initially to overcome the rigidity and acceleration limitations of serial mechanisms, PKMs offered a structurally superior alternative for tasks requiring both speed and accuracy. Their closed-loop architecture provides enhanced stiffness, lower inertia, and greater dynamic stability characteristics that make them particularly suitable for precise, high-speed machining. As robotic machining evolves, the principles and structural advantages of PKMs continue to influence hybrid designs and next-generation robotic platforms that aim to combine the flexibility of serial manipulators with the precision and stability of parallel architectures.

Unlike machine tools, which are inherently rigid and designed to maintain tight tolerances under dynamic cutting loads, robots possess limited structural stiffness and damping. These limitations stem from their lightweight link structures, serial kinematic chains, and gear-driven actuators. Consequently, when exposed to milling forces, robotic arms are highly susceptible to vibrations, structural deflections, and dynamic instabilities. One of the most prevalent and damaging of these instabilities is chatter, a self-excited vibration that can degrade surface quality, reduce tool life, and limit material removal rates (Iglesias,2016), (Zengxi ,2006), (Cordes,2019).

The challenge of applying robots in milling lies in their low-frequency structural dynamics. While conventional CNC machines typically exhibit natural frequencies well above the cutting force excitation range, robotic systems frequently possess dominant structural modes below 100 Hz. These modes can be easily excited during machining, resulting in chatter even under conservative cutting conditions (Dombovari,2025), (Lutfi ,2021), (Celikag,2021). This fundamental mismatch between structural behaviour and process demands requires a rethinking of traditional stability analysis approaches.

Robotic milling also introduces unique complexities which are not present in CNC systems. The robot's dynamic behaviour is configuration-dependent which means that its stiffness, damping, and natural frequencies vary as the tool moves through different positions in the workspace. A tool path that is stable in one pose may become unstable in another due to shifting modal properties. This nonuniform behaviour complicates both process planning and predictive modelling (Cordes,2019), (Ozturk,2007).

Historically, research into robotic machining has focused on mitigating these limitations through hardware augmentation such as adding passive support or increasing joint stiffness, or through advanced control strategies. However, these approaches offer limited adaptability and often increase system complexity or cost. A more foundational solution lies in understanding the physics of the cutting process and how it interacts with the directional flexibility of the robot's structure.

While classical chatter stability analyses rely heavily on process models incorporating cutting force coefficients and structural dynamics, the introduction of directional factor

matrices has enabled more refined predictions of stability, particularly in systems with spatially complex engagement geometries such as five-axis milling. In these formulations, the directional coefficient matrix captures how tool vibrations in various directions contribute to the regeneration of chip thickness, and it is typically expressed through Fourier series expansions in both single- and multi-frequency stability models (Budak ,2009), (Ozturk, 2010). However, these approaches generally treat the directional effects as periodic functions rather than scalar stability indicators. In contrast, the present thesis extends this framework by introducing the Mean Directional Factor (MDF) as a scalar projection of the directional matrix along the dominant mode shape of a flexible structure such as a robotic arm. This MDF serves as a stability criterion that unifies directional flexibility with mode-specific dynamics, showing that negative MDF values consistently correlate with low-frequency chatter, even at high tooth-passing frequencies. By doing so, the thesis bridges the gap between matrix-based stability theory and mode-shape-informed process planning, enabling more effective posture-aware chatter avoidance strategies in robotic milling.

This thesis addresses this core issue by advancing a directional stability framework based on the Mean Directional Factor (MDF) a scalar metric that encapsulates how the dominant direction of tool engagement interacts with the system's primary vibration mode. Unlike prior theories, which attribute chatter to mode coupling between multiple structural frequencies (Lejun ,2017), (Badiola,2019), the MDF approach posits that in low-frequency-dominated systems such as robots, chatter is governed primarily by the alignment of cutting force direction with the dominant mode shape (Dombovari,2025).

By building upon this concept, the work presented here aims to shift the focus of robotic milling stability analysis from system-wide modal interactions to directionally tuned engagement strategies. This will be further explored through detailed structural analysis, cutting force modelling, and experimental validation, with the ultimate goal of enabling chatter-free robotic milling through posture-aware and directionally informed tool path planning.

### 1.1.1 Robots and Structural Challenges

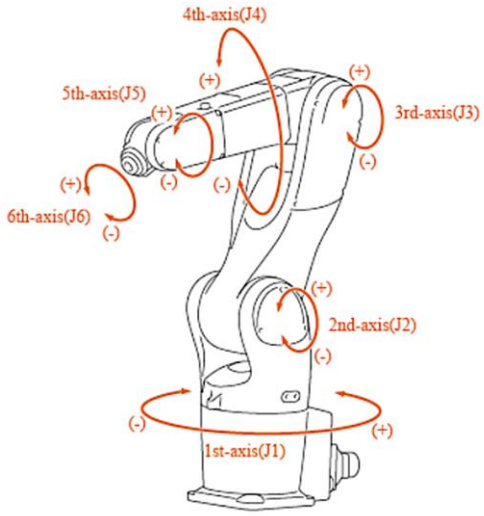


Figure 1.1 A 6th degree of freedom robot structure.

Industrial robots employed in milling tasks are typically serial manipulators composed of multiple revolute joints connected by lightweight links. This configuration provides high flexibility and reachability, enabling six or more degrees of freedom (DOF) in tool positioning and orientation. These capabilities make robots attractive for machining operations that require access to complex geometries or large workpieces (Hazarika,2018),(Cordes,2019),(Valente,2019).

However, the same kinematic structure that provides flexibility also introduces significant limitations in terms of structural rigidity. Unlike CNC machine tools, which are designed with heavy, rigid frames to maintain positional accuracy under high cutting forces, robots have compliant joints and slender link structures that reduce their ability to resist dynamic loads. The gearboxes and reducers embedded in each joint add further compliance and often introduce nonlinearities such as backlash and hysteresis (Lutfi ,2021), (Zengxi ,2006).

A fundamental characteristic of robotic structures is their posture-dependent stiffness and damping. The dynamic properties at the tool center point (TCP) including translational stiffness, rotational stiffness, and natural frequencies change substantially depending on

the robot's configuration. For example, in extended configurations where the arm is fully stretched, the structure behaves like a long cantilever beam, significantly reducing stiffness and natural frequency. In contrast, when the robot is retracted near its base, the dynamic properties improve due to the shorter load path (Cordes,2019), (Ozturk,2007).

Additionally, robot stiffness is anisotropic varying by direction. Experimental studies show that compliance is typically lowest along the direction of the end-effector's primary axis and highest in orthogonal bending directions. These anisotropies play a critical role in how the robot responds to cutting forces, particularly in high-force processes like milling where the tool engagement direction may align with the system's weakest axis (Lutfi ,2021), (Sanz-Calle,2024).

The natural frequencies of robot structures in milling configurations are generally low, with fundamental bending modes appearing between 20 Hz and 80 Hz, depending on the pose, payload, and support conditions (Cordes,2019), (Ozturk,2007). These frequencies are much lower than those of traditional CNC machines, which are engineered to have dominant modes well above 300 Hz to avoid interaction with the cutting excitation range. In robots, the low-frequency modes are often bending-dominated and involve deformation across multiple links and joints rather than localized structural elements.

Moreover, the frequency response function (FRF) at the tool tip critical for predicting chatter stability varies significantly across the robot's workspace. This makes the application of a single, fixed dynamic model impractical. Each machining posture requires individualized dynamic characterization to assess process stability and performance (Ozturk,2007), (Eynian,2009).

Due to these challenges, robotic milling demands a dynamic analysis framework that can accommodate posture-dependent flexibility, directional stiffness, and evolving tool–structure interaction. These characteristics form the foundation for chatter susceptibility, which is examined in later sections of this chapter.

### 1.1.2 Cutting Forces in Milling

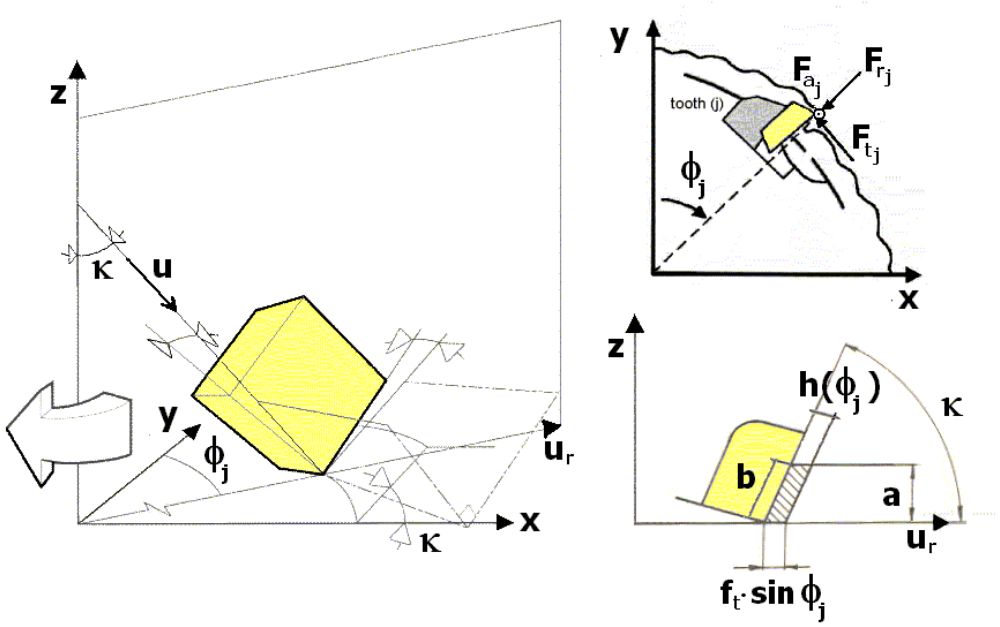


Figure 1.2 Geometry of the face milling (Munoa,2006)

The modeling of cutting forces in milling is fundamental to understanding the dynamics of machining processes, particularly for chatter prediction and stability analysis. Milling is characterized by the intermittent engagement of multiple teeth, each contributing to time-varying forces dependent on chip thickness and tool-workpiece interaction. To capture these phenomena, different force models are employed. This section presents and interprets three commonly used force models: the linear edge force model, the exponential average force coefficient model, and the exponential instantaneous force coefficient mode. (Budak,1996), (Budak,1996), (Munoa,2006)

Linear Edge Force Model

The linear force model assumes that the cutting forces are linearly dependent on the instantaneous chip thickness and include an additional edge or ploughing force component. The formulation is as follows (Budak,1996), (Munoa,2006):

$$\begin{aligned} F_{tj} &= \left(K_{tc} \cdot h(\phi_j) \cdot b + K_{te} \cdot S\right) \cdot g(\phi_j) \\ F_{rj} &= \left(K_{rc} \cdot h(\phi_j) \cdot b + K_{re} \cdot S\right) \cdot g(\phi_j) \\ F_{aj} &= \left(K_{ac} \cdot h(\phi_j) \cdot b + K_{ae} \cdot S\right) \cdot g(\phi_j) \end{aligned} \qquad \textbf{(1.1)}$$

In equation 1.1, the variables $F_{tj}$, $F_{rj}$, and $F_{aj}$ represent the tangential, radial, and axial force components acting on the $j$-th tooth, respectively. These cutting forces are governed by both the main cutting force coefficients $K_{tc}$, $K_{rc}$, and $K_{ac}$ and the edge or ploughing force coefficients $K_{te}$, $K_{re}$, and $K_{ae}$. The force generation is dependent on the instantaneous uncut chip thickness $h(\phi_j)$ at the angular position $\phi_j$, the axial depth of cut $b$, and the edge contact length $S$, which becomes significant when the chip thickness is small and accounts for rubbing effects. Finally, the engagement of each tooth with the material is represented by the step function $g(\phi_j)$, which equals 1 when the tooth is cutting and 0 otherwise. This model decomposes the total cutting forces into two main components: shear forces and edge forces. The shear forces are directly proportional to the product of the instantaneous chip thickness and the axial depth of cut, representing the dominant cutting mechanism during steady engagement. In contrast, edge forces become significant when the chip thickness is very small, such as during tool entry or exit, or under low feed rate conditions. The model operates under the assumption that force coefficients remain constant, thereby neglecting nonlinear behaviors or variations due to changing feed conditions.

**Exponential Average Force Coefficient Model**

This model introduces nonlinearity by expressing the cutting force coefficients as a function of the average chip thickness $h_a$. It models how the cutting forces increase disproportionately when chip thickness becomes very small, which is especially important for stability prediction at low feed rates (Budak,1996), (Munoa,2006).

$$\begin{Bmatrix} F_{tj} \\ F_{rj} \\ F_{aj} \end{Bmatrix} = K_T \cdot h_a^{-p} \cdot \begin{Bmatrix} 1 \\ K_R \cdot h_a^{-q} \\ K_R \cdot h_a^{-s} \end{Bmatrix} \cdot h(\phi_j) \cdot g(\phi_j) \cdot b \quad \text{where} \quad h_a = f_t \cdot \frac{\cos\phi_e - \cos\phi_s}{\phi_s - \phi_e} \tag{1.2}$$

In Eq. 1.2,$K_T$ is base tangential force coefficient, $K_R$ is scaling coefficient for radial and axial components. Additionally, $p, q, s$ are exponents controlling the sensitivity of each direction to chip thickness, while $h_a$ stands for average chip thickness, dependent on feed per tooth $f_t$ and tool engagement angles $\phi_s, \phi_e$. In Eq, force coefficients decrease with increasing $h_a$, reflecting experimental observations. Enables modelling of feed rate influence on stability, which is missing in the linear model. Appropriate for steady-state or time-invariant applications, but limited in dynamic resolution

**Exponential Instantaneous Force Coefficient Model**

This is the most advanced and precise model, where force coefficients depend on the instantaneous chip thickness $h(\phi_j)$ at every tooth engagement. It provides the most accurate dynamic behavior and is well-suited for chatter and stability analysis in both time and frequency domains (Budak,1998), (Budak,1996), (Munoa,2006).

$$\begin{Bmatrix} F_{tj} \\ F_{rj} \\ F_{aj} \end{Bmatrix} = K_T \cdot b \cdot \begin{Bmatrix} h(\phi_j)^{1-p} \\ K_R \cdot h(\phi_j)^{1-p-q} \\ K_A \cdot h(\phi_j)^{1-p-s} \end{Bmatrix} \cdot g(\phi_j) = K_T \cdot b \cdot \begin{Bmatrix} h(\phi_j)^{1-m_t} \\ K_R \cdot h(\phi_j)^{1-m_r} \\ K_A \cdot h(\phi_j)^{1-m_a} \end{Bmatrix} \cdot g(\phi_j) \quad \textbf{(1.3)}$$

In equation 1.3 the parameters $m_t$, $m_r$, and $m_a$ denote the nonlinearity exponents associated with the tangential, radial, and axial cutting force directions, respectively, capturing how cutting forces scale nonlinearly with chip thickness in each direction. The term $K_A$ refers to the axial cutting force coefficient, which quantifies the proportional relationship between axial force and chip thickness. The instantaneous uncut chip thickness is represented by $h(\phi_j)$, which varies as a function of the angular position $\phi_j$. All other terms retain their previously defined meanings. This model enables instant-by-instant calculation of cutting forces with direct sensitivity to tool vibrations, making it highly responsive to dynamic changes in tool position. It effectively captures regenerative effects, which are essential for the formation of chatter. Consequently, it serves as a foundational

element in frequency-domain stability analyses, including the Zero Order Approximation (ZOA) and multi-harmonic analysis methods.

In this thesis, all subsequent stability and chatter investigations will be based on the exponential instantaneous model, as it accurately reflects the nonlinear, vibration-sensitive nature of robotic milling processes.

### 1.1.3 Chatter Related Problems

Chatter is a dynamic instability that arises during machining processes and is characterized by self-sustained oscillations of the tool and/or workpiece. These vibrations degrade the surface finish, increase tool wear, and limit productivity. (Altintas,1992) Chatter is particularly significant in flexible systems such as industrial robots, where low structural stiffness and damping make them more susceptible to vibratory instabilities. Several types of chatter mechanisms have been identified in the literature; each associated with distinct dynamic behaviours and physical origins.

**1. Regenerative Chatter**

Regenerative chatter is the most dominant and extensively modelled type of chatter in milling. It occurs due to the regenerative effect: the waviness left on the surface by one tool pass affects the chip thickness encountered by the subsequent tooth. This creates a time-dependent feedback loop where tool vibration in the present interferes with vibrations from the past, leading to potential dynamic instability. (Merritt,1965), (Tobias ,1958)

**Dynamic Chip Thickness:**

The uncut chip thickness at time $t$ can be expressed as:

$$h(t) = f_z \cdot \sin(\phi) + x(t) - x(t - T) \quad \textbf{(1.4)}$$

Where:

The parameter $f_z$ represents the feed per tooth, while $\phi$ denotes the angular position of a specific tooth. The term $x(t)$ indicates the tool displacement at the current time, and $x(t - T)$ corresponds to the tool displacement from the previous tooth pass, capturing the regenerative effect. The tooth passing period $T$ is defined as $\frac{60}{N \cdot Z}$, where $N$ is the spindle speed in revolutions per minute (RPM), and $Z$ is the number of flutes on the tool. (Tlusty,1983)

**Dynamic Model:**

The governing dynamic equation for one degree of freedom (DOF) can be written as:

$$m\ddot{x}(t) + c\dot{x}(t) + kx(t) = F_c(t) \quad \textbf{(1.5)}$$

Substituting the cutting force $F_c(t)$, assumed proportional to chip thickness:

$$F_c(t) = K_c \cdot h(t) \quad \textbf{(1.6)}$$

$$\Rightarrow m\ddot{x}(t) + c\dot{x}(t) + kx(t) = K_c(f_z \cdot \sin(\phi) + x(t) - x(t - T)) \quad \textbf{(1.7)}$$

This delay differential equation introduces infinite-dimensional dynamics, where the stability depends on the time delay $T$ and the process parameters.

**Hopf Bifurcation in Milling**

Hopf bifurcation describes the mathematical condition under which a stable steady-state solution of a dynamical system becomes unstable and transitions into a limit cycle oscillation (i.e., sustained vibration). In the context of regenerative chatter, as the depth of cut or spindle speed increases, the real part of one or more eigenvalues of the time-delay system crosses zero and becomes positive. This signals a change from stable cutting to unstable vibration. The Hopf bifurcation point defines the boundary of the stability lobe diagram, which is commonly used to map chatter-free cutting zones (Honeycutt,2018), (Cordes,2019).

Mathematically, for a linearized single-DOF delay system:

$$\lambda^2 + 2\zeta\omega_n\lambda + \omega_n^2 - K_c e^{-\lambda T} = 0 \quad \textbf{(1.8)}$$

Where:

The symbol $\lambda$ represents the characteristic exponent, which determines the stability of the system based on its real and imaginary components. The natural frequency of the system is denoted by $\omega_n$, while $\zeta$ indicates the damping ratio, characterizing how quickly vibrations decay over time. The term $K_c$ is the cutting force coefficient, which quantifies the relationship between cutting force and chip load. Finally, $T$ refers to the time delay between successive tooth engagements, a critical factor in modeling regenerative chatter.

At the Hopf point, the solution satisfies:

$$\lambda = i\omega \quad \text{(purely imaginary)}$$

and any small change in system parameters can lead to:

$$\text{Re}(\lambda) > 0 \quad \Rightarrow \text{unstable (chatter)}$$

As conclusion, chatter is often associated with nonlinear bifurcation behavior in flexible systems. As process parameters such as depth of cut or feed direction approach critical thresholds, the system may exhibit sudden jumps in amplitude or switch between stable and unstable states. This is characteristic of a Hopf bifurcation, but more complex transitions such as quasi-periodicity or period-doubling may also occur in multi-modal systems.

These bifurcations introduce high sensitivity to small disturbances and make it difficult to maintain stability near the process limits. In robotic milling, this manifests as unpredictable onset of chatter, even under seemingly safe conditions, and requires conservative selection of cutting parameters unless real-time monitoring or control strategies are implemented.

**2. Mode Coupling Chatter**

Mode coupling chatter arises when two or more structural vibration modes interact during cutting (Altintas,2020), (Yuan,2018). This usually occurs when:

- The natural frequencies of the modes are closely spaced

- The cutting forces excite both directions
- Cross-axis coupling leads to energy exchange

The result is often an elliptical or spiralling tool motion, distinct from the sinusoidal pattern seen in regenerative chatter. The interaction is governed by a multi-DOF system:

$$\mathbf{M}\ddot{\mathbf{x}} + \mathbf{C}\dot{\mathbf{x}} + \mathbf{K}\mathbf{x} = \mathbf{F_c}(\mathbf{x}) \quad \textbf{(1.9)}$$

Where:

The vector $\mathbf{x} = [x_1, x_2]^T$ represents the displacements in two coupled directions, typically corresponding to the feed and normal directions in milling. The matrices $\mathbf{M}$, $\mathbf{C}$, and $\mathbf{K}$ denote the mass, damping, and stiffness properties of the system, respectively, capturing its dynamic response characteristics. The term $\mathbf{F_c}$ refers to the direction-dependent cutting force vector, which varies based on the tool's engagement angle and cutting conditions.

Mode coupling is traditionally observed in turning operations and compliant systems, but its presence in milling is conditional on structural characteristics and modal alignment (Gasparetto,1998).

While robotic machining systems are frequently dominated by a single flexible mode particularly at low frequencies, their configuration-dependent structural dynamics can give rise to multiple vibration modes with closely spaced natural frequencies. Under specific tool engagement directions or extended postures, such systems may exhibit modal interactions that do not align with the principal cutting force direction. These interactions can manifest as cross-axis vibrations or elliptical tool motion. However, they do not satisfy the fundamental conditions for classical mode coupling chatter, which assumes self-excitation based solely on the system's instantaneous (free) vibrations, independent of prior surface undulations.

In the literature, several studies have reported low-frequency chatter in robotic milling and attributed it to mode coupling mechanisms. Notably, Pan et al. (Zengxi ,2006) and Cen and Melkote (Lejun ,2017) associated such chatter with mode coupling behaviour due to the appearance of structural vibration modes not aligned with spindle harmonics. Furthermore,

Badiola et al. (Badiola,2019) extended state-space analysis to explore mode coupling phenomena in workpiece dynamics. However, as clarified by Celikag et al. (Celikag,2021), these interpretations are based on assumptions that contradict the kinematic and dynamic nature of milling. Specifically, the dynamic chip thickness in milling inherently depends on both the current and previously cut surface undulations due to the tool's rotary motion and intermittent engagement, which invalidates the core requirement for mode coupling chatter.

Consequently, even when modal interactions are present in robotic systems, the governing instability mechanism in milling remains fundamentally regenerative. Such interactions, while capable of amplifying vibrations and complicating dynamic responses, represent secondary effects within a regenerative framework. This distinction is critical for accurate chatter prediction and control, particularly in robotic applications where structural flexibility and cutting force directionality significantly influence process stability. Capturing these dynamics often requires higher-order modeling techniques or experimental modal identification to supplement traditional single-DOF regenerative models.

**3. Forced Vibration Chatter**

Forced vibration chatter occurs due to external periodic excitation, such as:

- Spindle imbalance
- Servo or motor harmonics
- Structural excitation from the environment

Unlike regenerative or mode coupling chatter, this form is not self-excited and typically appears at fixed frequencies corresponding to the excitation source (Altintas,2020). However, if the excitation frequency aligns with a structural mode of the robot or spindle, resonance may occur, producing vibration amplitudes similar to those seen in self-excited chatter.

## 1.3 Problem Definition and Research Objectives

Robotic milling is emerging as a cost-effective and flexible alternative to conventional CNC machining, especially in applications involving large or geometrically complex workpieces. However, the dynamic limitations of industrial robots particularly their low stiffness and posture-dependent compliance lead to a high susceptibility to chatter. This chatter frequently occurs at low frequencies, a regime not well explained by traditional stability theories.

In classical machine tools, chatter is commonly attributed to regenerative effects or mode coupling between closely spaced structural modes. These frameworks assume that the excitation of multiple modes or past tool vibrations drive instability. While these mechanisms are valid in rigid or multi-modal systems, they fall short in explaining chatter observed in single-mode dominant robotic configurations where only one vibratory direction is active and yet chatter still occurs. Several studies in literature (Lejun ,2017), (Badiola,2019) have proposed mode coupling as the root cause of low-frequency chatter in flexible systems. However, these models do not fully account for the directional characteristics of cutting forces or the pose-dependent anisotropy of robotic structures.

This thesis challenges the mode coupling hypothesis for robotic milling and instead proposes that low-frequency chatter in robots is governed by the directional interaction between cutting forces and structural flexibility. Specifically, the Mean Directional Factor (MDF) is introduced as a scalar metric to quantify the alignment between the tool engagement direction and the robot's dominant mode shape. When this alignment is negative, the regenerative feedback becomes destabilizing even in single-mode systems and leads to self-excited vibration. Conversely, positive MDF values correlate with stable cutting.

To rigorously investigate this hypothesis, the study employs a flexure-based fixture that mimics a single dominant mode, allowing for controlled and repeatable dynamic experiments. The setup is designed to replicate the low stiffness and low-frequency

characteristics of robotic milling while ensuring minimal influence from higher-order modes. Through this framework, a clear link between MDF and chatter onset is established.

The primary objective of this thesis is to demonstrate that the Mean Directional Factor (MDF) is the key factor governing chatter in robotic milling systems, particularly in low-frequency regimes where classical multi-mode or isotropic stiffness assumptions do not hold. Unlike traditional approaches, the MDF-based methodology incorporates both structural dynamics and cutting force geometry in a unified way.

**Research Objectives**

To investigate the hypothesis that low-frequency chatter in robotic milling is primarily governed by the alignment of cutting forces with a single dominant structural mode, the following specific objectives are defined:

1. Mathematically formulate the Mean Directional Factor (MDF) to quantify the alignment between the cutting force vector and the dominant mode shape of the robotic or compliant structure. The MDF expression will serve as the core analytical tool for predicting chatter onset.
2. Design and construct a single dominant mode fixture that mimics the low-frequency flexibility observed in robotic systems. This experimental platform will isolate the primary mode of vibration, allowing for controlled investigation of directional effects on stability.
3. Generate polar plots of MDF values and correlate them with experimental cutting results to determine chatter-free and unstable cutting zones as a function of engagement direction. These plots will visualize the relationship between feed angle and process stability.
4. Validate the MDF-based theory on a real industrial robot by performing robotic milling experiments. The effect of feed direction and robot posture on chatter behaviour will be analysed to confirm that MDF governs stability in practical robotic machining scenarios.

# 2. STABILITY LOBES IN MILLING

The stability lobes in milling can be predicted by different methods such as Frequency-Domain methods, Time-Domain methods, Semi-Analytical / Hybrid methods (Altintaş,1995). However, Analytical Frequency Domain models provide accurate understanding of the regenerative chatter process and easy predictions for Stability Lobe Diagrams (SLD) for many cases. In literature, one of the fundamental methods, which are based on Directional Dynamic Milling Force Model and Zero Order Approximation (ZOA), is provided by Budak and Altintas (Iglesias,2016). This study provides an easy to implement approach to predict SLDs by providing a deeper understanding of regenerative chatter in milling operations. On the other hand, Time Domain methods [45] can capture nonlinearities in chatter process and gives more accurate stability analysis for periodic delay systems for milling applications of accurate modeling of real, multi-DOF, helix tools, and variable pitch. For Time-Domain based analysis, Stépán (Insperger,2003) is one of the pioneers of delay-differential equation modeling in machining dynamics, especially in turning, milling, and orthogonal cutting.

## 2.1. Frequency Domain Solutions with ZOA for Stability Lobe Diagrams

**Dynamic Force Modelling**

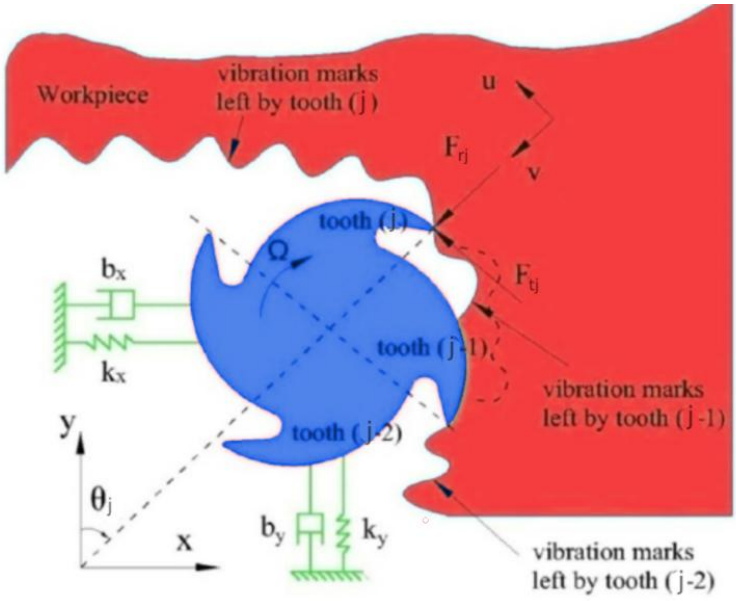


Figure 2.1 Dynamic model of milling with two degrees of freedom (Altintaş,1995)

The mathematical modelling of regenerative chatter in the milling process starts with defining chip thickness. The chip thickness formulation should capture both the static chip formation due to feed and dynamic modulation due to vibrations. The chip thickness equation is given by Eq.2.1

$$h(\phi_j) = \left[s_t \sin\phi_j + (v_{j,0} - v_j)\right] g(\phi_j) \quad \textbf{(2.1)}$$

where,

$\phi_j$: Angle of tooth j (its position as the tool rotates)

$h(\phi_j)$: instantaneous chip thickness for tooth $j$ at angular position $\phi_j$

$s_t$: feed rate per tooth

$v_j$: current vibration in radial direction

$v_{j,0}$: vibration at previous tooth pass (due to regenerative effect)

$g(\phi_j)$: step function (1 when the tooth is in cut; 0 otherwise)

In Eq.1, $s_t sin\phi_j$ represents the static part of chip thickness whereas dynamic regeneration term is represented via $(v_{j,0} - v_j)$.

The model reflects that chip thickness depends on the difference between tool positions at current and past engagements. At the dynamic part, the chip thickness is defined in the radial direction, but displacements are in Cartesian coordinates $(x, y)$.Therefore, projection is needed, and chip direction displacement projection is shown in Eq.2.2

$$v_j = -x\sin\phi_j - y\cos\phi_j \quad \textbf{(2.2)}$$

Eq.2 converts 2-D tool displacements $(x, y)$ into the direction of chip thickness formation, aligned with the cutting edge at angle $\phi_j$. This gives dynamic displacement in the chip direction, projecting the $(x, y)$ vibrations into the radial direction at each tooth's angular position.

If the projected vibrations (Eq.2.2) substituting into Eq.2.1, the simplified dynamic chip thickness equation can be obtained as shown in Eq.2.3

$$h(\phi_j) = [\Delta x\sin\phi_j + \Delta y\cos\phi_j]g(\phi_j) \quad \textbf{(2.3)}$$

Where: $\Delta x = x - x_0$ , $\Delta y = y - y_0$ : difference in tool position between current and previous revolution. Eq.2.3 represents a more accurate form of Eq. (2.1) showing chip thickness variation directly in terms of vibration difference.

Mechanistic force model (Altintas,2012) tells us that cutting forces are proportional to chip thickness. Therefore, the cutting force per tooth can be described as in Eq.2.4.

$$F_{tj} = K_t a h(\phi_j), \quad F_{rj} = K_r F_{tj} \quad \textbf{(2.4)}$$

In Eq.2.4, $F_{tj}$ is tangential cutting force, $F_{rj}$ is radial cutting force while $K_t$ represents tangential cutting force coefficient, and $K_r$: ratio of radial to tangential force. Additionally, $a$ is axial depth of cut that demonstrates cutting forces are proportional to chip thickness in Eq.2.4.

Milling is a rotating process, and the cutting forces are evaluated in a rotary frame in Eq 2.4. However, in this method, radial and tangential forces into fixed machine frame directions $(x, y)$ which makes easier compared to other methods. Therefore, force transformation to Cartesian Axes is given in Eq.2.5 for a tooth:

$$F_{xj} = -F_{tj}\cos\phi_j - F_{rj}\sin\phi_j$$
$$F_{yj} = +F_{tj}\sin\phi_j - F_{rj}\cos\phi_j \quad \textbf{(2.5)}$$

The total force is the sum over all active teeth engaged in cutting and can be represented as shown in Eq.2.6. N represents the number of flutes.

$$F_x = \sum_{j=0}^{N-1} F_{xj}\,, \quad F_y = \sum_{j=0}^{N-1} F_{yj} \quad \textbf{(2.6)}$$

The multiple teeth are engaged at different times which makes Eq.2.6 as time dependent and can be described as matrix from by using time-varying matrix $A(t)$.

$$\begin{Bmatrix} F_x \\ F_y \end{Bmatrix} = \frac{1}{2} a K_t \begin{bmatrix} a_{xx} & a_{xy} \\ a_{yx} & a_{yy} \end{bmatrix} \begin{Bmatrix} \Delta x \\ \Delta y \end{Bmatrix} \quad \textbf{(2.7)}$$

In Eq.2.7 $A(t)$ is written in open form and, the matrix elements ( $a_{ij}$ ) illustrate directional cutting force coefficients (depending on engagement angle and number of teeth). The $A(t)$ matrix is called time-varying directional matrix. This matrix captures time-varying directional coefficients caused by rotating teeth and changing chip engagement. Each element of time-varying directional matrix can be written as illustrated in Eq.2.8.

$$\begin{aligned} a_{xx} &= \sum_{j=0}^{N-1} -g_j\left[\sin 2\phi_j + K_r(1-\cos 2\phi_j)\right] \\ a_{xy} &= \sum_{j=0}^{N-1} -g_j\left[(1+\cos 2\phi_j) + K_r \sin 2\phi_j\right] \\ a_{yx} &= \sum_{j=0}^{N-1} g_j\left[(1-\cos 2\phi_j) - K_r \sin 2\phi_j\right] \\ a_{yy} &= \sum_{j=0}^{N-1} g_j\left[\sin 2\phi_j - K_r(1+\cos 2\phi_j)\right] \end{aligned} \quad \textbf{(2.8)}$$

In Eq.2.8, $a_{xx}$ represents how x-vibration causes force in x, $a_{xy}$ represent how y-vibration causes force in x, $a_{yx}$ illustrates how x-vibration causes force in y, and lastly $a_{yy}$ shows

how y-vibration causes force in y. The time-domain form of the force equation in Eq.2.7 can be written as shown in Eq.2.9.

$$\{F(t)\} = \frac{1}{2} a K_t [A(t)]\{\Delta(t)\} \quad \textbf{(2.9)}$$

Where

$[A(t)]$: 2×2 time-dependent directional matrix

$\Delta(t) = \{x(t) - x(t-T), y(t) - y(t-T)\}$: regenerative displacement

However, like the milling forces, $[A(t)]$: is periodic at tooth passing frequency or tooth period. Thus, time-dependent directional matrix can be expanded into Fourier series as shown in Eq.2.10.

$$[A(t)] = \sum_{r=-\infty}^{\infty} [A_r] e^{ir\omega t} \quad \textbf{(2.10)}$$

In the open form of Eq.2.10, $[A_o]$ can be excepted as the direct current (DC) term which does not affect time varying effects the average over one period. $[A_r]$ for are the AC (alternating current) or oscillating terms, they capture the time-varying fluctuations.

DC term $[A_0]$ is the average value of this matrix over one tooth passing period:

$$[A_0] = \frac{1}{T} \int_0^T [A(t)] dt \quad \textbf{(2.11)}$$

This is called the Zero Order Approximation (ZOA) to simplify analysis. In ZOA, we assume:

- Higher-order harmonics $r = \pm 1, \pm 2, \ldots$ have a lesser effect
- The dominant dynamics are captured well enough by the average cutting behavior

This results in completely analytical equations for chatter, a stable, closed-form prediction, and good performance with minimal computation.

The DC term $[A_0]$ is over engagement angles can be represented as in Eq.2.12.

$$[A(0)] = \frac{1}{\phi_p}\int_{\phi_{st}}^{\phi_{ex}} [A(\phi)]\, d\phi = \frac{N}{2\pi}\begin{bmatrix}\alpha_{xx} & \alpha_{xy}\\ \alpha_{yx} & \alpha_{yy}\end{bmatrix} \quad \textbf{(2.12)}$$

Where

$\phi_p = 2\pi/N$: tooth pitch angle

$\phi_{st}, \phi_{ex}$: start and exit angles of engagement

$[A(\phi)]$ is the direction-dependent force coefficient matrix at angular immersion $\phi$

In Eq.2.12, the integral calculates the average value of this matrix over the tooth immersion range $[\phi_{st}, \phi_{ex}]$. The result is a constant matrix $[A(0)]$ that represents the average dynamic stiffness behavior over the cutting engagement. This matrix is used back in Eq. 2.9 giving result by the simplified dynamic force equation as Eq.2.13:

$$\{F(t)\} = \frac{1}{2} a K_t [A(0)]\{\Delta(t)\} \quad \textbf{(2.13)}$$

In Eq.12 the overall cutting force in milling represented as a simplified form using average coefficients and can be called as Average Cutting Coefficient Matrix as simplified in Eq.2.14.

$$[A(0)] = \frac{N}{2\pi}\begin{bmatrix}\alpha_{xx} & \alpha_{xy}\\ \alpha_{yx} & \alpha_{yy}\end{bmatrix} \quad \textbf{(2.14)}$$

In Eq.2.14, $a_{ij}$ are derived by analytically integrating the milling force directional components over angle $\phi$, using trigonometric identities and cutter geometry as shown in Eq.2.15 in an explicit form.

$$\begin{aligned}
\alpha_{xx} &= \frac{1}{2}[\cos 2\phi - 2K_r\phi + K_r \sin 2\phi]_{\phi_{st}}^{\phi_{ex}}\\
\alpha_{xy} &= \frac{1}{2}[-\sin 2\phi - 2\phi + K_r \cos 2\phi]_{\phi_{st}}^{\phi_{ex}}\\
\alpha_{yx} &= \frac{1}{2}[-\sin 2\phi + 2\phi + K_r \cos 2\phi]_{\phi_{st}}^{\phi_{ex}}\\
\alpha_{yy} &= \frac{1}{2}[-\cos 2\phi - 2K_r\phi - K_r \sin 2\phi]_{\phi_{st}}^{\phi_{ex}}
\end{aligned} \quad \textbf{(2.15)}$$

In this method, rotary radial and tangential forces into fixed machine frame directions $(x, y)$ which makes easier compared to other methods .Thus, instead of summing tooth-by-

tooth, it is obtained an analytical way to compute the average force contribution of a full tool rotation by the help of Eq.2.15 .This enables critical for fast, closed-form stability analysis. As a result, the final form of the force equation becomes as indicated in Eq.2.13.

**Chatter Stability Lobes**

After obtaining dynamic force, in this section, it will be moved to frequency-domain analysis to find chatter boundaries. The dynamic compliance matrix (frequency response function) can be represented as in Eq.2.16. This value can be obtained from modal analysis.

$$[G(i\omega)] = \begin{bmatrix} G_{xx}(i\omega) & G_{xy}(i\omega) \\ G_{yx}(i\omega) & G_{yy}(i\omega) \end{bmatrix} \quad \textbf{(2.16)}$$

The displacement in frequency domain can be obtained as shown in Eq.2.17.

$$\begin{aligned} \{r(i\omega)\} &= [G(i\omega)]\{F\}e^{i\omega t} \\ \{r_0(i\omega)\} &= e^{-i\omega T}\{r(i\omega)\} \end{aligned} \quad \textbf{(2.17)}$$

Where $r$ is current displacement, $r_0$ is delayed displacement (due to previous tooth), and $T = \frac{2\pi}{\Omega Z}$ tooth passing period. Therefore, relative displacement in frequency domain can be expressed as illustrated in Eq.2.18

$$\{\Delta(i\omega)\} = \{r(i\omega)\} - \{r_0(i\omega)\} = \left[I - e^{-i\omega T}\right]\{r(i\omega)\} \quad \textbf{(2.18)}$$

Eq.2.18 captures the regenerative delay which can be also identified as current motion minus motion from the last pass.

If we rewrite Eq.2.13 in the frequency domain, $\{\Delta(t)\}$ can be written in the form of Eq.2.18. Thus, the final form of dynamic milling force becomes as shown in Eq.2.19.

$$\{F\}e^{i\omega t} = \frac{1}{2}aK_t[A(0)]\left[I - e^{-i\omega T}\right]\{r(i\omega)\} \quad \textbf{(2.19)}$$

Now if we substitute $\{r(i\omega)\} = [G(i\omega)]\{F\}e^{i\omega t}$:

$$\{F\}e^{i\omega t} = \frac{1}{2}aK_t[A(0)]\left[I - e^{-i\omega T}\right][G(i\omega)]\{F\}e^{i\omega t} \quad \textbf{(2.20)}$$

If we cancel $e^{i\omega t}$,and rearrange Eq.2.20:

$$I = \frac{1}{2} a K_t [A(0)]\left[I - e^{-i\omega T}\right][G(i\omega)] \tag{2.21}$$

Eq.2.21 represents a matrix eigenvalue problem. Chatter occurs when any eigenvalue has positive real part, meaning exponential growth. Solving for the maximum stable $a$ (axial depth of cut) gives the chatter boundary.

The characteristic equation can be rewritten for Eq.2.21 in the following form:

$$\det[I + \Lambda G_0(i\omega_c)] = 0 \tag{2.22}$$

Where Λ is eigenvalues of the closed-loop dynamic milling system. The eigenvalues can be written as shown in Eq.2.23 which is the key parameter describing system response to periodic forcing. $G_0(i\omega_c)$ is transfer function matrix projected via force direction.

$$\Lambda = -\frac{N}{4\pi} a K_t (1 - e^{-i\omega_c T}) \tag{2.23}$$

$G_0(i\omega_c)$ represents the scalarized form of $[G(i\omega)]$ based on how force is applied. The open form of $G_0(i\omega_c)$ is shown in Eq.2.24.

$$[G_0(i\omega_c)] = \begin{bmatrix} \alpha_{xx}G_{xx} + \alpha_{xy}G_{yx} & \alpha_{xx}G_{xy} + \alpha_{xy}G_{yy} \\ \alpha_{yx}G_{xx} + \alpha_{yy}G_{yx} & \alpha_{yx}G_{xy} + \alpha_{yy}G_{yy} \end{bmatrix} \tag{2.24}$$

In Eq.2.22, non-trivial solutions exist when this determinant = 0. This defines stability boundaries. If two orthogonal directions are considered in feed (X) and normal direction (Y), this consideration makes cross terms ($G_{yx}, G_{xy}$) zero in Eq.2.24. Therefore, the determinant of Eq.2.22 can be reorganized in the following form:

$$a_0\Lambda^2 + a_1\Lambda + 1 = 0 \tag{2.25}$$

Where

$a_0 = G_{xx}(i\omega) \cdot G_{yy}(i\omega) \cdot (\alpha_{xx}\alpha_{yy} - \alpha_{xy}\alpha_{yx})$

$a_1 = \alpha_{xx}G_{xx}(i\omega) + \alpha_{yy}G_{yy}(i\omega)$

$a_0$ is the determinant of the oriented transfer matrix $[G_0]$, and captures both the structure dynamics and the directional cutting interaction. $a_1$ is the first-order contribution, often dominant in 1DOF systems. From Eq.2.25, the eigenvalue solution can be obtained as shown in Eq.2.26

$$\Lambda = \frac{-1}{2a_0}\left(a_1 \pm \sqrt{a_1^2 - 4a_0}\right) \tag{2.26}$$

Eq.2.26 gives you two complex eigenvalues. The one with positive imaginary part indicates instability (chatter). This complex eigenvalue governs system stability and needs to be separated real and imaginary parts of the complex eigenvalue as shown in Eq.2.27.

$$\Lambda = \Lambda_R + i\Lambda_I \tag{2.27}$$

Then plug into the eigenvalue form from before shown in Eq.2.23 before:

$$\Lambda = -\frac{N}{4\pi} a K_t (1 - e^{-i\omega_c T}) \tag{2.28}$$

In Eq.2.28, $e^{-i\omega_c T}$ can be rewritten according to Euler's formula as

$$e^{-i\omega_c T} = \cos(\omega_c T) - i\sin(\omega_c T) \tag{2.29}$$

Then, $(1 - e^{-i\omega_c T})$ can be rewritten by separating the exponential term as stated in Eq.2.

$$1 - e^{-i\omega_c T} = 1 - \cos\omega_c T + i\sin\omega_c T \tag{2.30}$$

Now equate imaginary and real parts in this expression to get conditions for purely real depth of cut:

$$a_{\text{lim}} = -\frac{2\pi}{NK_t}\left[\frac{\Lambda_R(1 - \cos\omega_c T) + \Lambda_I \sin\omega_c T}{1 - \cos\omega_c T} + i \cdot \frac{\Lambda_I(1 - \cos\omega_c T) - \Lambda_R \sin\omega_c T}{1 - \cos\omega_c T}\right] \tag{2.31}$$

For real axial depth of cut, imaginary part of numerator must vanish:

$$\Lambda_I(1 - \cos\omega T) - \Lambda_R \sin\omega T = 0 \tag{2.32}$$

If the Eq.2.32 is reconsidered in the following form by defining $\kappa$ as defined ratio of imaginary to real part of eigenvalue.

$$\kappa = \frac{\Lambda_I}{\Lambda_R} = \frac{\sin\omega T}{1 - \cos\omega T} \tag{2.33}$$

This lets us rewrite the final depth of cut formula as stated in Eq. 2.34. This equation relates to chatter frequency, transfer function, and depth of cut.

$$a_{\text{lim}} = \frac{-2\pi\Lambda_R}{NK_t}(1 + \kappa^2) \tag{2.34}$$

In regenerative chatter theory, the system's characteristic equation leads to complex eigenvalues as indicated in Eq.2.27. This eigenvalue appears in the exponential solution of the form:

$$x(t) = x_0 e^{\Lambda t} \tag{2.35}$$

Here in Eq.2.35, $\Lambda_R$ is real part which controls amplitude growth or decay, and $\Lambda_I$ is the imaginary part that controls oscillation frequency. In complex analysis, any complex number $\Lambda$ can be written in polar form as shown in Eq.2.36.

$$\Lambda = |\Lambda| e^{i\psi} \tag{2.36}$$

Where:

$|\Lambda| = \sqrt{\Lambda_R^2 + \Lambda_I^2}$

$\psi = \arg(\Lambda)$ is the phase angle. Then, by definition of argument of a complex number becomes to the form indicated in Eq.2.37.

$$\psi = \arg(\Lambda) = \tan^{-1}\left(\frac{\Lambda_I}{\Lambda_R}\right) \tag{2.37}$$

So, the phase angle ( $\psi$) can be defined as

$$\kappa = \frac{\Lambda_I}{\Lambda_R} \quad \Rightarrow \quad \psi = \tan^{-1}(\kappa) \tag{2.38}$$

Phase delay per tooth can be described based on Eq.2.38 as follows:

$$\kappa = \frac{\Lambda_I}{\Lambda_R} \quad \Rightarrow \quad \psi = \tan^{-1}(\kappa) \tag{2.39}$$

Then, the angular phase relation can be expressed as in Eq.2.40 which defines time delay that aligns with tool vibration.

$$\omega_c T = \cos^{-1}\left(\frac{\kappa^2 - 1}{\kappa^2 + 1}\right) = 2\psi \tag{2.40}$$

Where $\psi$ is the phase delay between teeth due to vibration. Then add multiples of $2\pi$ to get the complete family of lobes:

$$\omega_c T = \epsilon + 2k\pi = \pi - 2\psi + 2k\pi \tag{2.41}$$

Where

$k = 0,1,2,\ldots$: the lobe number, $\epsilon$ is total phase shift, and $\omega_c$: chatter frequency

Once $\omega_c T$ is known, spindle speed from tooth period can be calculated as shown in Eq.2.42. (Remember that $T = \frac{60}{\mathrm{nN}}$ tooth passing period.)

$$T = \frac{1}{\omega_c}(\epsilon + 2k\pi), \quad n = \frac{60}{NT} = \frac{60\omega_c}{N(\epsilon + 2k\pi)} \tag{2.42}$$

**Application of the Zero Order Approximation (ZOA) for a SDOF structure**

Milling of Single Degree of Freedom Structure can be derived from analytical formula shown at Eq.2.34.

$$a_{\mathrm{lim}} = \frac{2\pi}{N\alpha_{xx}K_t \cdot \mathrm{Re}[G_{xx}(i\omega_c)]} \tag{2.43}$$

In Eq.2.43 the depth of cut is represented as a simple SDOF system, meaning vibrations occur only in one direction (here: x-direction). The transfer function in X direction can be stated as in Eq.2.44.

$$G_{0x}(i\omega) = \alpha_{xx} \cdot \frac{\omega_n^2}{\omega_n^2 - \omega^2 + i2\xi\omega_n\omega} \tag{2.44}$$

This is the standard SDOF FRF scaled by immersion-dependent directional coefficient $\alpha_{xx}$, which comes from Eq.2.12. Now substitute this into the chatter depth equation (Eq. 2.43) to get:

$$a_{\text{lim}} = \frac{2\pi}{N\alpha_{xx}K_t \cdot \text{Re}[G_{xx}(i\omega_c)]} \tag{2.45}$$

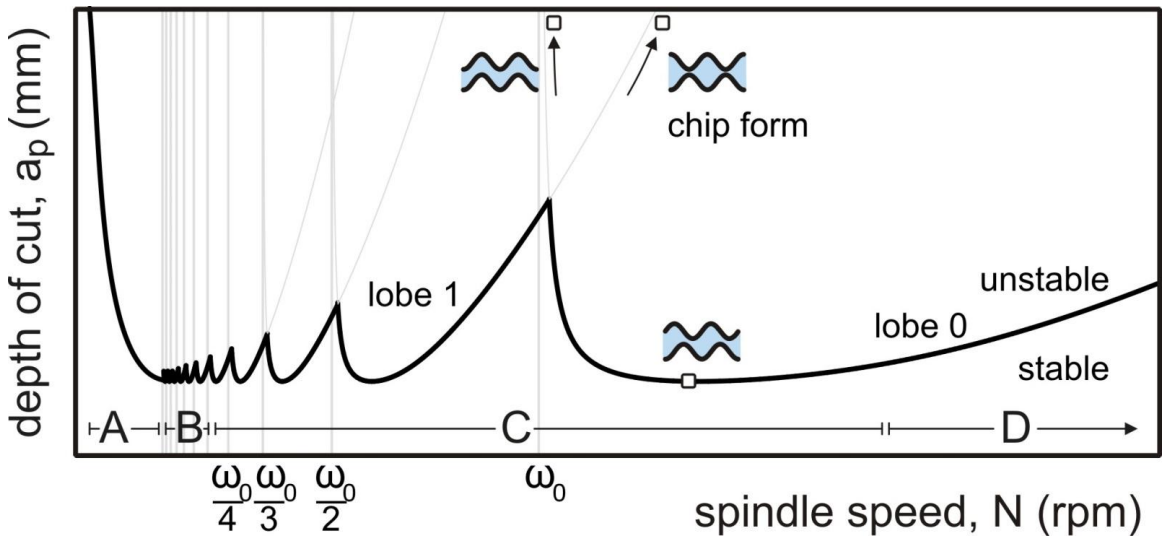


Figure 2.2 Example stability lob diagram

## 2.2 Time Domain Solutions for Stability Lobe Diagrams

To be able to do fast, analytical estimates for chatter lobes the frequency domain solutions (Altintaş,1995) give the option for in high-speed full immersion milling where tooth engagement is nearly constant, and for parameter optimization loops where speed matters more than modelling richness. However, the frequency domain solutions are not accurate for partial immersion and multi-tooth engagement cases. The frequency domain solutions require complex Fourier approximation for directionality to be extended to nonlinear dynamics or state-dependent delays. As a solution to the mentioned drawbacks and to be able to demonstrate some nonlinear phenomena in chatter like double period chatter (Munoa,2016) triggered the application of time domain-based methods. Normally, in classical chatter, where the vibration is strictly periodic with the same period as the tooth passing frequency. However, there might be cases where the vibration pattern of the tool does not repeat every tooth pass but instead repeats every two tooth passes. This is called as double period chatter, and it's a form of period-doubling bifurcation, a common phenomenon in nonlinear time-delay systems. The time domain-based solutions can be categorized as Gamma-distribution based expansions (Guillem,2011), The Semi-Discretization Method (SDM), Full discretization techniques, The collocation method, Time-domain finite element methods, and the Galerkin method which are more time consuming compared to frequency domain methods. Among these methods, the Semi-Discretization Method (SDM) represented by Stephan et. al. (Insperger,2003) has wide usage in turning, milling and grinding applications [45]. Therefore, in this thesis, the semi discretization method will be introduced in the following chapter.

**Semi Discretization Method**

The Semi-Discretization Method (SDM) reformulates the delay differential equation (DDE) that governs regenerative chatter into a discrete-time linear system through a systematic multi-step procedure. The process begins with the discretization of the time domain into small, uniform intervals, thereby enabling a piecewise representation of the system dynamics. In the next step, the time-varying cutting forces are approximated as constant within each subinterval, which simplifies their mathematical treatment. Subsequently, the resulting ordinary differential equations (ODEs) are solved over each time segment based on these constant-force approximations. Finally, a matrix recursion is

applied to propagate the state of the system over a complete tooth passing period. The dynamic stability of the system is then evaluated by examining the eigenvalues of the resulting state-transition matrix. If all eigenvalues lie within the unit circle in the complex plane, the system is considered stable under the given machining conditions, in accordance with Floquet theory (Insperger,2003).

The dynamic model for a single-degree-of-freedom milling process with chatter can be expressed as Eq 2.46 in DDE form.

$$\ddot{x}(t) + 2\zeta\omega_n\dot{x}(t) + \left(\omega_n^2 - \frac{b}{m}K_s(t)\right)x(t) = \frac{b}{m}K_s(t)x(t-\tau) \qquad \textbf{(2.46)}$$

In Eq. 2.46, $x(t)$ is tool displacement in cutting direction, and $\dot{x}(t), \ddot{x}(t)$ stand for velocity, acceleration. The natural frequency of the tool is shown as $\omega_n$, where the damping ratio is $\zeta$, while modal mass is $m$. The depth of cut is $b$, and $\tau$ is time delay between teeth (tooth passing period). As last, $K_s(t)$ is specific cutting force, varies with tool position, reflects up/down milling, immersion, etc.

After revealing the full DDE at Eq.2.46, the semi-discretized DDE can be represented as shown in Eq.2.47. In The core idea in Eq 2.47 is discretizing time and assuming $K_s(t)$ is constant over each small interval, which turning the DDE into a standard second-order ODE with known forcing input from the past.

$$\ddot{x}(t) + 2\zeta\omega_n\dot{x}(t) + \left(\omega_n^2 - \frac{b}{m}K_{s_i}\right)x(t) = \frac{b}{m}K_{s_i}x_{i-M} \quad \text{for } t \in [t_i, t_{i+1}) \qquad \textbf{(2.47)}$$

Here in Eq 2.47:

$t_i$: discretized time points $t_i = i\Delta t$
$K_{s_i}$: average value of $K_s(t)$ over interval $[t_i, t_{i+1}]$
$x_{i-M}$: delayed value of $x$, with $\tau = M\Delta t$

Specific cutting force $K_s(t)$ varies with tool position, and reflects up/down milling, immersion, etc. However, in Eq.2.47 it is assumed as an average value. Instead of using

the exact shape of $K_s(t)$, use its average value in each interval, making the system easier to solve as shown in Eq.2.48.

$$K_{s_i} = \frac{1}{\Delta t}\int_{t_i}^{t_{i+1}} K_s\,(t)\,dt \tag{2.48}$$

In Eq.2.4, DDE is turned into an ODE which is much simpler to solve. The next steps will be solving the second-order ODE from $t_i$ to $t_{i+1}$, given: Initial values $x_i, \dot{x}_i$, and constant forcing from $x_{i-M}$. The displacement update can be written as in Eq.2.49, whereas the velocity update is given in Eq.2.50.

$$x_{i+1} = a_{00}x_i + a_{01}\dot{x}_i + b_{0M}x_{i-M} \tag{2.49}$$

$$\dot{x}_{i+1} = a_{10}x_i + a_{11}\dot{x}_i + b_{1M}x_{i-M} \tag{2.50}$$

In Eqs.2.49 and Eqs.2.50, $a_{00}, a_{01}, a_{10}, a_{11}$ are coefficients from solving homogeneous part of ODE, and $b_{0M}, b_{1M}$: contributions from delayed force input $x_{i-M}$ These equations give us numerical rules to compute the tool's next displacement and velocity, based on: Current state and delayed state from $M$ steps ago.

After defining the difference equations (Eqs.2.49 and Eqs.2.50), a discrete-time map is obtained. The next move will be defining a finite state vector including all necessary history to be able to define a finite dimensional linear system. Then, it will be no longer "infinite" like a PDE or DDE. The finite state vector is illustrated in Eq.2.51.

$$\mathbf{y}_i = \begin{bmatrix} \dot{x}_i \\ x_i \\ x_{i-1} \\ \vdots \\ x_{i-M} \end{bmatrix} \tag{2.51}$$

Then, a recursive state update can be written in finite form as shown in Eq.2.52

$$\mathbf{y}_{i+1} = \mathbf{B}_i\,\mathbf{y}_i \tag{2.52}$$

In Eq.2.53, $\mathbf{B}_i$ is described as transition matrix, and this matrix updates the full state vector to the next step. It applies the dynamics via $a$- and $b$-coefficients and shifts previous values to track the delay.

$$\mathbf{B}_i = \begin{bmatrix} a_{11} & a_{10} & 0 & \cdots & b_{1M} \\ a_{01} & a_{00} & 0 & \cdots & b_{0M} \\ 0 & 1 & 0 & \cdots & 0 \\ 0 & 0 & 1 & \cdots & 0 \\ \vdots & \vdots & \vdots & \ddots & \vdots \\ 0 & 0 & 0 & \cdots & 1 \end{bmatrix} \quad \textbf{(2.53)}$$

State after k steps can be written as in Eq 2.54. Here, each $\mathbf{B}_i$ describes a small-time step. Then, we need to multiply them to simulate a full period.

$$\mathbf{y}_k = \mathbf{B}_{k-1} \cdot \mathbf{B}_{k-2} \cdots \mathbf{B}_0 \cdot \mathbf{y}_0 \quad \textbf{(2.54)}$$

Then, according to Floquet teorem, it is needed to satisfy the Eq.2.55.

$$\mathbf{y}_k = \Phi . \mathbf{y}_0 \quad \textbf{(2.55)}$$

Then, the Floquet transition matrix is described as show in Eq.2.56

$$\Phi = \mathbf{B}_M \cdot \mathbf{B}_{M-1} \cdots \mathbf{B}_0 \quad \textbf{(2.56)}$$

Where, the eigenvalues of $\Phi$ (called Floquet multipliers) determine stability. The matrix $\Phi$ maps the initial state $\mathrm{y}_0$ to the state after one full period. According to Floquet theorem,

The eigenvalues of $\Phi$ determine stability:

If all $|\lambda| < 1 \rightarrow$ stable

If any $|\lambda| > 1 \rightarrow$ unstable (chatter).

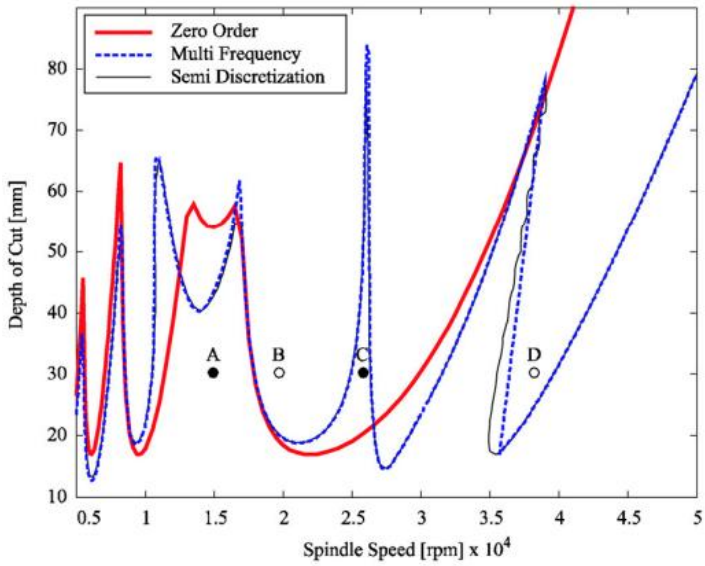


Figure 2.3 Stability lobe diagram with zero order, multi frequency, semi discretization methods

## 2.3 Directional Matrix and Mean Directional Factor

Milling is a rotating and transmitted process, and the cutting forces are evaluated in a rotary frame in general. However, Directional Matrix (DM) introduced by Budak et. al. (Iglesias,2016) in which, radial and tangential forces project into fixed machine frame directions $(x, y)$ which makes it easier compared to other methods. The DM method also applied to multifrequency and Semi Discretization methods by (Altintaş,1995). Additionally, the Zero Order Approximation (ZOA) to simplify analysis. In ZOA, we assume:

- Higher-order harmonics $r = \pm 1, \pm 2, \ldots$ have a lesser effect
- The dominant dynamics are captured well enough by the average cutting behaviour

The ZOA approach results in completely analytical equations for chatter, a stable, closed-form prediction, and good performance with minimal computation. The ZOA can be applied to Mean Directional Factor (MDF) to ease the computation (Dombovari,2025).

The earlier developed approaches by pioneers like Tlusty (Hagele,2016) were one of the first introduced the term of closed loop-of self-exciting system for chatter as shown in Fig X.

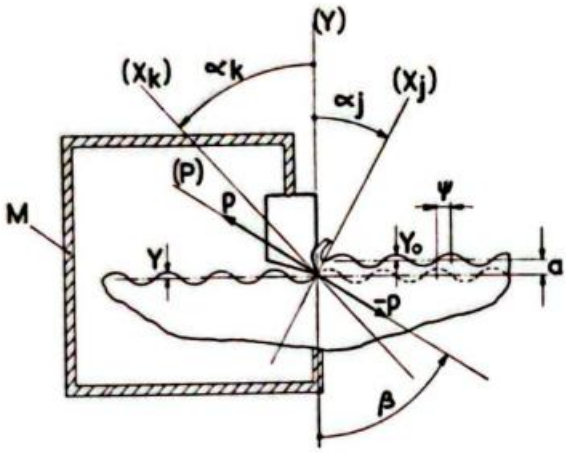


Figure 2.4 Basic Diagram for the process of self-excited tool vibration (Koegnisberger ,1970)

This is (Fig. 2.4) a 1-DOF frequency-domain chatter model with directional interaction between: structural vibration direction (X), (Here again subscripts j, and k describe structural modal vibration direction in 2D space), cutting force direction (P), and surface normal direction (Y). Since the system is introduced as a self-exciting system by Tlusty (Koegnisberger ,1970), the regenerative chip thickness equation is identified as shown in Eq.2.57.

$$h = Y - Y_0 \tag{2.57}$$

According to Eq.2.57, ( $Y$) is surface normal, $Y_0$ is undulation from previous cut, and $Y$ is current vibration in same direction. Cutting force is proportional to chip thickness, which is stated in Eq.2.58. Here, $b$ stands for axial depth of cut (chip width), $r$ is specific cutting force constant and $P$ is cutting force in direction ($P$).

$$P = -b \cdot r \cdot (Y - Y_0) \tag{2.58}$$

Then, vibration response in frequency domain ($\omega$) can be represented as shown in Eq. 2.59. Here in Eq.2.59, Tlusty only considered cross-receptance to simplify the system. Because chatter is fundamentally caused by a multi-directional loop:

- Where Force applied in direction P

- Resulting in vibration in direction X
- Which alters the chip thickness in direction Y
- Which then feeds back into force in direction.

Thus, according to this multi-directional loop, chatter in turning and milling is fundamentally driven by directional interactions between tool vibration direction and cutting force direction. Tlusty focuses on cross-receptance to capture the energy feedback loops across directions that leads to self-excited vibration.

$$Y(\omega) = P(\omega) \cdot \Phi(\omega) \tag{2.59}$$

In Eq. 2.59, $\Phi(\omega)$ represents system cross-receptance from force direction $P$ to vibration direction $(Y)$ whereas $Y(\omega)$ is tool vibration response. By doing this, Tlusty is analysing a single-degree-of-freedom (1-DOF) vibration system but in an arbitrary direction. In this approach, the key is rotating the coordinate system so that vibration happens along some modal direction (X), and cutting force is applied along a different direction (P). The relevant response is along (Y) (the surface normal), which affects chip thickness. Thus, Tlusty needs the projection of the vibration response in the force direction, not in the structural direction as in the case of Directional Matrix approach as introduced by Budak [2,1].

The projection of the vibration response in the force direction can be made by introducing angles as shown in Fig. 2.4. Here the defined angles are as follows:

$\alpha$: angle between vibration direction $(X)$ and surface normal $(Y)$
$\beta$: angle between cutting force direction $(P)$ and surface normal $(Y)$

Then, the directional factor at this moment (instantaneous directional factor) can be described as shown in Eq. 2.60. This factor weighs the contribution of the structural mode to the regenerative loop.

$$u = \cos(\alpha) \cdot \cos(\alpha - \beta) \tag{2.60}$$

The projection of the vibration response in the force direction in Eq. 2.60 which also we can describe as instantaneous directional factor ($u$) can be easily discarded by Fig 2.4 for a single degree of system illustrated (Koegnisberger ,1970).

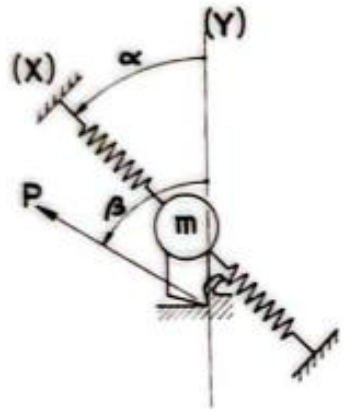


Figure 2.5 Diagram for a single degree of freedom system (Koegnisberger ,1970)

Then, according to instantaneous directional factor, the directional structural response can be obtained via Eq. 2.61 by using the cross directional factor.

$$\Phi(\omega) = u \cdot G(\omega) \tag{2.61}$$

Where, $G(\omega)$ is the real part of the structure's frequency response in its own modal direction, and $u$ is scalar factor projecting that mode into cutting/vibration direction.

The feedback loop for chatter becomes unstable if the real part of the loop gain crosses a threshold which is 1. This comes from the requirement that the loop gain must remain below 1 to avoid positive feedback from control theory. Then, this yields the chatter limit chip width:

$$b_{\text{lim}} = \frac{1}{2r \cdot G_{\text{lim}}} \tag{2.62}$$

Where, $G_{\text{lim}} = \min_{\omega}(u \cdot G(\omega))$ is minimum value of directional real receptance, and $r$ is cutting coefficient. This is important because it was one of the first frequency-domain models that showed how orientation of structural modes affects chatter. Tlusty's method works for turning or 1-DOF milling cases.

Another approach to define instantaneous directional factor is developed by Zatarain et. al. (Zatarain,2010) by only using modal coordinates instead of blending them with surface-normal / modal but embedded in physical frame as in the case of Tlusty. Additionally, in this approach, the angle approaches are more intuitively separated from each other.

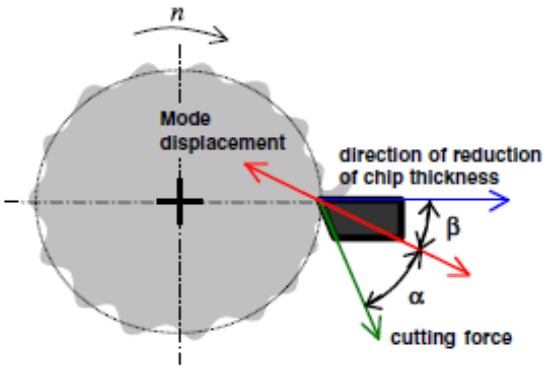


Figure 2.6 Cutting force and mode and chip directions (Zatarain,2010)

In this approach (Zatarain,2010) a modal-coordinate-based formulation of regenerative chatter dynamics, with a single mode of vibration, an instantaneous directional factor ($u$) derived from angular relationships, and a physically clear projection of both the cutting force and the chip thickness regeneration direction onto the mode displacement direction. Here the defined angles are as follows:

$\alpha$: angle between mode displacement and direction of chip thickness
$\beta$: angle between mode displacement and cutting force.

According to this representation of angels in Fig. 2.5, the directional projection can be made based solely on the model displacement. In Tlusty's approach the directional projection was made based on the normal surface (Y).

In a time-invariant system, the equations of motion of a cutting process can be written in modal form as indicated in Eq. 2.63.

$$\ddot{q} + 2\zeta\omega_n\dot{q} + \omega_n^2 q = f\cos\alpha \qquad \textbf{(2.63)}$$

Where q is modal coordinate (displacement in mode direction), f is dynamic cutting force and α is angle between cutting force and mode direction, whereas $\zeta$ is damping ratio and $\omega_n$ signifies natural frequency. The Eq.2.63 shows that only the component of cutting force that acts in the direction of the mode contributes to vibration.

Later, the chip thickness can be defined as shown in Eq.2.64.

$$h = -\phi \cdot (q(t) - q(t-\tau)) \cdot \cos\beta \quad \textbf{(2.64)}$$

Where, $\phi$ is relative amplitude of motion, and $\beta$ is angle between chip thickness direction and mode direction. The Eq. 2.64 shows that the vibration projected onto chip thickness variation direction drives the regenerative feedback. Then, if the force equation is written by using Equations 2.63 and 2.64,

$$f = -k \cdot b \cdot \phi \cdot \big(q(t) - q(t-\tau)\big) \cdot \cos\beta \quad \textbf{(2.65)}$$

The final chatter loop equation becomes as in Eq. 2.66

$$\ddot{q} + 2\zeta\omega_n\dot{q} + \omega_n^2 q = -k \cdot b \cdot \phi \cdot \cos\alpha \cdot \cos\beta \cdot (q(t) - q(t-\tau)) \quad \textbf{(2.66)}$$

Eq.65 leads us to the directional factor ( $u$) as in Eq.2.67.

$$u = \cos\alpha \cdot \cos\beta \quad \textbf{(2.67)}$$

In Zatarain's approach (Zatarain,2010), it strictly uses modal analysis and does not transform anything into X-Y or machine coordinates. Instead: It stays in the mode coordinate $q$, and projects both the cutting force, and the regenerative chip variation, onto that mode direction. So, it is the product of cosine projections of:

- The cutting force direction onto the mode $\cos\alpha$,
- The chip thickness variation direction onto the mode $\cos\beta$.

Before explaining the Mean Directional Factor approaches available in the literature, it is important to comment on what the directional projections are on. In the Tlusty's approach (Koegnisberger ,1970) projection is made on surface normal direction (Y), and it was a blended approach between machine coordinates and modal interactions. On the other hand, the approach provided by Zatarin et. al. (Zatarain,2010) is based on modal displacements. These projections are hard to obtain analytically; it requires experimental effort and cannot be determined before the cutting operations. Lastly, the DM approach introduced by Budak provides a fast analytical solution based on machine tool coordinates but again this directionality factor is impossible to determine beforehand according to cutting conditions. Thus, if someone wants to be able determine the directional factor according to cutting

conditions, the directional factor projections should be based on feed and average chip thickness direction. Therefore, during process planning, the sign (positiveness and negatives) of the directional factor can be determined. The formulation of the directional factor and mean directional factor will be explained in Section 3.

The Mean Directional Factor (MDF) is a scalar value that represents the average effectiveness of cutting force direction in exciting machine tool vibrations, usually over an entire engagement cycle. Therefore, in time in variant systems like turning operations or idealized cases like 1-DOF and one tooth milling operations, the instantaneous directional factor ($u$) can be considered as same with mean directional factor. However, in milling processes, due to the rotating nature of the tool, the geometry of cutting engagement changes constantly. This makes chatter stability analysis more complex than in continuous cutting processes like turning as shown in Fig. X.

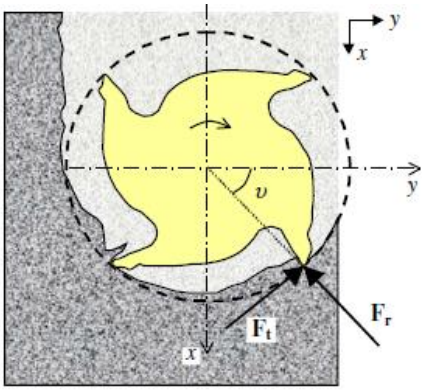


Figure 2.7 Cutting forces in milling process (Zatarain,2010)

For the discontinuous nature of milling, one must account for the fraction of time each tooth spends on the cut (arc length), and the number of teeth involved in the process. So, the limit depth of cut b (Zatarain,2010) for milling can be approximated as in Eq.2.68.

$$b = \frac{-1}{2 \cdot k_c \cdot u_{\text{av}} \cdot \frac{\Delta v}{2\pi} \cdot z \cdot R} \qquad \textbf{(2.68)}$$

Where, $u_{\text{av}}$ is the mean directional factor, $\Delta v$ is the angular range of tool-workpiece contact, $z$ is number of teeth, and $R$ is cutter radius, and $k_c$ is the cutting force coefficient.

For the calculation of Mean Directional Factor for milling according to immersion angles $(v)$ , Opitz (Opitz,1979) proposed calculating $u_{av}$ as the average value of the directional factor over the contact arc as indicated in Eq. 2.69.

$$u_{av} = \frac{1}{v_{ex} - v_{st}} \int_{v_{st}}^{v_{ex}} u\,(v)\, dv \qquad \textbf{(2.69)}$$

Where $v_{st}$, $v_{ex}$ are the angular positions where cutting starts and ends,$u(v)$ is instantaneous directional factor at angular position $v$. Alternatively, Tlusty (Koegnisberger ,1970) proposed a simpler approximation using the geometric mean or midpoint evaluation of the arc as shown in Eq.2.70.

$$u_0 = \frac{v_{st} + v_{ex}}{2} \qquad \textbf{(2.70)}$$

Later, Altintas and Budak later showed that when you model the directional behaviour of the cutting force using a Fourier expansion of the directional matrix, the first (DC) term of the expansion gives a result that matches exactly with Opitz's mean directional factor method.

# 3. IMPORTANCE OF MEAN DIRECTIONAL FACTOR FOR CHATTER-FREE ROBOTIC MILLING

## 3.1 Stability Model for Milling with a Single Dominant Mode

### 3.1.1 Equation of Motion with a Single Dominant Mode

A linearized dynamic model for a robotic milling process under periodic cutting forces is described in this section via Eq.3.1.

$$\mathbf{M}\ddot{u}(t) + \mathbf{C}\dot{u}(t) + \mathbf{K}u(t) = K_{ct}\, a\, \mathbf{A}(t)(u(t) - u(t-T)) \qquad \textbf{(3.1)}$$

Where M, C, K are mass, damping, and stiffness matrices of the robot/machine structure respectively. $u(t)$ is the displacement, and $K_{ct}$is tangential cutting force coefficient, $a$ is axial depth of cut. $\mathrm{A}(t)$ is time-dependent directional matrix, $T = \frac{1}{Z\Omega}$: Tooth passing period, a function of number of teeth and spindle speed. Then, this time-periodic delay differential equation (DDE) model, where the dominant vibration mode is extracted via modal transformation can be rewritten.

$$\ddot{q}(t) + 2\zeta\omega_n\dot{q}(t) + \omega_n^2 q(t) = -\frac{\omega_n^2}{k}\cdot\frac{K_{ct}\, a}{\sin\kappa}\cdot B(t)(q(t) - q(t-\tau)) \qquad \textbf{(3.2)}$$

$q(t)$ is displacement in modal coordinates, $\omega_n$, $\zeta$ are natural frequency and damping ratio of the dominant mode. $k$ is modal stiffness. $\kappa$ is lead angle, $B(t)$is time-dependent directional coefficient (similar to $A(t)$ but scalar). $\tau$ is delay period (same as the tooth passing period).

### 3.1.2 Physical Description of Mean Directional Factors of a Mode

The Directional Factor is a scalar projection coefficient that quantifies how much regenerative displacement in a certain direction contributes to the resultant dynamic cutting force. In Section 2.3, the directional factor was introduced based on different projection approaches from the literature [1,4,5]. Additionally, it was commented on available methods for directional factors based on machine tool coordinates and mode displacements which a machine operator cannot intervene during the machining process. Therefore, to accurately determine the directional factor under specific cutting conditions, the projections should be referenced with respect to the feed direction and the average chip thickness direction. This approach enables process planners to predict the sign (positive or negative) of the directional factor in advance. The formulation of the directional factor and mean directional factor based on average feed direction will be explained in this section.

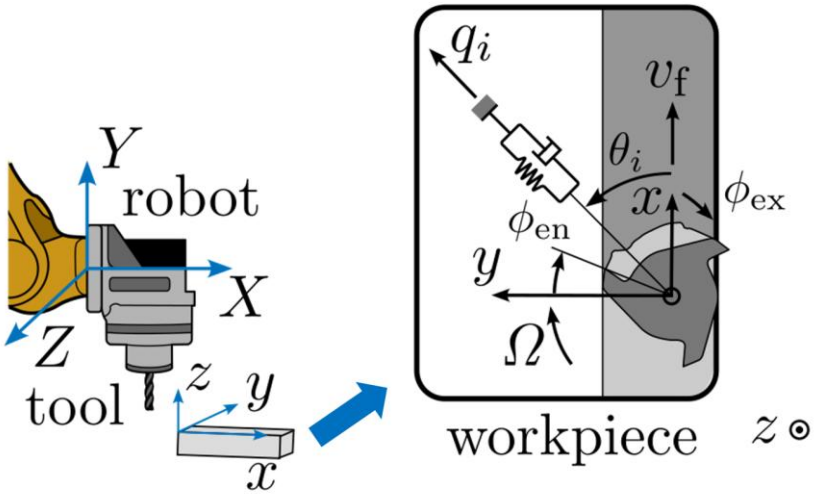


Figure 3.1 XY plane robotic milling

Fig. 3.1 explains how the cutting force, chip thickness, and vibration mode direction interact in milling (e.g., robotic milling or flexible machining systems). This interaction governs chatter. In Fig 3.1, the left side shows a robotic spindle with tool and workpiece. X, Y, Z are global Cartesian directions of machine, and x, y, z are tool coordinate directions. These frames matter because modal vibrations and cutting forces may occur in different frames. In the milling cutting process shown in Fig. X as boxed, the immersion

angles are represented as $\phi_{st}$ for start and $\phi_{ex}$ for exit. Additionally, $\vec{v}_f$ is feed direction, $\vec{v}$ is average chip thickness direction, which can also be described as direction in which the thickness of material removed varies. Lastly, $\vec{q}_i$ is mode direction, and $\theta_i$is angle between mode direction $\vec{q}_i$ and feed, and spindle speed is defined as $\Omega$. These angles govern how regenerative forces couple with vibrations. In this representation, for a single mode and single tooth, the directional factor can be calculated. However, to be able to do this calculation the projection angles between the cutting force, mode shape and average chip direction needs to be identified. This identification is made in Fig. 3.2.

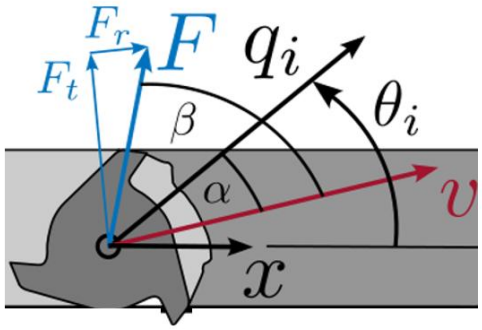


Figure 3.2 Cutting force, mode, chip directions for directional factors for avg. chip thickness

In Fig. 3.2, $\vec{F}$ is cutting force, $\vec{q}_i$ is mode direction, and $\theta_i$is angle between mode direction $\vec{q}_i$ and feed, and $\vec{v}$ is average chip direction. Here, the projections angels will be defined based on average chip direction where:

$\alpha$: angle between mode direction $\vec{q}_i$ and average chip direction $\vec{v}$
$\beta$: angle between cutting force $\vec{F}$ and average chip direction $\vec{v}$

Let's derive the instantaneous directional factor $(u)$ from projection principles. This requires a double projection as indicated in Eq. 3.3. The first one is projection chip regeneration onto mode direction. The second one is projection force onto the modal direction which determines modal excitation.

$$u = \cos(\alpha) \cdot \cos(\beta - \alpha) \quad \textbf{(3.3)}$$

Thus, the Eq.3.1 represents the effective energy transfer from regenerative displacement into vibration via cutting force.

**(a)** Positive Directional Factor

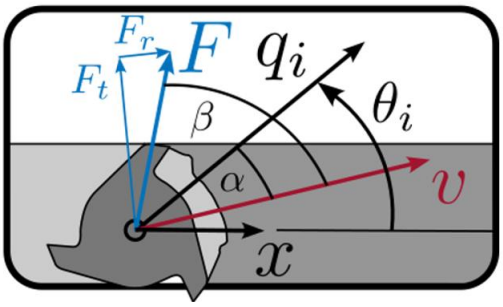


**(b)** Negative Directional Factor

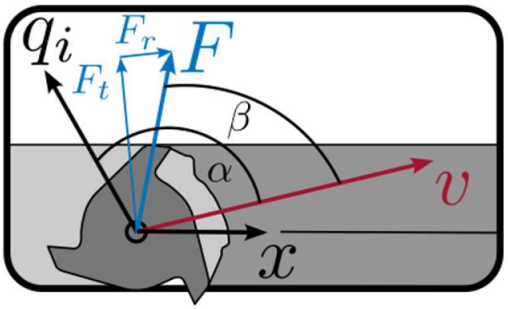


Figure 3.3 Positive and Negative directional factors based on average chip thickness

The instantaneous directional factor $(u)$ is strongly influenced by the angle $\theta_i$, which defines the direction of the mode shape. So, if the vibration mode is aligned with the direction of cutting force or chip thickness variation, the force has a strong component along the vibration direction that leading to a non-zero instantaneous directional factor $(u)$.However, if the mode direction is perpendicular to either: the resultant cutting force vector $\vec{F}$, or the chip thickness direction $\vec{v}$. Then the projection becomes zero, and so does the instantaneous directional factor $(u)$. In this case, the force cannot excite the vibration in that mode direction, and the system behaves as if decoupled from dynamic instability in that specific mode.

For a non-zero instantaneous directional factor $(u)$ can have positive or negative values in which:

**Positive instantaneous directional factor $(u)$ – Stabilizing Effect (Fig. 3.3 (a))**

When the instantaneous directional factor $(u)$ is positive, it indicates that the direction of the cutting force is such that it tends to oppose the vibration. That is:

- As the tool begins to move away from the workpiece (due to vibration),
- The cutting force pulls it back toward a stable position,
- The net effect is damping, or energy dissipation, which helps to suppress chatter.

In this case, the system is self-stabilizing, and vibrations naturally die out over time.

**Negative instantaneous directional factor $(u)$ – Destabilizing Effect (Fig. 3.3 (b))**

When the instantaneous directional factor $(u)$ becomes negative, a chatter risky situation occurs:

- The cutting force reinforces the vibratory motion of the tool.
- If the tool moves into the workpiece due to a vibration, the force acts in a way that encourages more penetration.
- This leads to a positive feedback loop, where vibrations grow with each tool pass, resulting in chatter.

This is a classic case of regenerative chatter, where tool vibrations from a previous revolution modulate the current chip thickness, and the cutting force amplifies the motion. In the next section, the effect of the directional factor will be explained better on stability limit diagrams, but a general summary is given in Table 3.1 for instantaneous directional factor $(u)$ .

Table 3.1 The effect of the directional factor on cutting stability

| DF Value | Projection Situation | Physical Effect | Result |
|---|---|---|---|
| **> 0** | Force resists vibration | Stabilizing force | Stable cut |
| **< 0** | Force amplifies vibration | Positive feedback | Chatter risk |
| **= 0** | Orthogonal vectors | No energy transfer | Neutral |

### 3.1.3 Stability of The System with One Dominant Mode

As discussed in the previous section, the mean directional factor can affect the chatter risk. In literature, robotic machining can be shown as associated with Hopf and Flip related bifurcations (Dombovari,2025), but the typical machining conditions for high-speed Machining (HSM) in robotic milling correspond to the ultra-high spindle speed zone when the robot posture dependency is neglected. In general, these nonlinearities (bifurcations) are also associated with structural and tool vibration interactions. However, in high-speed machining (HSM), milling at spindle speeds so high that the tooth passing frequency (ZΩ) becomes much greater than any natural frequency of the robot structure. This situation

means that tooth engagement happens so rapidly that structural vibrations cannot keep up with the dynamic cutting force variations. In mathematical terms, this can be identified as shown in Eq.3.4.

$$Z \cdot \Omega \gg 5\text{–}50 \cdot max_j \omega_{n,j} \tag{3.4}$$

A conventional robotic milling operation can be considered with evenly spaced $Z$ number of teeth and spindle speed $\Omega$, resulting in a tooth passing period T (s) = 1/ (Z $\Omega$ (Hz)). This indicates that the spindle speed is far beyond the range traditionally associated with Hopf and flip-related 'lobe structures.

Another indication about directional factors for such high speeds is that, in lower-speed milling, Fourier harmonics of the force, due to tooth entry/exit, create time-periodic excitation. But if $Z\Omega \gg \omega_n$, the structure is effectively low pass filtered which can be simplified as it only "feels" the average force. Therefore, the ZOA approach (Altintaş,1995) can be applied to time varying directional matrix with a constant Mean Directional scalar (MDF) $\beta_0$.

$$B(t) = \sum_{i=1}^{Z} g\big(\varphi_i(t)\big) b\big(\varphi_i(t)\big) \tag{3.5}$$

$$\beta_0 = \frac{Z}{2\pi} \int_{\varphi_{\text{en}}}^{\varphi_{\text{ex}}} b(\varphi)\, \mathrm{d}\varphi, \tag{3.6}$$

This simplification provides closed-form stability equations for a single DOF system as shown in Eq. 3.7.

$$a(\omega_c) = \frac{-\pi \cdot \sin\kappa}{K_{ct} \cdot Z \cdot \beta_0 \cdot \Re\{\Phi(\omega_c)\}} \tag{3.7}$$

$\omega_c$ is chatter frequency, $\kappa$ is lead angle (can be considered as 90 to simplify the equation more.) $K_{ct}$ is tangential cutting coefficient, $Z$ is number of flutes, and $\beta_0$ is Mean Directional Factor and lastly $\Re\{\Phi\}$ is real part of FRF in modal coordinates.

This defines the limiting axial depth of cut as shown in Eq.3.8.

$$\Omega_j(\omega_c) = \frac{\omega_c}{Z}((2j+1)\pi + 2\psi(\omega_c)) \tag{3.8}$$

The Eq. 77 gives spindle speed where chatter will occur for a specific mode and chatter frequency. Therefore, by checking Eq. 76 and 77, a key insight can be given as follows:

Stability has a linear relation with loop gain, MDF and the real part of the FRF, and for stability it should be negative:

$$\text{Loop gain} \propto \beta_0 \cdot \Re\{\Phi(\omega)\}$$

Therefore:

If $\beta_0 > 0$: system is destabilized by negative FRF real part.
If $\beta_0 < 0$: system is destabilized by positive FRF real part.

This flips the chatter frequency zone left or right of the resonance as shown in Fig. 3.4.

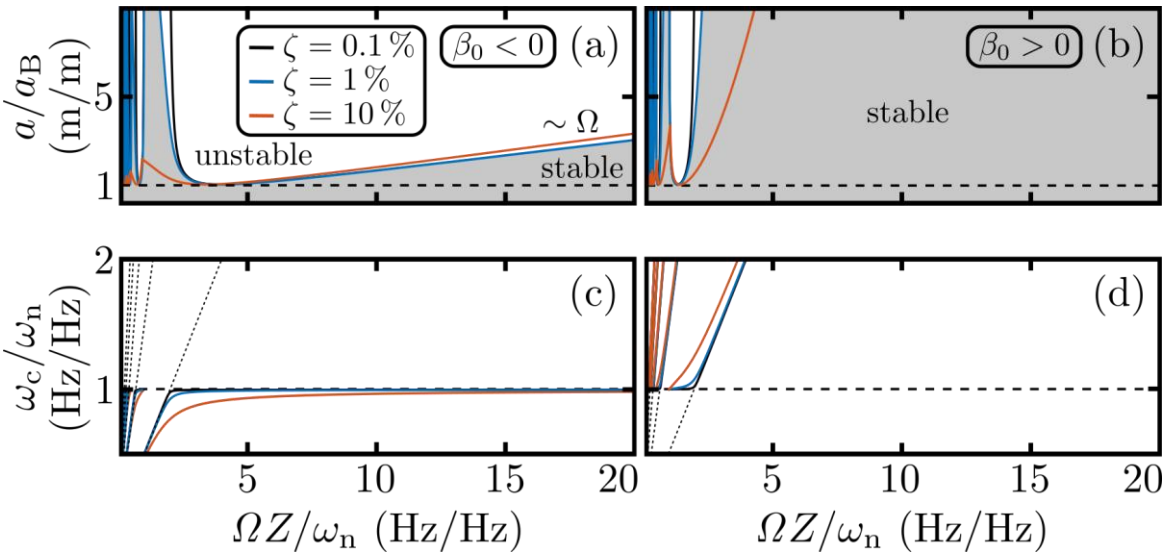


Figure 3.4 Stability of 1 DOF System (a) Negative MDF (N-MDF) and (b) Positive MDF (P-MDF) (c) Chatter frequency chart for N-MDF and (d) Chatter frequency chart for P-MDF.

Notable distinctions between negative and positive Modal Damping Factors (MDFs) become apparent in the high-speed regime, where the ratio of tooth-passing frequency to the system's natural frequency exceeds 5. Within this range, only negative MDFs can limit stability, leading to the emergence of chatter at a frequency slightly below the natural frequency (see Fig. 3.4(c)). Conversely, for positive MDFs, chatter occurs at a frequency

above the natural frequency (see Fig. 3.4(d)). This stability behavior is influenced by spindle speed, setting it apart from traditional mode-coupling chatter mechanisms.

When examining stability lobe diagrams (SLDs), negative MDFs lead to only modest improvements in stability at elevated spindle speeds, whereas positive MDFs result in significantly enhanced stability. Due to this pronounced contrast, achieving a positive MDF is highly advantageous and can be attained by carefully selecting radial immersion and feed direction. Therefore, this study emphasizes the importance of avoiding negative MDFs to ensure optimal performance in robotic milling. This approach represents a shift from conventional methods that mainly consider the direct projection of cutting force magnitude onto the critical mode associated with mode-coupling chatter (Gurney ,1962).

### 3.1.4 High Tooth Passing Frequency Asymptote for Negative-MDF

To derive a piecewise linear approximation of the stability limit (i.e., depth of cut $a(\Omega)$) for a single-mode system under negative MDF ($\beta_0 < 0$), it is needed to approximate the minimum stable depth of cut as a function of spindle speed $\Omega$, particularly when the dominant vibration mode is at low frequency. This is possible by analyzing the slope of the stability boundary. The slope of the stability boundary is examined as chatter frequency $\omega_c$ approaches the natural frequency $\omega_n$. In that limit, the depth of cut vs. spindle speed becomes linear, and its slope $s$ is:

$$\mathrm{s} = \lim_{\omega_c \to \omega_n} \frac{\partial a(\omega_c)}{\partial \Omega_0(\omega_c)} = -\frac{4\pi k\zeta}{\omega_n K_{ct}\beta_0} \qquad \textbf{(3.9)}$$

Where $a(\Omega)$ is depth of cut as a function of spindle speed, $\omega_n$is the natural frequency of the dominant mode, $\omega_c$ is chatter frequency. $Z$ is the number of teeth on the cutter, and $\zeta$is damping ratio of the mode. $\beta_0$ is mean directional factor (MDF), while $K_{ct}$is cutting force coefficient. $k$ is a modal projection factor (relates force to vibration), and $\Omega_0 = \omega_c/Z$ is tooth passing frequency. The Eq.3.9 means that as spindle speed increases such that chatter frequency approaches the natural frequency, the stability boundary becomes approximately linear, and the slope of this linear part depends inversely on $\beta_0$ and directly on damping $\zeta$.

Since $\beta_0 < 0$, this slope $s > 0$, meaning the linear region of the stability diagram, increases with speed.

The lowest possible depth of cut before instability always occurs is derived by minimizing the stability function. This minimum, denoted $a_B$, is given by Eq. 3.10.

$$a_B = \frac{4\pi k(\zeta - 1)\zeta}{K_{ct} Z \beta_0} \tag{3.10}$$

According to Eq.3.10; if $\zeta < 1$, then $(\zeta - 1) < 0 \rightarrow a_B > 0$ (since $\beta_0 < 0$, so negative denominator cancels). This defines the flat portion of the stability boundary: no matter how slow the spindle speed, the depth of cut must stay below $a_B$ to remain stable.

Then, the transition point between the flat region and the sloped region can be identified as in Eq.3.11.

$$\Omega^* = \frac{(1 - \zeta)\omega_n}{Z} \tag{3.11}$$

The Eq.3.11 is important because:

- For spindle speeds $\Omega \leq \Omega^*$: system is governed by the flat floor of minimum stability $a_B$.
- For $\Omega > \Omega^*$: system enters a linearly increasing stable region with slope $s$.

From these results, the final piecewise approximation of the stability curve can be constructed as shown in Eq.3.12.

$$a(\Omega) \approx \tilde{a}(\Omega) = \begin{cases} a_B, & \text{for } \Omega \leq \Omega^* \\ s\Omega, & \text{for } \Omega > \Omega^* \end{cases} \tag{3.12}$$

The Eq. 3.12 shows that geometrically, it's a horizontal line $a = a_B$ up to $\Omega^*$, then a straight line with slope $s$ beyond that. These lines intersect at the point $(\Omega^*, a_B)$, ensuring continuity. This piecewise model simplifies a complex stability lobe diagram into two easily interpreted regions. This model helps to estimate chatter limits quickly without full numerical computation. Additionally, as shown by the presented model, the negative MDF leads to limited stability growth with speed (unlike positive MDFs, which produce large lobes). This is important, stability is limited by the low-frequency mode only when the

MDF is negative. Therefore, to optimize machining performance in the ultra-high-speed range, it is essential to avoid conditions associated with negative MDF.

## 3.2 Polar Coordinates for Optimal Robotic Machining

### 3.2.1 Calculation of Feed Direction Dependent MDF

In this section, the instantaneous directional factor under a simplified 2D polar force model will be presented. The Instantaneous Directional Factor $b(\phi)$ is a geometric scalar that quantifies effectively the cutting force at a given cutter angle $\phi$ projects onto a given vibration mode direction $\vec{q}_i$. It's defined purely by vector directions. Mathematically, it can be defined as:

$$b(\phi) = (\text{cutting force direction}) \cdot (\text{mode direction}) \tag{3.13}$$

The cutting force vector $\vec{F}(\phi)$ as a sum of tangential and radial components:

$$\vec{F}(\phi) = F_t \cdot \hat{t}(\phi) + F_r \cdot \hat{r}(\phi)) \tag{3.14}$$

Where:

$\hat{t}(\phi) = [\cos(\phi), \sin(\phi)]$: tangential unit vector at φ

$\hat{r}(\phi) = [-\sin(\phi), \cos(\phi)]$: radial unit vector at φ

$\kappa_{c,r} = \frac{F_r}{F_t}$: ratio of radial to tangential force

Then, the total force direction vector can be written as:

$$\vec{F}(\phi) = \hat{t}(\phi) + \kappa_{c,r} \cdot \hat{r}(\phi) = \begin{bmatrix} \cos(\phi) - \kappa_{c,r}\sin(\phi) \\ \sin(\phi) + \kappa_{c,r}\cos(\phi) \end{bmatrix} \tag{3.15}$$

The mode shape direction as a unit vector:

$$\vec{q}_i = \begin{bmatrix} \cos(\theta) \\ \sin(\theta) \end{bmatrix} \tag{3.16}$$

Then the projection of the force vector onto the mode is:

$$b(\phi) = \vec{F}(\phi) \cdot \vec{q}_i \tag{3.17}$$

Compute the dot product:

$$b(\phi) = [\cos(\phi) - \kappa_{c,r}\sin(\phi)]\cos(\theta) + [\sin(\phi) + \kappa_{c,r}\cos(\phi)]\sin(\theta) \tag{3.18}$$

Group terms:

$$b(\phi) = \cos(\phi - \theta) + \kappa_{c,r}\sin(\phi - \theta) \tag{3.19}$$

If the Eq.88 is integrated over engagement:

$$\beta_0 = \frac{Z}{2\pi}\int_{\phi_{\text{en}}}^{\phi_{\text{ex}}} \big(\cos(\phi - \theta) + \kappa_{c,r}\sin(\phi - \theta)\big)\, d\phi \tag{3.20}$$

Let $u = \phi - \theta$, so:

$$\beta_0 = \frac{Z}{2\pi}\int_{\phi_{\text{en}}-\theta}^{\phi_{\text{ex}}-\theta} \big(\cos(u) + \kappa_{c,r}\sin(u)\big)\, du \tag{3.21}$$

Then integrate:

- $\int \cos(u)\, du = \sin(u)$
- $\int \sin(u)\, du = -\cos(u)$

So:

$$\beta_0 = \frac{Z}{2\pi}\big[\sin(u) - \kappa_{c,r}\cos(u)\big]_{\phi_{\text{en}}-\theta}^{\phi_{\text{ex}}-\theta} \tag{3.22}$$

Now plug in:

$$\beta_0 = \frac{Z}{2\pi}\big[\sin(\phi_{\text{ex}} - \theta) - \sin(\phi_{\text{en}} - \theta) - \kappa_{c,r}(\cos(\phi_{\text{ex}} - \theta) - \cos(\phi_{\text{en}} - \theta))\big] \tag{3.23}$$

Then, this leads to the following equation after applying some trigonometric identities:

$$\beta_0 = \frac{1}{4}\big[2\sin(2\theta - \phi_{en} - \phi_{ex}) \cdot \sin(\phi_{en} - \phi_{ex}) - \kappa_{c,r}(2\phi_{en} - 2\phi_{ex} + \sin(2(\theta - \phi_{en})) - \sin(2(\theta - \phi_{ex})))\big] \quad \textbf{(3.24)}$$

As a result, the MDF for a specific feed direction is defined by Eq.3.24.

### 3.2.2 Radial Engagement Polar Plots

Traditionally, polar plots in milling dynamics depict the feed direction along the angular axis and the depth of cut along the radial axis (Lutfi ,2021). In this study, a modified polar plot tailored for robotic milling process planning. In the revised format, the angular axis continues to represent the feed direction, but the radial axis now indicates the radial engagement ratio ($\psi = a_e/D$), while the colormap visualizes the limiting depth of cut for a given spindle speed, assuming a high ratio of tooth-passing frequency to mode natural frequency (e.g., ratio of 10 in Fig. 3.5(a)). Alternatively, the colormap can be used to represent the Mean Directional Factor (MDF), as shown in Fig. 3.5(b).

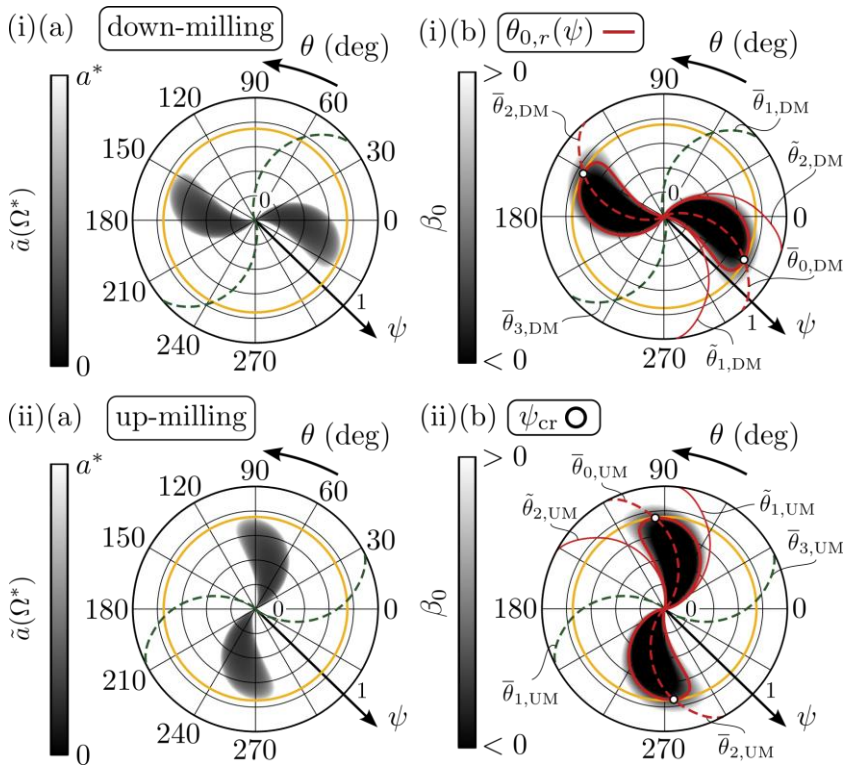


Figure 3.5 (a) Stability limit depth of cut $\tilde{a}$ at high spindle speed. $Z\ \Omega\ \ = K \max_j \omega_{\mathrm{n},j}\ , K = 10$ (b) MDF in polar coordinates. (i) DM and (ii) UM.

Up-milling (UM) and down-milling (DM) strategies are characterized by their respective entry and exit angles: $(\phi_{en}, \phi_{ex}) = (0, \varphi)$ for UM, and $(\pi-\varphi, \pi)$ for DM. This approach enables the visualization of single-mode dynamic behaviour in polar coordinates. Figure 3.5 illustrates how both the high-speed stability limits ã and the MDF vary with feed direction (θ) and radial immersion ψ. Several key insights arise from these plots:

- Regions exhibiting low allowable depths of cut correspond directly to areas with negative MDF.
- There is a sharp transition from highly stable (chatter-free) to unstable (chatter-prone) cutting conditions.

In particular, full slotting (ψ = 1) tends to suppress low-frequency mode excitation, promoting stable cutting with high depth of cut. Moreover, stability remains high up to a critical immersion value $\psi_{cr}$ (highlighted by an orange circle in Fig. 3.5), beyond which the MDF remains strictly positive effectively eliminating chatter.

These polar plots serve as a practical tool to select feed directions and engagement ratios that maximize stability, as highlighted by the white zones. Conversely, the shaded zones indicate 'stability-destructive' feed directions associated with negative MDF, which should be avoided particularly in robotic machining applications. Notably, the polar plot based on limiting depth of cut is broadly applicable and remains valid for systems with multiple vibration modes.

### 3.2.3 Minimum Radial Engagement for Chatter Free Machining

In this study, MDF is specialized to assess milling process stability for different feed directions and immersion values. The MDF becomes zero at boundary curves $\theta_0, r(\psi)$, which represent marginally stable conditions. These boundary curves are visualized as thick red lines in Fig. 3b and indicate where the cutting process transitions to instability.

ψ is the normalized radial immersion which can be described as a fraction representing the portion of the cutter engaged with the material. And $\psi_{\text{cr}}$ is the minimum radial immersion needed to ensure the MDF remains positive which also ensures the process is stable. It can be derived from solving $\beta_0(\theta, \psi) = 0$, where $\beta_0$ relates to directional dynamics.

To approximate $\psi_{\text{cr}}$, a harmonic sum model is used as shown in Eq.3.25.

$$\psi_{\text{cr}}(\kappa_{\text{cr}}) \approx \sum_{i=1}^{2} a_i \sin(b_i \kappa_{\text{cr}} + c_i) \qquad \textbf{(3.25)}$$

Where: $\kappa_{\text{cr}}$: relative radial cutting coefficient

Constants: $a_i = (2.49, 1.79)$, $b_i = (2.01, 2.42)$ , and $c_i = (0.60, 3.37)$

In this section, the following conclusions can be drawn:

low-frequency chatter can emerge even when the tooth-passing frequency significantly exceeds the natural frequency of the system. Importantly, this instability arises in the presence of a single dominant vibration mode, without contributions from mode coupling or multi-modal interactions that confirm that it is driven purely by the regenerative effect.

A key finding is that avoiding negative Minimum Directional Factor (MDF) is essential for ensuring stable robotic milling. The use of radial engagement polar plots proves effective in identifying optimal feed directions and engagement conditions. These plots help define a critical radial immersion threshold, beyond which the MDF remains entirely positive, ensuring a stable cutting process.

To experimentally validate the feed direction optimization framework in polar coordinates, a custom-designed flexure structure with consistent dynamic properties is employed. This flexure is specifically designed to mimic the low dynamic stiffness of industrial robots, featuring a single dominant low-frequency mode. In Section 4, the development of this flexure structure will be explained. Additionally, machining tests conducted along both circular and linear tool paths successfully revealed distinct zones of positive and negative MDF, verifying the theoretical predictions and confirming the effectiveness of the polar-based optimization approach in Section 6.

# 4. FIXTURE DESIGN TO REPRESENT ROBOTIC MILLING

## 4.1 Fixture Design

To investigate the stability behaviour observed in robotic milling, a custom flexure-based fixture was developed that emulates the dominant dynamic features of industrial robots in a simplified and controlled setup. Robotic systems typically exhibit very low structural and dynamic stiffness, with dominant low-frequency modes often below 30 Hz linked to bending-type deformations in a specific direction. This anisotropic compliance means that one principal direction is significantly more flexible, while others remain relatively stiff. To replicate these characteristics, the fixture was designed to possess a single dominant linear bending mode in figure 4.1, with all other modal responses (e.g., torsional or lateral bending) pushed to higher, non-interfering frequency ranges. The fixture was designed to exhibit a directionally compliant yet spatially consistent dynamic response mimicking the behaviour of an industrial robot in an extended configuration while avoiding the posture-dependent and nonlinear characteristics typically present in actual robotic systems. This allows for repeatable dynamic testing and direct validation of theoretical models that focus on low-frequency chatter driven by negative mean directional factors (MDFs). By enforcing single-mode dominance, the fixture isolates the critical dynamics responsible for chatter onset, creating an ideal testbed for studying how directional cutting forces interact with structural flexibility, a cornerstone of the MDF-based chatter theory.

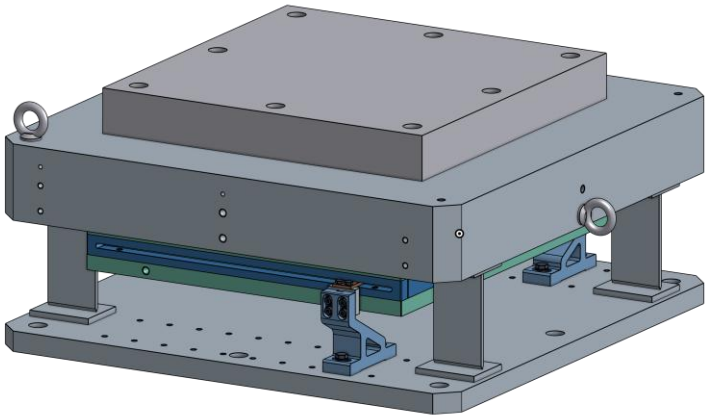

Figure 4.1 Fixture CAD design

Key design principles for the fixture included:

Low Directional Stiffness: The fixture was engineered to have a substantially lower stiffness in one lateral direction, yielding a fundamental bending mode in the 20–30 Hz range (to mimic a robot's first flexible mode). This required slender, compliant elements in the target direction while maintaining rigidity in other axes.

Modal Control: The geometry ensures that one bending mode dominates the dynamic response, with all other modes (orthogonal bending, torsion, axial modes) pushed to much higher frequencies. This was achieved via a symmetric layout and careful proportioning of members to raise non-bending modes out of the critical frequency range. For example, a symmetric four-post support configuration was chosen to inherently resist torsional deformation of the top platform, thereby elevating the natural frequency of torsional modes well above the first bending mode.

Ease of Integration: The fixture needed to accommodate test components (workpieces, sensors, and dampers) and mount securely in a lab setting. A broad steel base plate with standard hole patterns allows rigid bolting of the fixture to a massive support (e.g. a granite table or machine bed), ensuring a well-defined boundary condition. The top platform likewise includes tapped holes for attaching a workpiece or adapter plate. The overall size

500 × 500 mm and height 195 mm were selected to fit within the typical lab test equipment while providing sufficient space for instrumentation and a workpiece.

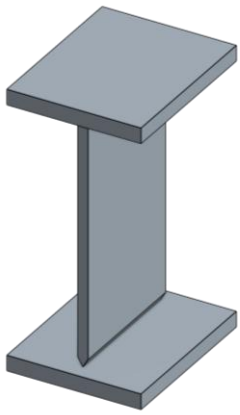

Figure 4.2 CA design of fixture support element

The fixture support element shown in figure 4.2 is a welded I-section assembly, consisting of a vertical web plate joined to two horizontal flange plates. To ensure structural integrity and stiffness under dynamic loading, all three components are fully welded together. The vertical plate features chamfered edges at both ends, specifically designed to facilitate full-penetration welds between the web and flanges. This ensures a strong, uniform connection and prevents weak points at the weld root critical for reliable behaviour under vibration.

Additionally, the horizontal flange plates are welded directly to the fixture's top and bottom plates, creating a continuous structural path from the top plate through the support to the base. This welded interface eliminates any joint slip or bolted compliance, making the connection effectively monolithic. As a result, the support behaves as a rigid, directionally compliant element, allowing bending only in the designed X coordinate direction while remaining stiff in all others.

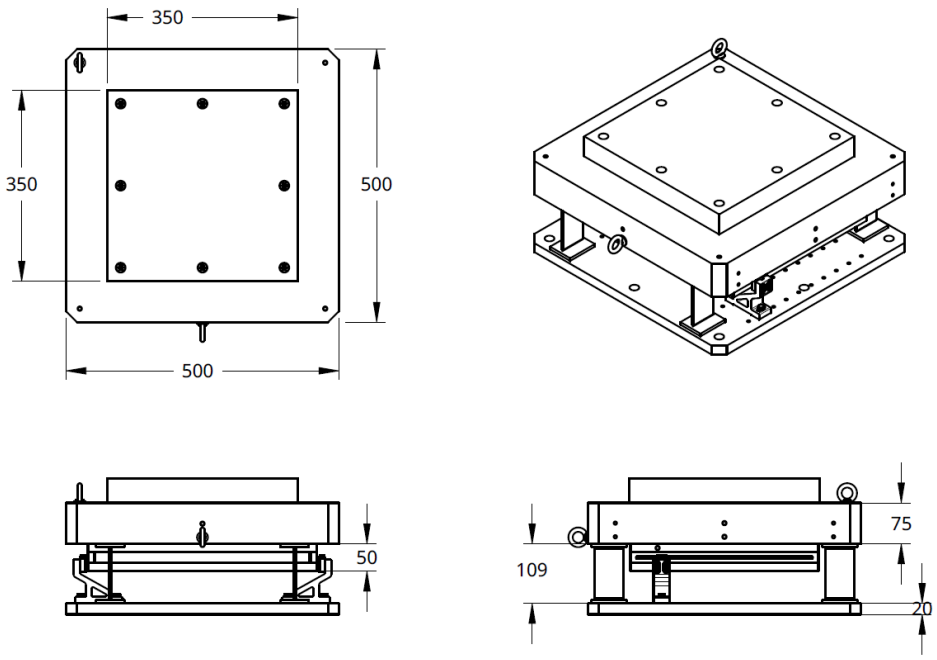


Figure 4.3 Technical drawing of fixture design

The resulting fixture shown in Figure 4.3 consists of a rigid steel base plate and a lighter aluminum top plate, connected at the corners by four welded flexural support elements. Each support is constructed from three welded steel plates forming a vertical I-section column that connects the top and bottom plates. These flexural supports are intentionally thin in the front-back direction perpendicular to the side view shown in the bottom right of the technical drawing which serves as the weak axis, while remaining stiff in the lateral and torsional directions. As a result, the fixture behaves like a platform supported by four compliant struts, allowing easy bending motion in the front-back direction while resisting deformation in all other axes.

The dominant mode of vibration arises from the symmetric bending of all four flexural supports, causing the top to move in simultaneously along the compliant axis, as if mounted on a soft spring foundation. This primary bending mode is deliberately tuned to occur at a low natural frequency (< 30 Hz) with most of the modal mass participating in the front-back translational direction. In contrast, higher-order modes such as lateral bending or torsional twisting require deformation along stiffer structural axes and are consequently pushed to much higher frequencies (typically above 100 Hz), as verified in simulation and experiments.

In effect, the fixture operates as a single-degree-of-freedom spring–mass system within the frequency range of interest. This design mimics the behavior of an industrial robot exhibiting a single flexible bending mode, enabling controlled, repeatable investigation of dynamic stability phenomena such as low-frequency chatter driven by directional compliance.

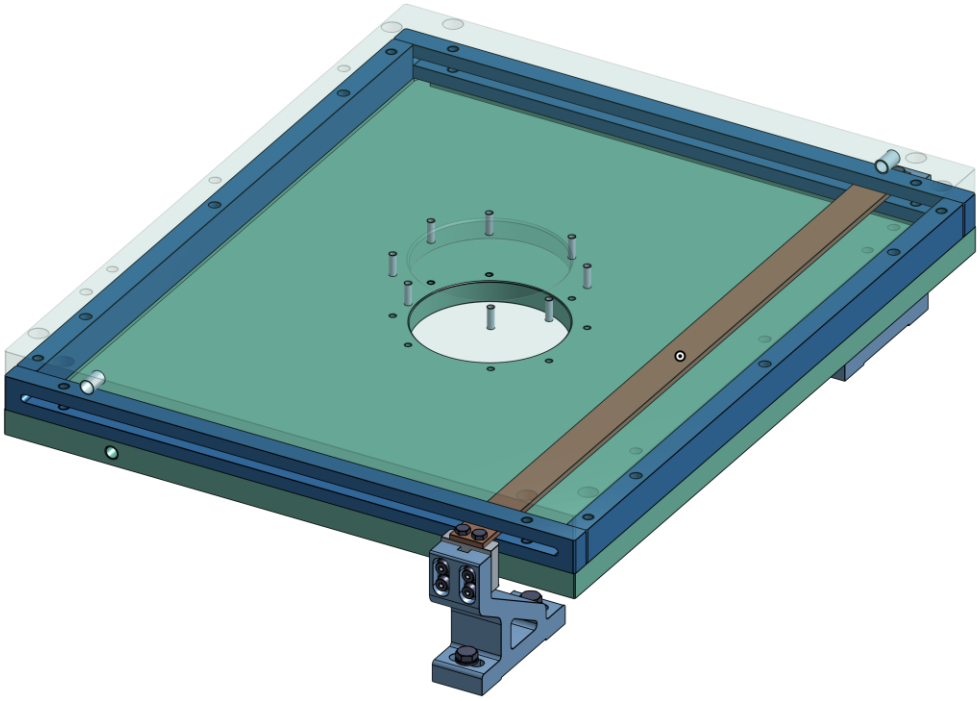

Figure 4.4 The design of eddy current damping system

As can be seen on figure 4.1, practical features were incorporated to enhance the fixture's functionality. The bottom base plate is made of steel (grade S355), chosen for its high stiffness, mass. The upper plate is aluminium (Al7075-T6), which reduces the moving mass and helps maintain the natural frequency within the desired low-frequency range, while also being non-magnetic to facilitate clean magnetic interactions.

To emulate a robot's inherently low damping and to provide a tuneable damping mechanism, in figure 4.4, an eddy-current damping system was integrated into the fixture. A 46 kg neodymium magnet is rigidly mounted to the underside of the aluminium top plate. In the baseline (undamped) configuration, this setup introduces only minimal damping, when there is no conductive copper plate between the magnets.

To enable controlled damping, copper plates can be inserted into the magnetic gap, inducing eddy currents when the top plate vibrates. These plates are held in place by custom-designed 3D-printed holders, which are designed to allow adjustable vertical positioning of the copper sheets. This ensures precise alignment while preventing any physical contact with the magnet, which could otherwise introduce nonlinear behaviour or mechanical interference. The height adjustability also makes it possible to fine-tune the damping effect based on air gap distance, maximizing flexibility without altering the structural design.

Additionally, the top plate includes a standardized mounting interface for test specimens. In this study, a $350 \times 350$ mm aluminium workpiece made of Al7075 is bolted onto the fixture for cutting test The added workpiece mass reduces the resonant amplitude of the frequency response function (FRF) and slightly lowers the natural frequency, without altering the overall mode shape. This configuration allows dynamic testing under cutting loads while preserving the fixture's intended single-mode-dominant behaviour.

## 4.2 Finite Element Modelling and Modal Analysis

A finite element (FE) model of the flexure-based fixture was developed using Siemens Simcenter 3D to analyse its modal behaviour and validate the experimental results presented in the following section. The model was constructed to predict the structure's natural frequencies and mode shapes under idealized boundary conditions. The objective of the simulation was to capture the dominant global modes that govern the dynamic behaviour relevant to low-frequency chatter in robotic milling systems.

The fixture model was composed of the base plate, four welded flexure supports, and the top platform. The geometry was meshed using 8-node linear hexahedral (CHEXA) solid elements with a global element size of 6 mm, as defined in the meshing parameters. Local mesh refinements were applied at the welded joints between the flexures and the plates to improve resolution in high-gradient deformation zones. The final mesh comprised 31,008

elements and 38,642 nodes, offering sufficient spatial resolution for the frequency range of interest as can be seen on figure 4.5. A summary of the mesh configuration is provided in Table 4.1

Table 4.1 Mesh information

| **Mesh Parameter** | **Value** |
|---|---|
| Element Type | CHEXA (8-node) |
| Global Element Size | 6 mm |
| Total Elements | 31,008 |
| Total Nodes | 38,642 |

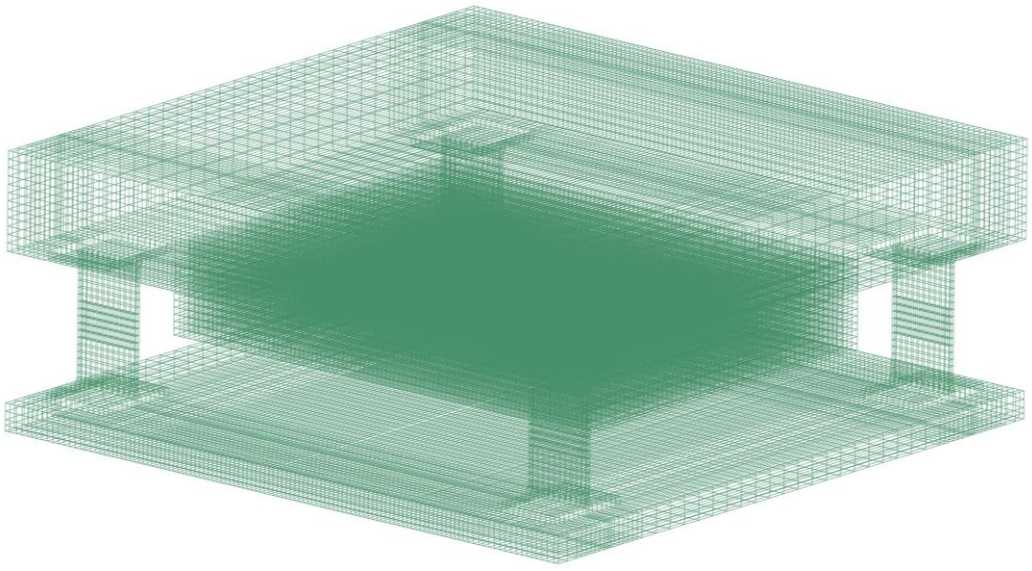

Figure 4.5 Meshed design of the fixture with wireframe view

Material definitions included isotropic steel (S355) for the base and flexures, and Al7075-T6 aluminium for the top plate and material properties can be seen in table 4.2. The material properties were specified as homogeneous and linear elastic, and no damping was included in this undamped modal analysis. Boundary conditions were applied to simulate the real-world bolted configuration by fixing all six degrees of freedom at the bottom face of the steel base plate.

Table 4.2 Material Properties list

| Property | Steel (S355) | Al7075-T6 |
|---|---|---|
| Young's Modulus (GPa) | 210 | 71.7 |
| Density (kg/m³) | 7850 | 2810 |
| Poisson's Ratio | 0.3 | 0.33 |

The modal analysis was executed using the Lanczos solver in Simcenter Nastran, targeting the first six global modes up to 600 Hz. Higher-order modes beyond this range exhibited localized deformation in non-critical regions and were excluded from further evaluation. The extracted modes, depicted in Figures 4.6 through 4.8, provide a clear representation of the fixture's dominant vibrational characteristics.

a) b)

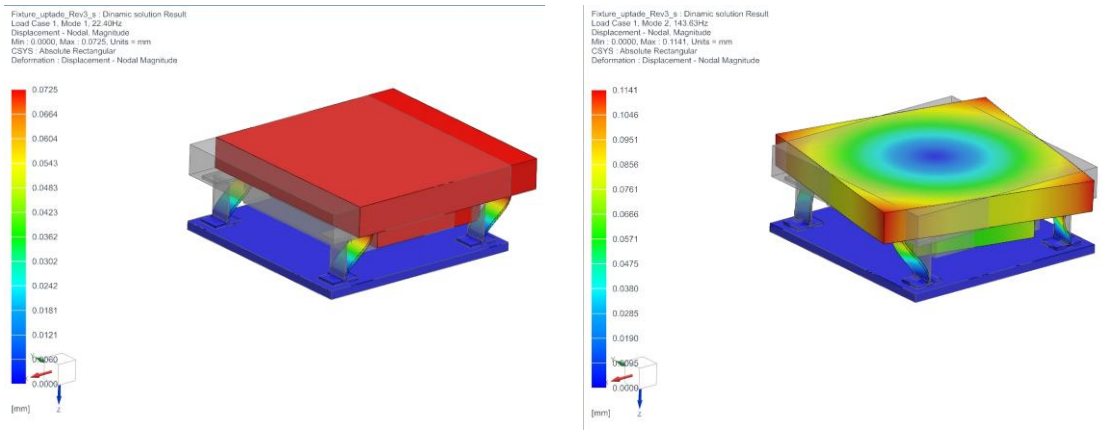


Figure 4.6 FEM mode shapes a) 22.4 Hz mode b) 143.6 Hz mode

The first mode, at 22.4 Hz, primarily shows bending in the X-direction and corresponds to rigid-body-like translational motion of the top plate (Figure 4.6.(a)). This mode dominates the fixture's dynamic compliance and is particularly relevant for chatter susceptibility in robotic milling applications. The second mode, at 143.6 Hz, involves torsional deformation around the Z-axis (Figure 4.6 (b)), while the third mode at 164.8 Hz corresponds to bending in the orthogonal Y-direction (Figure 4.7.(a)). These two modes, though relatively close in frequency, exhibit distinct deformation mechanisms.

a) b)

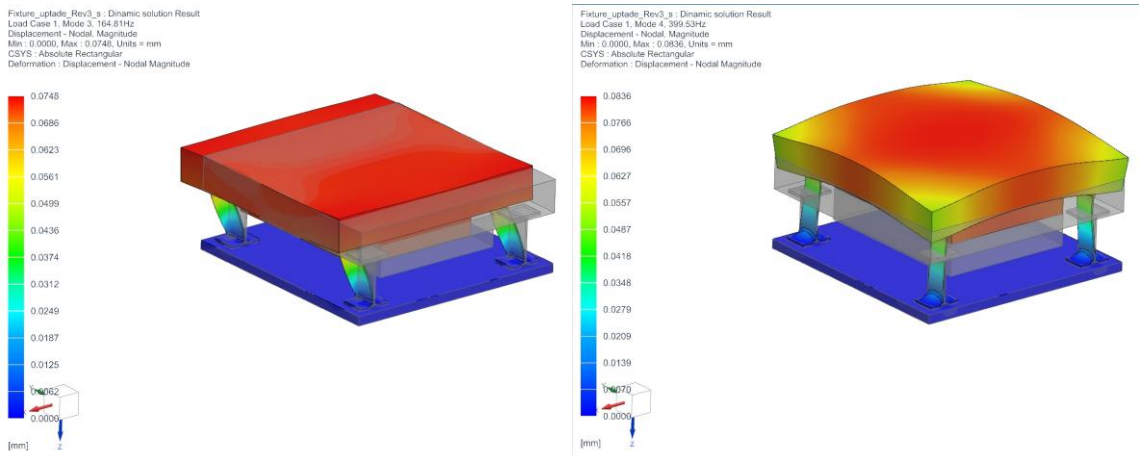


Figure 4.7 FEM mode shapes a) 164.8 Hz mode b) 399.5 Hz mode

The fourth mode, occurring at 399.5 Hz, is characterized by out-of-plane bending along the Z-axis, producing a dome-like deformation of the top plate (Figure 4.8.(b)). The fifth and sixth modes, at 510.1 Hz and 513.7 Hz respectively, display torsional behaviour around the X and Y axes (Figures 4.8.(a) and 4.8.(b)). These higher modes are less dynamically compliant and energetically stiffer, making them less significant for low-frequency vibration scenarios.

a) b)

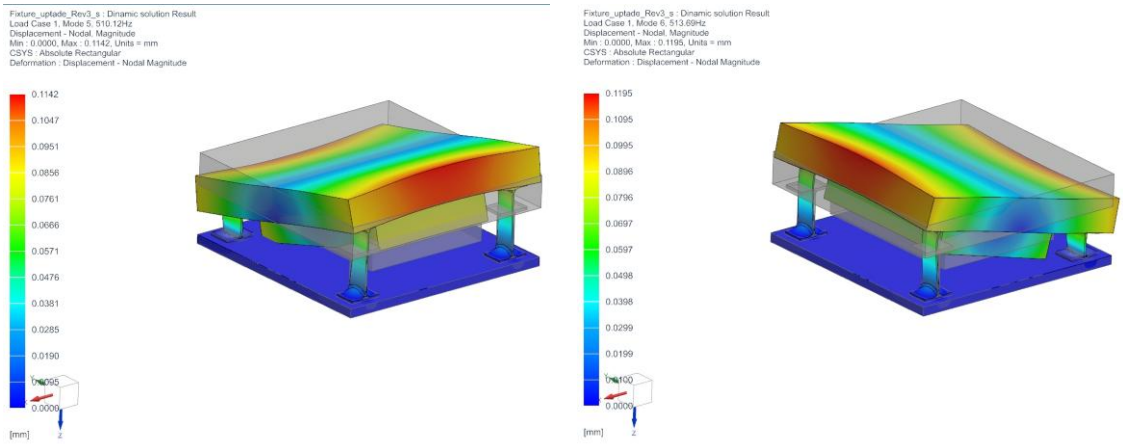


Figure 4.8 FEM mode shapes a) 510.1 Hz mode b) 513.6 Hz mode

Overall, the FE results confirm the fixture is designed to exhibit a clear single-mode dominance at low frequency, fulfilling the design objective for controlled dynamic testing.

The significant frequency separation between the first mode and the subsequent modes supports its applicability in isolating and studying the effect of a single vibration mode in chatter analysis.

## 4.3 Experimental Modal Analysis (EMA) and Modal Assurance Criteria (MAC)

### Experimental Modal Analysis Setup and Methodology

To validate the finite element (FE) predictions of the fixture's dynamics, an experimental modal analysis (EMA) was performed using impact hammer tests. In the EMA, the fixture was excited at a single point with a modal hammer (PCB 086D20), and responses were measured with accelerometer (Dytran 3263A) at multiple points on the structure a single input multi output (SIMO) test configuration. This approach (also known as a roving accelerometer) kept the hammer impact location fixed while moving the accelerometer to different measurement nodes. By always hitting the same location on the fixture as illustrated in Figure 4.9, which marks the impact point, we ensured consistent input excitation for all measurements. The chosen impact location was selected using insight from the FE mode shapes, avoiding nodal positions and targeting an anti-node of the dominant mode. Exciting the structure at a point of large modal displacement helps ensure all important modes are sufficiently excited. The hammer was instrumented with a force transducer, and a lightweight accelerometer was used to record response acceleration at each test point. The selection of measurement points for the experimental modal analysis was guided by the finite element (FE) model. Initially, four corner nodes were selected based on their high modal participation and accessibility. A reduced FE model was solved using only these four nodes, and the extracted mode shapes were compared against the full FE dynamic solution using the Modal Assurance Criterion (MAC). As illustrated in Figure 4.10(a), the MAC matrix shows that even with only four nodes, the main mode shapes can be successfully extracted, achieving high diagonal values. However, the frequency

accuracy for the higher modes (Modes 4–6) was notably poor, indicating limited accuracy in capturing the dynamic content at higher frequencies.

To reduce the frequency difference and shape fidelity, four additional measurement points were added at the midpoints of each side of the top plate, as shown in Figure 4.12(a). The corresponding MAC results demonstrate a clear improvement in both modal correlation and frequency accuracy. A stronger diagonal pattern is observed, and the frequency deviation for the higher-order modes is significantly reduced illustrated in 4.10(b).

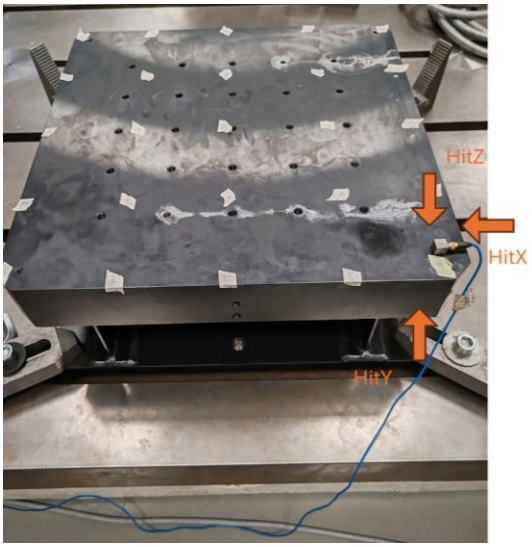


Figure 4.9 Fixture EMA test setup and hammer hit location

a)

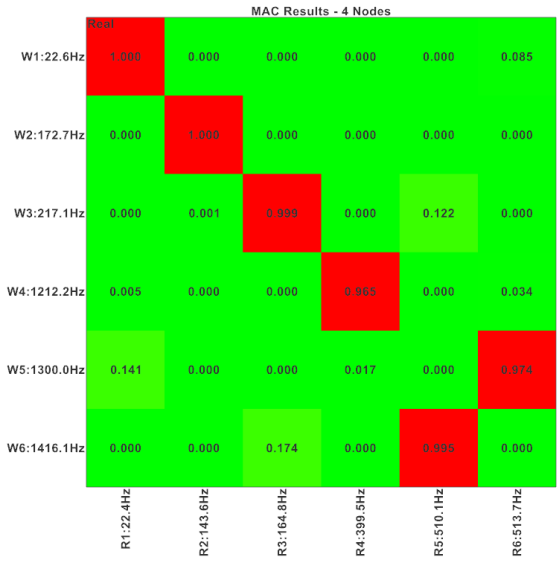


b)

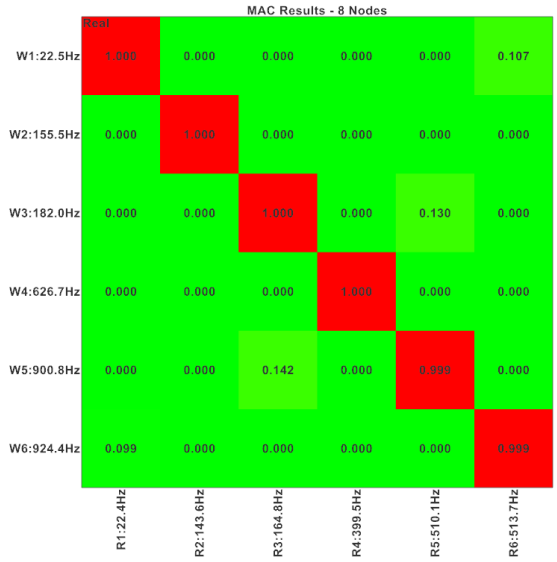

Figure 4.10 MAC correlation between dynamic solution a) 4 nodes b) 8 nodes

Further refinement was achieved by adding four more nodes, resulting in a total of 12 measurement points. The MAC results in Figure 4.11(a) confirm that the dominant mode shapes exhibit excellent correlation, with only slight improvements in frequency matching compared to the 8-node configuration. From this stage, it was evident that 8 nodes are generally sufficient for identifying the principal mode shapes with acceptable accuracy.

However, for enhanced visualization and to further reduce inconsistency in higher-frequency modes, a set of 29 nodes was distributed across the fixture surface (see Figure 4.12(b)). This configuration ensured comprehensive spatial coverage and higher fidelity in shape extraction. The MAC matrix in Figure 4.11(b) confirms near-perfect modal correlation across all modes, with minimal frequency error, thus validating both the experimental measurement strategy and the A total of 29 measurement points, each measured in three translational directions (X, Y, Z), yielded a complete set of 87 frequency response functions (FRFs) used in the analysis.

a)

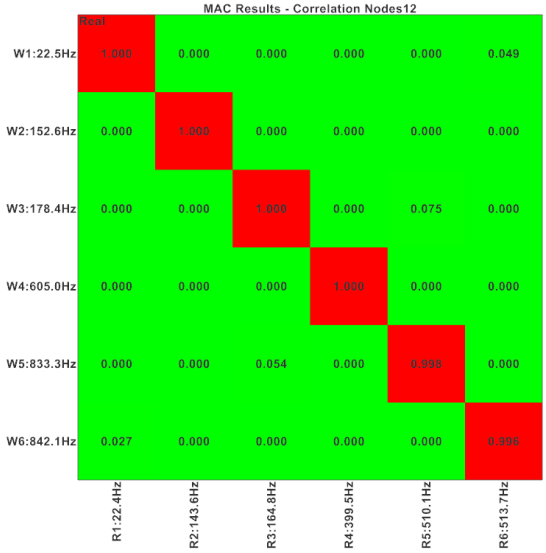


b)


Figure 4.11MAC correlation between dynamic solution a) 12 nodes b) 29 nodes

a) b)

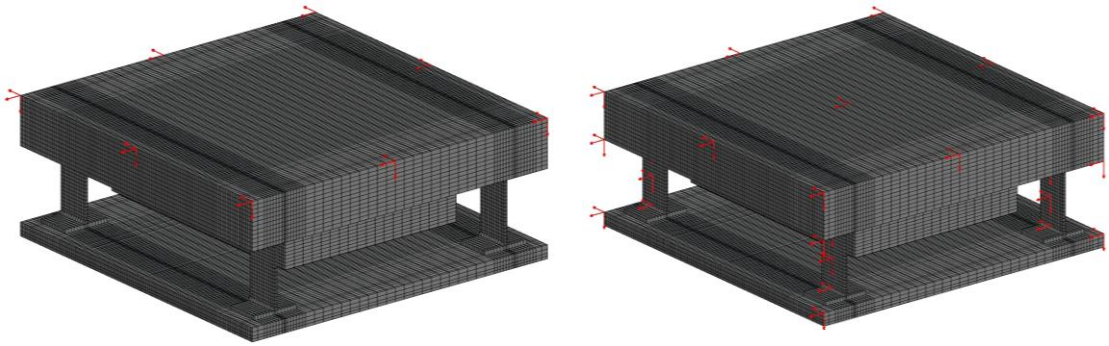

Figure 4.12 FE model and nodes location a) 8 nodes b)29 nodes

During testing, each impact response was sampled and processed to obtain frequency response functions (FRFs). The FRFs were initially measured in the inertance form (acceleration/force, m/s² per N) using the accelerometer signals and were later integrated to the receptance form (displacement/force, μm/N) for ease of modal interpretation. Using displacement-based FRFs (receptance) is common in machining dynamics to directly assess static deflection per unit force. The data acquisition parameters were tuned for the frequency range of interest – since the fixture's first mode was expected around ~20–30 Hz, a frequency range up to a five hundred Hz was analysed with fine resolution of 0.1 Hz to clearly resolve the low-frequency mode. Four impacts were averaged at each location to improve FRF quality, and exponential windowing was applied to the response signals to reduce leakage, as per standard modal testing practice. The measured FRFs showed a clear resonance at roughly 23.8 Hz, corresponding to the fixture's fundamental bending mode. Figure 4.13 shows an example FRF (magnitude of receptance vs. frequency) obtained at one of the measurement points. A sharp peak is evident at 23.8 Hz, indicating a lightly damped first mode with damping ratio of 0.6% and amplitude of the first mode is 2.7 mm/N. Apart from the first mode, only the second mode exhibits a clearly distinguishable peak in the displacement-based frequency response function, indicating significant modal participation within the measured frequency range.

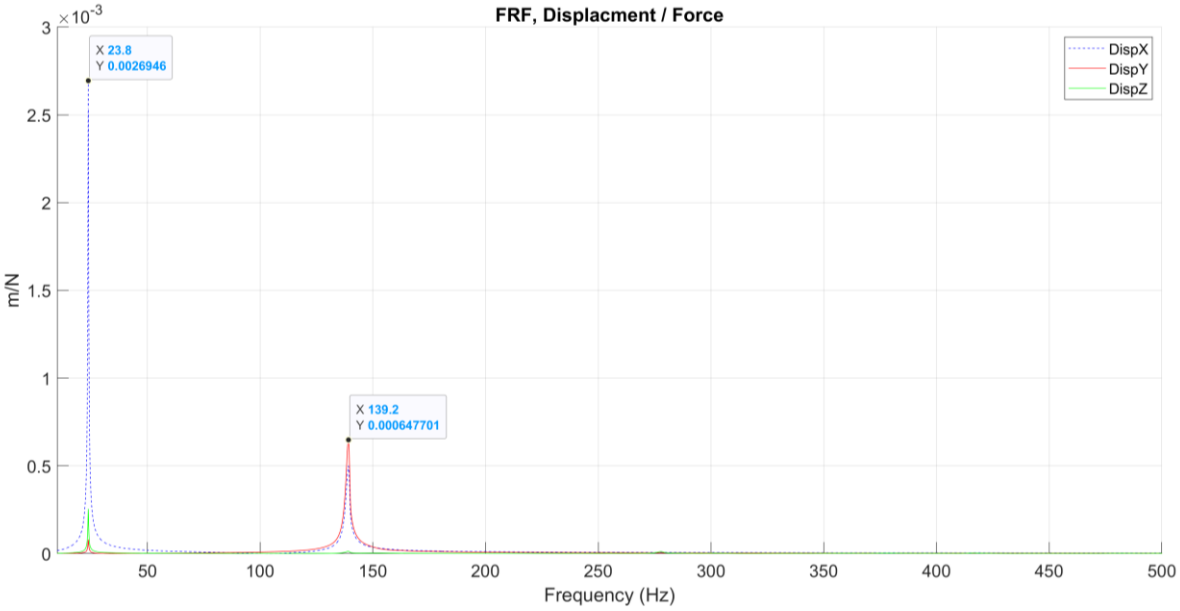

Figure 4.13 FRF measurement of the fixture at point 1

Modal parameter identification was conducted using the multi-degree-of-freedom (MDOF) curve fitting algorithm available in Siemens LMS Test.Lab. This algorithm enables simultaneous estimation of multiple modal parameters from the measured frequency response function (FRF) data, producing a coherent global modal model. The FRFs used in this analysis were obtained from all 29 accelerometer locations, each with three translational degrees of freedom.

As shown in Figure 4.14, the acceleration-over-force ($m/s^2/N$) FRFs from all channels reveal a clear and dominant peak corresponding to the first bending mode. The second mode is also distinctly visible across most FRFs. Higher-order modes, however, exhibit less prominent peaks and require more careful inspection and judgment for accurate identification. To reduce uncertainty, only cross-FRFs measured between different directions were considered for mode identification due to their superior sensitivity to modal contributions.

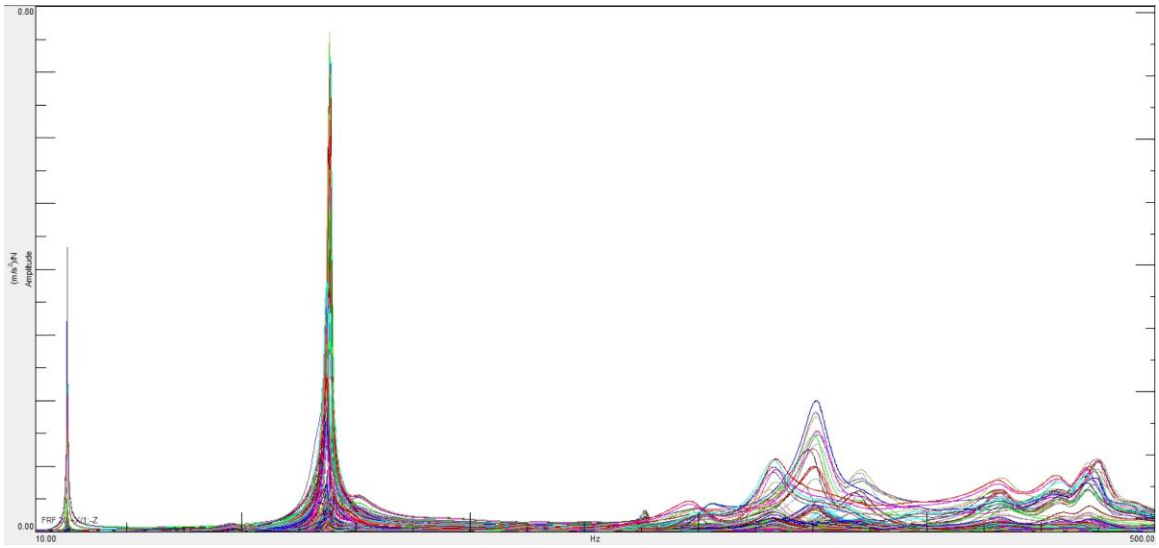

Figure 4.14 FRF of Acceleration/Force ($m/s^2/N$) for all the 87 measurments

Mode identification was supported by Simcenter's automated estimation tools, which provide preliminary mode indicators. However, final determination and validation of the modes remained user-guided and were cross-checked against expected deformation patterns and FE simulation results. Figure 4.15 presents the Simcenter mode location visualization, where estimated mode shapes are plotted across the fixture geometry. The stabilization of poles is marked by different symbols: "o" indicates an unstable pole, "f" denotes frequency stability, "d" represents frequency and damping stability, "v" indicates vector stability, and "s" marks a completely stable pole. Stable streaks of "s" characters identify consistent modal frequencies extracted across model orders.

In total, six distinct modes were identified within the frequency range of interest. These included three bending modes, and three torsional modes associated with the principal structural axes (X, Y, and Z). The experimentally extracted mode shapes were subsequently compared to those predicted by the FE model using the MAC criterion, ensuring the reliability of the identification process and confirming the accuracy of the FE representation.

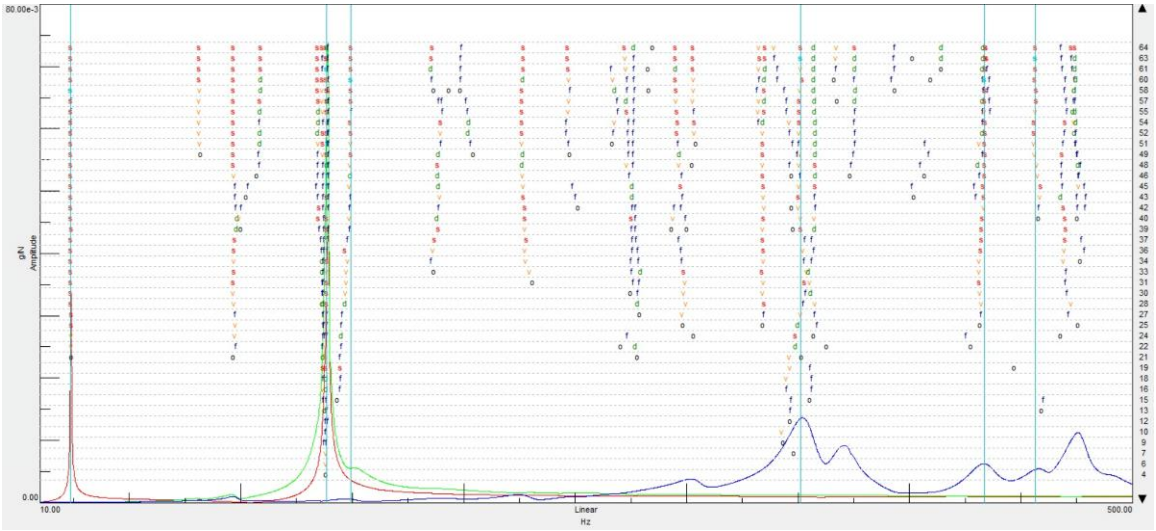

Figure 4.15 Stabilization diagram from experimental modal analysis.

A total of six prominent structural modes were identified through experimental modal analysis using 29 accelerometer locations (three degrees of freedom each), yielding 87 FRFs. These modes were classified based on the observed deformation patterns and dominant direction of motion:

Mode 1: 23 Hz Bending in X-direction this mode corresponds to a rigid-body-like bending motion of the entire top plate along the X-axis. The deformation is symmetric across the Y-axis, and the motion is primarily translational in nature. This mode exhibits the highest displacement amplitude, measured at 4.53 mm/N, and a damping ratio of 0.65%, as listed in Table 4.X. It represents the dominant flexible direction of the fixture, highlighting its primary dynamic compliance [Figure 4.16(a)].

Mode 2: 138 Hz Torsion around Z-axis this mode involves a twisting motion of the top plate around the vertical (Z) axis. Opposing corners of the top plate rotate in opposite directions, producing an antisymmetric shape. The flexural supports exhibit significant rotational compliance in this mode and its amplitude is 2.32 mm/N [Figure 4.16(b)].

a) b)

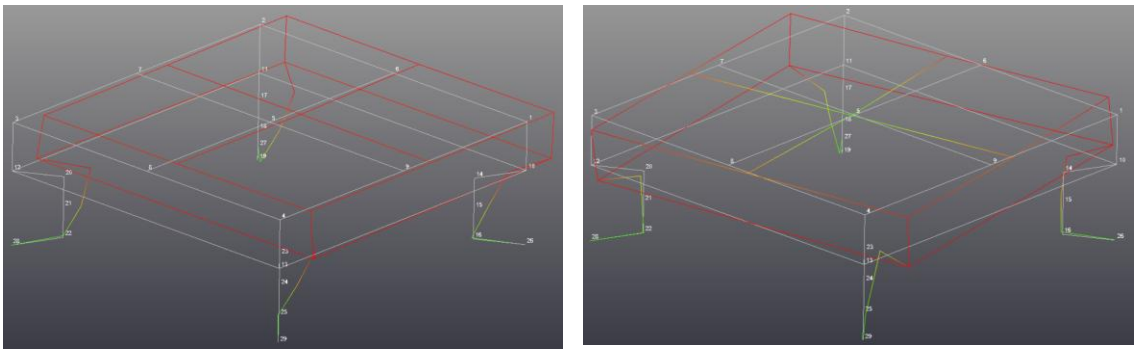

Figure 4.16 EMA mode shapes a) 23.8 Hz b) 138.7 Hz

Mode 3: 149 Hz Bending in Y-direction the third mode is characterized by a bending deformation along the Y-axis. This motion is similar to Mode 1 but oriented orthogonally, indicating lateral flexibility of the fixture in the Y-direction and its amplitude is 1.19 mm/N [Figure 4.17(a)].

Mode 4: 303 Hz Bending in Z-direction a higher-frequency bending mode, characterized by significant out-of-plane deformation. In this mode, the center of the top plate exhibits pronounced vertical displacement while the corners remain relatively stationary, capturing the global Z-axis bending flexibility of the structure. The corresponding modal amplitude reaches a peak displacement magnitude of 0.53 mm/N, indicating the dynamic compliance of the structure at this frequency [Figure 4.17(b)].

a) b)

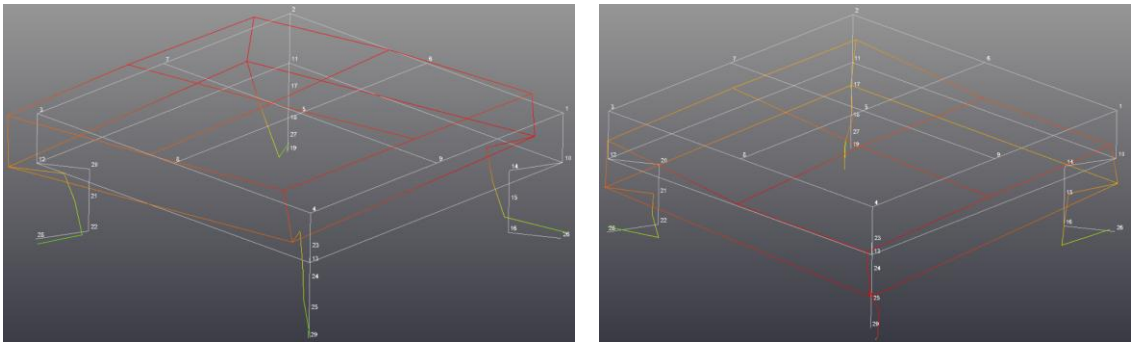

Figure 4.17 EMA mode shapes a) 149.8 Hz b) 304.1 Hz

Mode 5: 351 Hz Torsion around Y-axis This mode exhibits torsional deformation primarily about the Y-axis. Opposite-phase rotational motion is observed at the front and rear edges

of the top plate, indicating that the structure permits twisting along the longitudinal axis due to the compliance of the supporting legs. The peak modal displacement amplitude reaches 1.41 mm/N, reflecting a relatively high dynamic flexibility in torsion around the Y-direction [Figure 4.18(a)].

Mode 6: 457 Hz – Torsion around X-axis in the sixth mode, a twisting deformation occurs about the X-axis, primarily involving rotational motion of the top plate's side edges. The out-of-plane stiffness of the support limits the deformation, resulting in a relatively higher mode frequency and its maximum deformation amplitude is 0.93 mm/N [Figure 4.18(b)].

a) b)

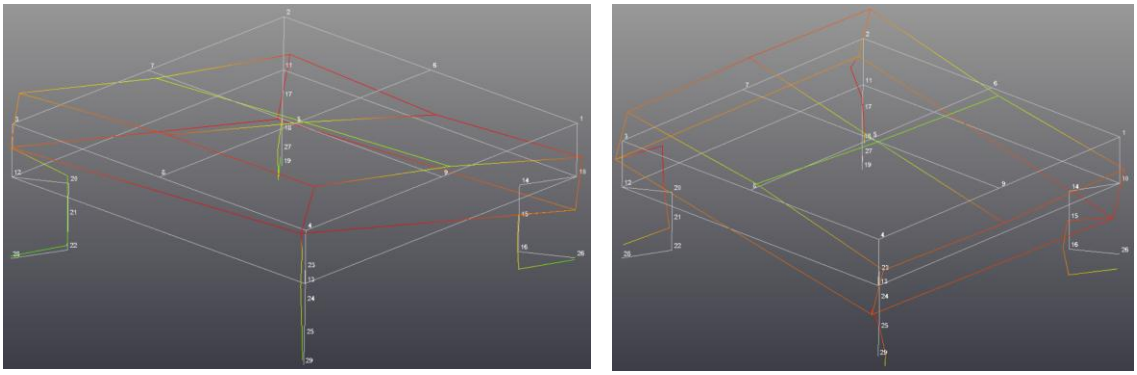

Figure 4.18 EMA mode shapes a) 351.7 Hz b) 457.4 Hz

Table 4.3 Measured natural frequencies, damping ratios and displacement amplitudes

| MODE | FREQUENCY (Hz) | DAMPING (%) | Amplitude |
|---|---|---|---|
| 1 | 23.77 | 0.65 | 4.53 mm/N |
| 2 | 138.68 | 0.26 | 2.32 mm/N |
| 3 | 149.78 | 2.46 | 1.19 mm/N |
| 4 | 303.31 | 0.94 | 0.53 mm/N |
| 5 | 351.77 | 1.68 | 1.41 mm/N |
| 6 | 457.26 | 1.81 | 0.93 mm/N |

**Correlation of Experimental and Numerical Modal Parameters**

The experimentally extracted modal data were imported from Siemens Test.Lab into Simcenter 3D to enable direct correlation with the finite element (FE) model. The EMA geometry (shown in blue) was aligned with the FE geometry (shown in grey) to ensure coordinate consistency illustrated figure 4.19. Subsequently, a Modal Assurance Criterion (MAC) analysis was performed to quantify the similarity between the experimental and numerical mode shapes.

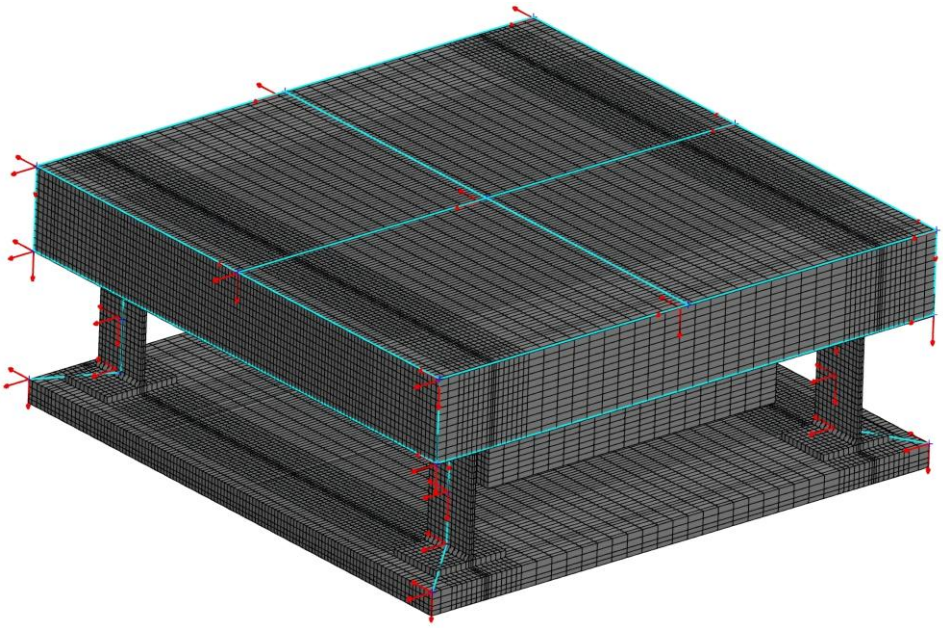

Figure 4.19 FE model and EMA model overlapped

The experimental modal analysis (EMA) confirmed that the fixture behaves as a single-mode dominant system at low frequencies, consistent with its design intent. The first mode is characterized by a rigid-body-like bending of the four vertical supports, resulting in in-phase translational motion of the top plate dominates the sub-100 Hz spectrum as can be seen on figure 4.20. This mode was clearly captured in both the finite element (FE) simulation and experimental measurements, with excellent agreement in shape and a small frequency deviation (22.4 Hz in simulation vs. 23.7 Hz experimentally). This mode is of primary interest, as it mimics the dominant flexible mode typically observed in robotic machining systems.

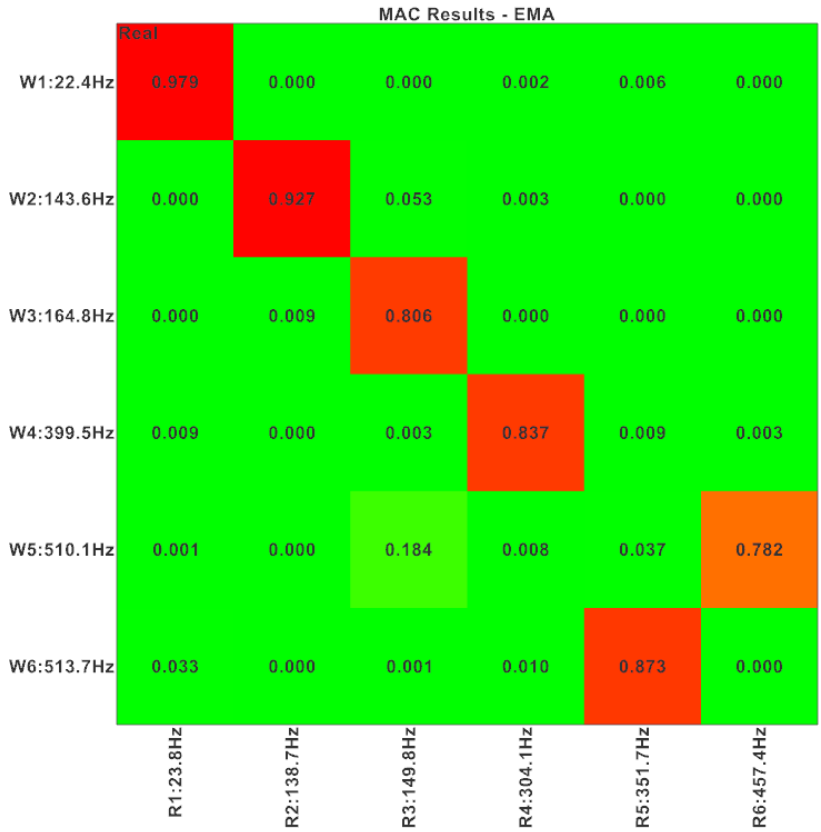


Figure 4.20 MAC correlation between theoretical and experimental modes

Higher-order modes, although less critical for low-frequency chatter phenomena, were also identified with good accuracy. These include torsional and bending modes in the 138–457 Hz range. While some slight discrepancies in natural frequencies were observed between the FE model and the experimental results (in table 4.4), the modal shapes were found to be consistent, with high Modal Assurance Criterion (MAC) values across all identified modes.

Table 4.4 Frequency deviations between theoretical and experimental modes

| Mode | Analytical Frequency (Hz) | Experimental Frequency (Hz) | Deviation (%) |
|---|---|---|---|
| 1 | 22.4 | 23.8 | 5.88 |
| 2 | 143.6 | 138.7 | 3.53 |
| 3 | 164.8 | 149.8 | 10.01 |
| 4 | 399.5 | 304.1 | 23.90 |
| 5 | 513.7 | 351.7 | 31.67 |
| 6 | 510.1 | 457.4 | 10.33 |

The MAC analysis conducted in Simcenter 3D provided a quantitative assessment of the correlation between EMA and FE mode shapes. To facilitate comparison, the EMA model (R) was imported into the FE environment and geometrically aligned with the FE model (W). The MAC matrix revealed strong agreement, with five out of six modes exhibiting MAC values above 0.90 and one mode at 0.78, which is still considered acceptable. The highest correlation was observed for the first bending mode (MAC ≈ 0.98), confirming that both models capture the same deformation pattern. Minor frequency mismatches were attributed to modeling simplifications, such as idealized boundary conditions, material property assumptions, and the omission of joint compliance or preload effects in the FE model.

It is important to highlight that the fifth and sixth modes in the FE model are closely spaced in frequency (approximately 3 Hz apart). This proximity can lead to mode shape mixing during the correlation process, potentially causing off-diagonal MAC values. Nevertheless, the overall MAC analysis confirms the consistency and reliability of the experimental modal extraction relative to the FE predictions.

Overall, the strong MAC values and visually matched mode shapes validate the fidelity of the FE model. The low frequency bending mode, essential for the study of chatter in robotic machining, was verified experimentally and found to be consistent with the design objective.

# 5. LINEARITY ASSESSMENT OF THE FIXTURE

## 5.1. Summary

The experiments conducted in this study aim to validate the hypothesis that negative Mean Directional Factor (MDF) leads to low-frequency chatter in robotic milling, and to demonstrate the effectiveness of slotting operations for chatter-free machining. There for it is important to have a fixture with only one significant mode. One significant mode plays a crucial role in determining the dynamic behavior of the fixture. The dominant mode, typically associated with the fixture's fundamental resonance, dictates the overall stability and vibrational characteristics of the system. Maintaining linearity in this mode is critical, as it ensures predictable and stable performance under varying load conditions. Linearity is essential in fixture dynamics because non-linear behavior can lead to unpredictable resonances, excessive vibrations, and potential structural failures.

## 5.2. Introduction

The study of fixture dynamics is a crucial aspect of machining stability, influencing both precision and efficiency. Since robotic milling has high flexibility and low stiffness, a custom-designed flexure setup was used to simulate robotic machining dynamics in a repeatable and controlled manner. The specially designed fixture has the following specifications:

- The workpiece was mounted on a flexure system designed to replicate low stiffness similar to industrial robots.

- This ensures low-frequency dominant mode behavior, mimicking robotic milling conditions.
- The flexure was designed with thin-walled structures to create dominant bending modes.
- Attached masses were added to control natural frequency and match robotic stiffness characteristics.
- The fixture was engineered to reduce torsional modes, ensuring that only low frequency bending modes influenced chatter.

To be able to satisfy all these aspects vibrationally, designing a single mode dominant fixture is essential.

### 5.2.1. Significance of Single-Mode Dominance in Fixture Dynamics

In many practical machining scenarios, one dominant mode significantly influences the system behavior, particularly at lower frequencies (Iglesias,2016). This is known as single-mode dominance, where a single natural frequency dictates the overall dynamic response of the structure. The effect of this single mode on the stability of machining operations has been extensively discussed in literature, particularly in relation to low-frequency chatter in robotic milling applications (Altintas,2020).

A single-mode dominant system allows for simplified stability analysis since higher-order modes contribute minimally to vibration amplitudes in a desired frequency range. In this study the fixture is designed to have a low frequency bending mode to be the dominant contributor to vibrations. This mode is directly influenced by the structure's stiffness, damping mechanisms, and the presence of a workpiece. The addition of damping elements, such as eddy current dampers, alters this single-mode response by increasing energy dissipation and reducing amplitude magnitudes.

### 5.2.2. Eddy Current Damping and Its Role in Fixture Stability

Damping in fixtures can be achieved through various mechanisms, one of which is eddy current damping (Hahn ,2002). This type of damping is generated when conductive materials are subjected to changing magnetic fields, leading to the induction of circulating currents (eddy currents). These currents generate opposing magnetic fields, which resist motion and dissipate energy as heat. Eddy current damping is widely used in precision

machining applications due to its non-contact nature, minimal wear, and ability to provide consistent energy dissipation across a range of frequencies (Smith ,2018).

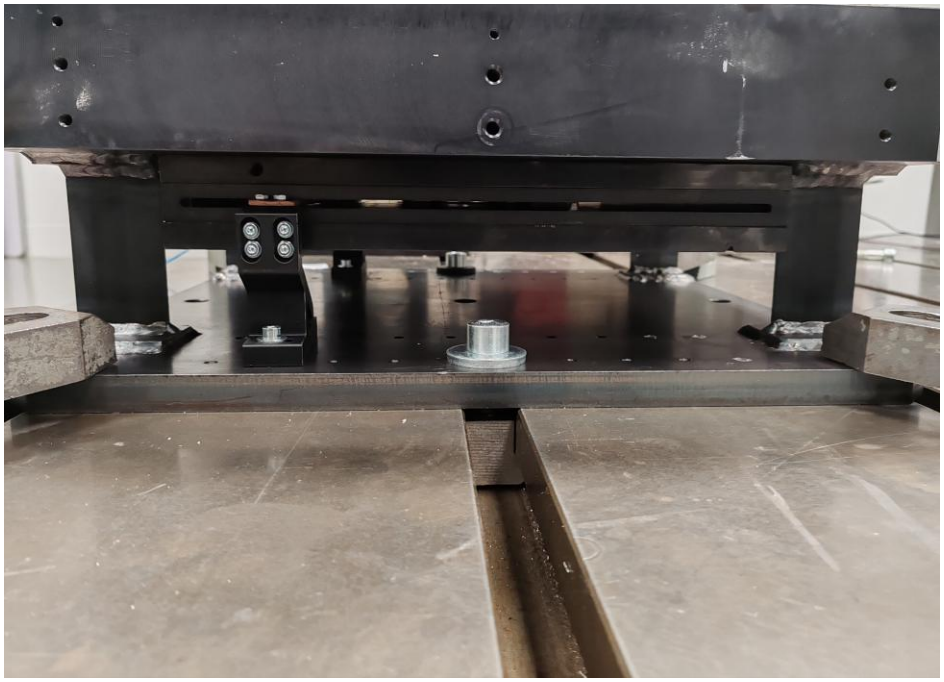

Figure 5.1: Fixture Materials and Magnet for Eddy Current

To be able to use eddy current induced magnetic forces are important. Therefore, the presence of magnetic materials in workpieces and fixtures is necessary. However, it is still possible to use eddy current damping when the workpiece is nonmagnetic. As demonstrated in figure 1, in this study, the lower plate of the fixture is made of steel, and the upper is made of aluminum while there is 40 kg magnet placed between them by assembling the magnet specifically the upper aluminum plate. The workpiece is made of Aluminum Alloy (AL7075-T6).

The primary objective of this chapter is to evaluate the linearity of the fixture system with and without a workpiece while adjusting the damping ratio using an eddy current damper.

To be able to evaluate the linearity, chirp tests are used. A chirp test is a frequency-sweeping technique used in structural dynamics and vibration analysis to evaluate the FRF of a system. In this test, a sinusoidal waveform with continuously varying frequency (chirp signals) is used as an excitation input, allowing to analyze how the system responds across a chosen range of frequencies. In fixture design incorporating eddy current damping, the

most suitable chirp test is the sine-sweep chirp test with a logarithmic frequency variation (logarithmic chirp) which is used in this study due to the following reasons (Iglesias,2022):

- Eddy current damping is proportional to frequency—at higher frequencies, the induced currents increase, leading to greater damping.
- A logarithmic chirp test provides higher resolution at lower frequencies, making it ideal for capturing low-frequency fixture dynamics and the transition of damping behavior as frequency increases.

Logarithmic chirp excitation method is employed to measure the FRF under different damping conditions. The effect of damping on system linearity is assessed by comparing FRFs across a force range of 5 N to 40 N for six different damping configurations:

1. No damping
2. No damping with workpiece
3. One copper slot damping
4. One copper slot damping with workpiece
5. Two copper slots damping
6. Two copper slots damping with workpiece

Additionally, together with chirp excitation, impact hammer tests are recorded to establish a reference for all cases mentioned above. This study aims to determine the impact of damping levels and workpiece mass on linearity, frequency shift, and amplitude response in the fixture design where one significant mode dominates.

## 5.3. Experimental Setup and Methodology

The fixture was designed to exhibit a dominant vibrational mode that requires controlled damping to regulate its dynamic response. Eddy current damping was introduced by positioning conductive copper plates near a fixed magnetic field, allowing for tunable damping ratio.

a) b)

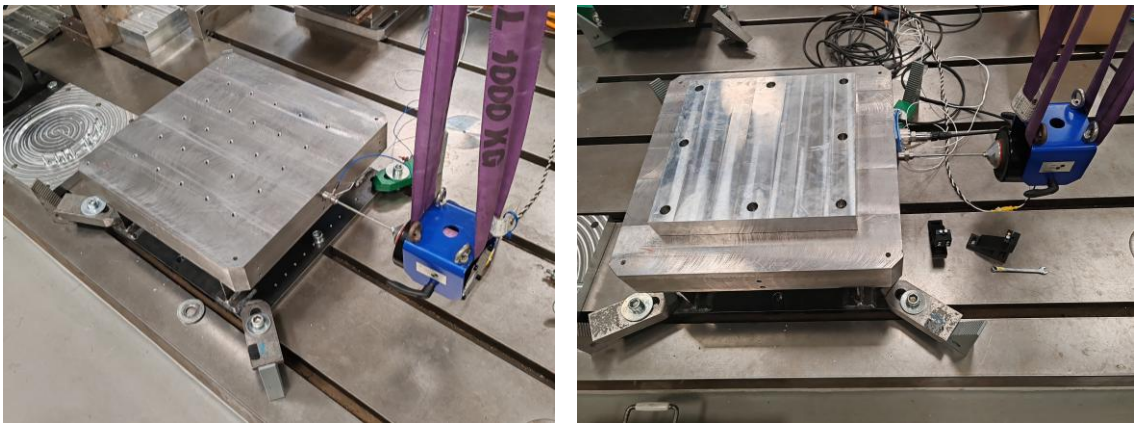

Figure 5.2 Linearity experiment setup

A logarithmic chirp excitation method was used to capture the system's FRF under different damping conditions. As can be seen on figure 2 the experimental setup involved applying controlled excitation forces that range from 5 N to 40 N, while the accelerometer recording the system's response. The damping ratio was tuned by introducing copper modules, which influenced the level of eddy current dissipation. The experiment was conducted under two primary scenarios:

-The first case is without a workpiece: This case is aiming assessing the inherent system response and damping effects.
-The second case is with a workpiece: This case is evaluating how the added mass influences system linearity and damping behavior.
Furthermore, impact hammer test was performed to validate chirp excitation results, ensuring that the frequency shifts and amplitude reductions were consistent.

## 5.4. Results and Discussion

### Case 1: Without Damping

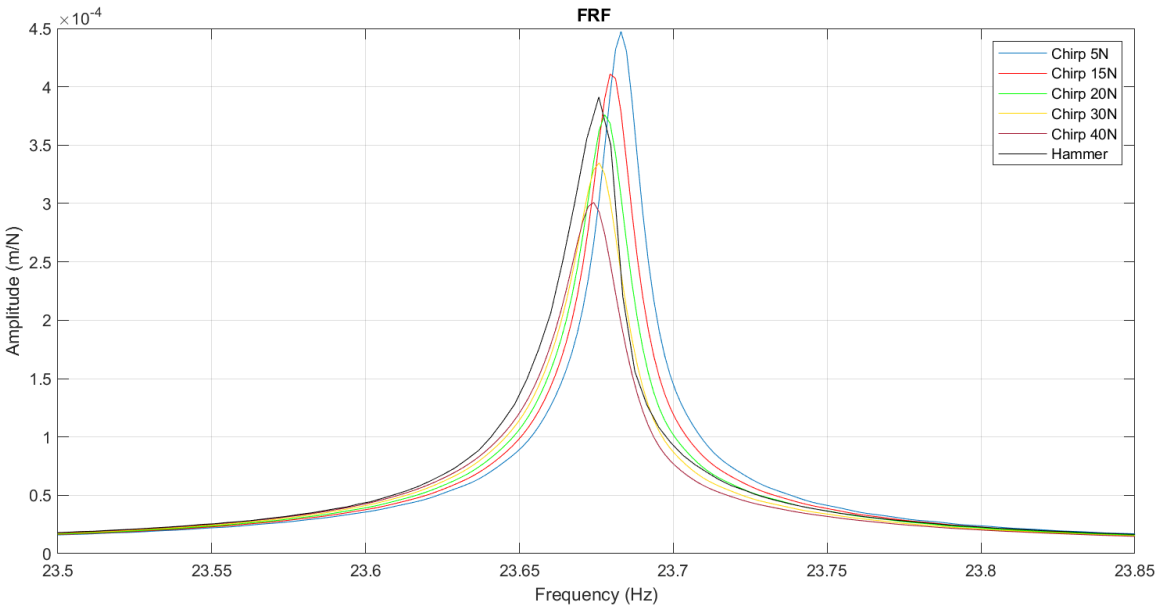


Figure 5.3 FRFs obtained by chirp excitation at different force levels without workpiece without damping

Table 5.1 Resonance frequency, amplitude and damping values without workpiece without damping

| STREGTH | FREQUENCY (Hz) | D/F (μm/N) | DAMPING (%) |
|---|---|---|---|
| Hammer | 23.6758 | 391.27 | 0.0399 |
| 5 N | 23.6830 | 447.38 | 0.0300 |
| 15 N | 23.6794 | 411.03 | 0.0319 |
| 20 N | 23.6777 | 376.08 | 0.0325 |
| 30 N | 23.6759 | 334.88 | 0.0376 |
| 40 N | 23.6741 | 300.89 | 0.0412 |

As can be shown in figure 3, in the absence of damping elements, the FRF results indicate a slight decrease in resonant frequency with increasing force, ranging from 23.68 Hz at 5N to 23.67 Hz at 40N (table 1). This minor shift suggests a softening effect, likely due to microstructural deformations or fixture compliance variations under higher impact forces.

The amplitude is 447.38 μm/N at 5N and shifts to 300.89 μm/N at 40N, indicating a stiffening response where the fixture exhibits reduced compliance at higher force levels. This behavior might be attributed to contact nonlinearity, and boundary constraints, which contribute to increased resistance to deformation.

The damping percentage increases slightly, from 0.03% at 5N to 0.04% at 40N, implying enhanced energy dissipation mechanisms, potentially due to internal friction and micro-slip at contact interfaces. Despite this increase, the overall damping remains low, indicating the fixture's limited inherent capacity for vibration attenuation.

In summary, as applied force increases, resonant frequency slightly decreases, FRF amplitude reduces, and damping marginally increases, suggesting a predominantly linear system with minor nonlinear softening effects. Given its low damping characteristics, the fixture remains prone to sustained oscillations, highlighting the necessity for additional damping mechanisms in robotic machining applications.

### Case 2: Without Damping with Workpiece

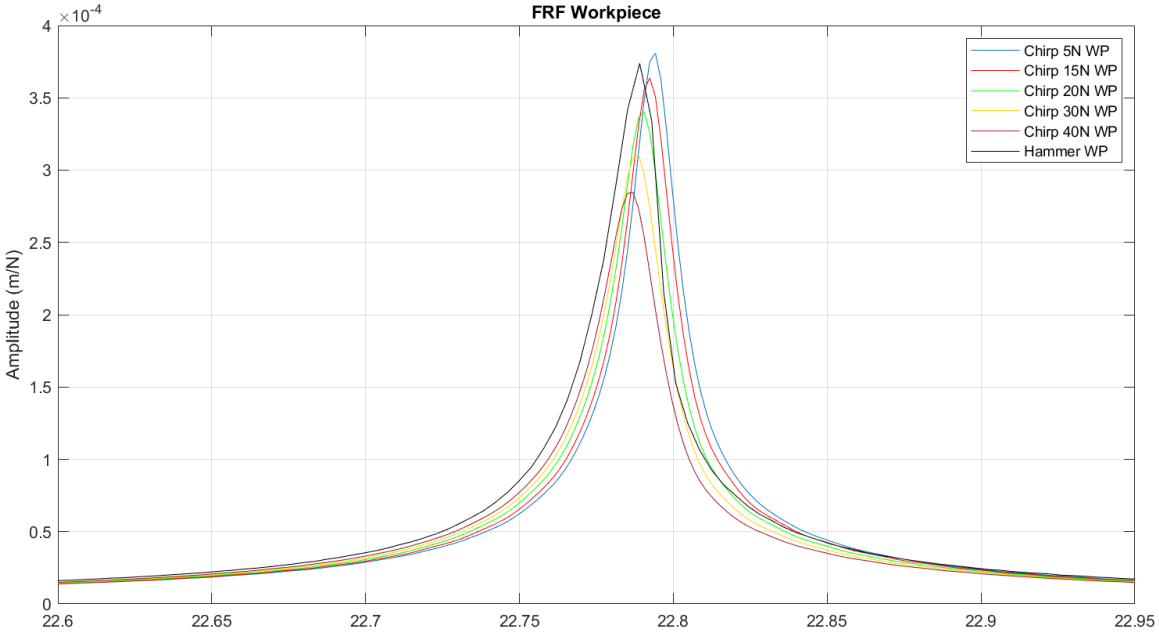


Figure 5.4 FRFs obtained by chirp excitation at different force levels with workpiece without damping

Table 5.2 Resonance frequency, amplitude and damping values with workpiece without damping

| STREGTH | FREQUENCY (Hz) | D/F (μm/N) | DAMPING (%) |
|---|---|---|---|
| Hammer | 22.7891 | 373.84 | 0.0388 |
| 5 N | 22.7942 | 380.82 | 0.0318 |
| 15 N | 22.7923 | 363.81 | 0.0331 |
| 20 N | 22.7905 | 340.18 | 0.0360 |
| 30 N | 22.7887 | 310.57 | 0.0369 |
| 40 N | 22.7869 | 284.59 | 0.0402 |

Introducing a workpiece into the fixture modifies the system's dynamic response by increasing its effective mass and altering its stiffness distribution (figure 4). The FRF results for this case indicate a very slight reduction in resonant frequency, ranging from 22.794 Hz at 5N to 22.786 Hz at 40N, which is slightly lower than in the undamped case without a workpiece. This frequency shift is attributed to the slight increased mass of the system, which reduces the overall stiffness-to-mass ratio, leading to lower vibrational frequencies.

The amplitude values also decrease, with a maximum of 380.82 µm/N at 5N and a minimum of 284.59 µm/N at 40N, both resulting lower values than those recorded in the first case (table 2). This reduction suggests that the workpiece enhances fixture stiffness, reducing structural compliance and limiting vibratory displacement. Additionally, the fixture-workpiece contact interface introduces constraints, further restricting system flexibility.

The damping exhibits a slight increase, ranging from 0.032% at 5N to 0.0402% at 40N, nearly same with the previous case. In summary, the introduction of a workpiece lowers the system's natural frequency. The following section examines the effect of damping slots in further modifying fixture dynamics.

**Case 3: One Copper Slot Damping**

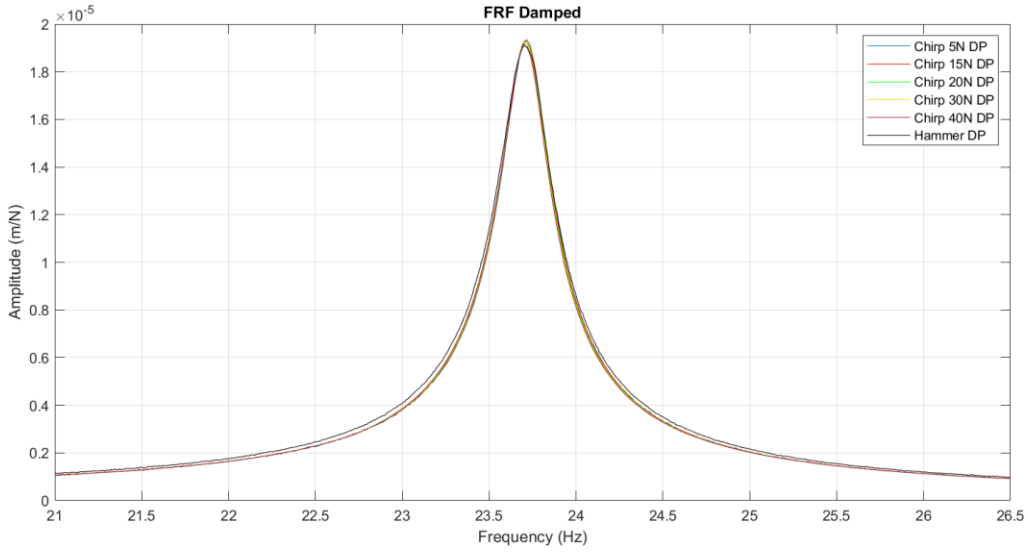

Figure 5.5 FRFs obtained by chirp excitation at different force levels without workpiece with damping

Table 5.3 Resonance frequency, amplitude and damping values without workpiece with one slot damping

| STREGTH | FREQUENCY (Hz) | D/F (μm/N) | DAMPING (%) |
|---|---|---|---|
| Hammer | 23.7031 | 19.14 | 0.6592 |
| 5 N | 23.7119 | 19.28 | 0.6086 |
| 15 N | 23.7145 | 19.34 | 0.6087 |
| 20 N | 23.7093 | 19.24 | 0.6088 |
| 30 N | 23.7067 | 19.17 | 0.6089 |
| 40 N | 23.7042 | 19.08 | 0.6142 |

Introducing one copper slot damping alters the fixture's dynamic response by enhancing energy dissipation and modifying local stiffness distribution. The FRF results indicate that the dominant frequency remains relatively stable, ranging from 23.7119 Hz at 5N to 23.7042 Hz at 40N, suggesting that the copper slot primarily influences damping rather than mass-induced frequency shifts.

The amplitude exhibits a significant reduction, with values ranging from 19.28 μm/N at 5N to 19.08 μm/N at 40N, demonstrating a significant decrease in the amplitude compared to the undamped cases. This reduction suggests that the copper slot increases localized stiffness and suppresses dynamic displacement, likely due to its ability to introduce eddy current damping effects, which dissipate vibratory energy more efficiently.

The damping percentage shows a prominent increase, reaching 0.659 % at the hammer impact and maintaining values above 0.607% across all force levels. This substantial enhancement confirms that the copper slot serves as an effective damping mechanism, significantly improving the fixture's ability to attenuate oscillations by converting mechanical energy into heat through induced electrical currents. The next section examines the combined effect of the copper slot and workpiece, further evaluating its influence on fixture dynamics.

**Case 4: One Copper Slot Damping with Workpiece**

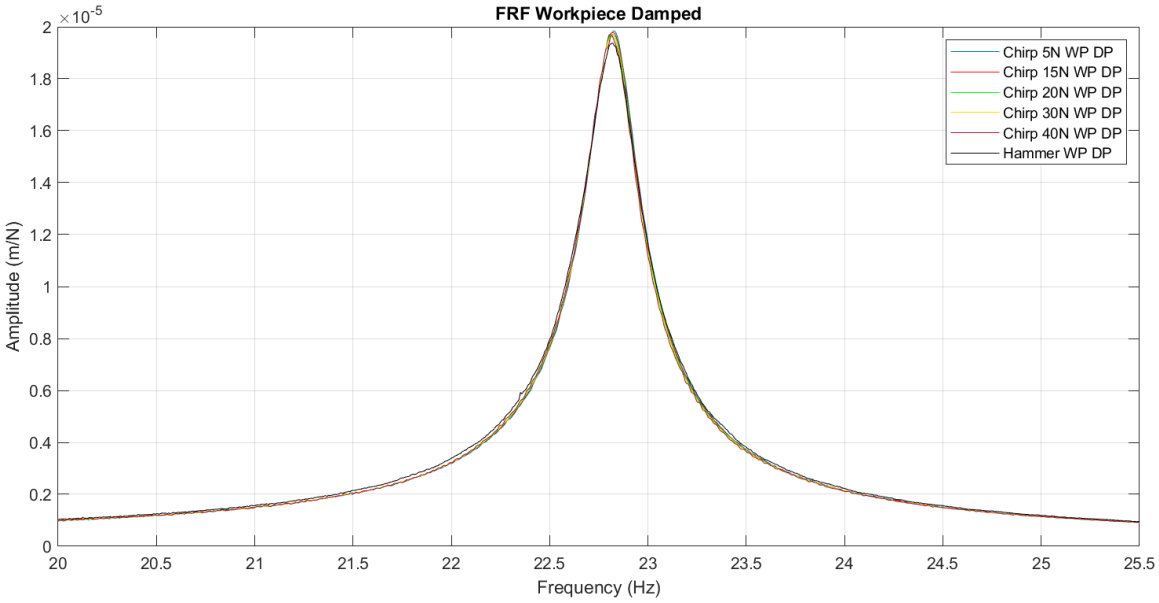


Figure 5.6 FRFs obtained by chirp excitation at different force levels with workpiece with damping

Table 5.4 Resonance frequency, amplitude and damping values with workpiece with one slot damping

| STREGTH | FREQUENCY (Hz) | D/F (μm/N) | DAMPING (%) |
|---|---|---|---|
| Hammer | 22.8203 | 19.37 | 0.6345 |
| 5 N | 22.8279 | 19.85 | 0.5927 |
| 15 N | 22.8201 | 19.78 | 0.5931 |
| 20 N | 22.8175 | 19.71 | 0.5932 |
| 30 N | 22.8175 | 19.62 | 0.5987 |
| 40 N | 22.8150 | 19.67 | 0.5987 |

The inclusion of a workpiece alongside one copper slot damping further modifies the fixture's dynamic response by increasing mass, enhancing stiffness, and improving energy dissipation mechanisms as can be seen in figure 6. The resonant frequency exhibits a slight reduction, ranging from 22.83 Hz at 5N to 22.81 Hz at 40N, reflecting the influence of the increased effective mass, which lowers the system's natural frequency.

The amplitude ratio decreases further, with values from 19.85 μm/N at 5N to 19.67 μm/N at 40N. The damping percentage increases, reaching 0.635% under hammer impact and exceeding 0.593% across all force levels (table 4). This suggests that the combined effect of the workpiece and copper slot enhances energy dissipation, likely through frictional

damping at the contact interface and eddy current effects within the copper slot. The next section examines the influence of an additional copper damping slot on fixture dynamics.

### Case 5: Two Copper Slot Damping

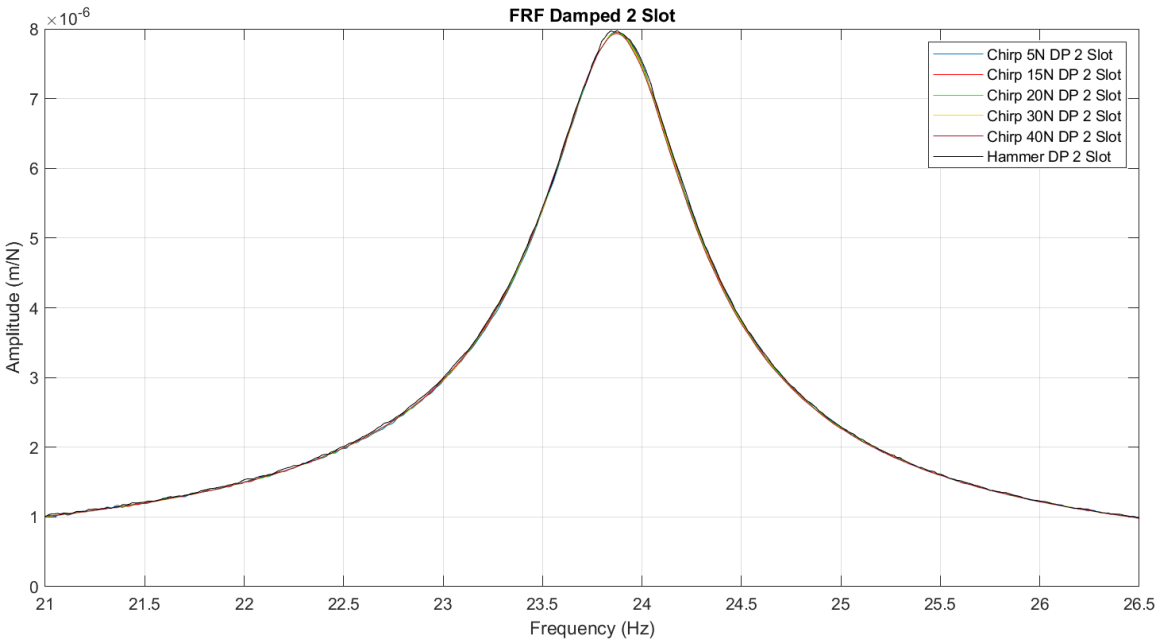


Figure 5.7 FRF obtained by chirp excitation at different force levels without workpiece with 2 slot damping

Table 5.5 Resonance frequency, amplitude and damping values without workpiece with two slot damping

| STREGTH | FREQUENCY (Hz) | D/F (μm/N) | DAMPING (%) |
|---|---|---|---|
| Hammer | 23.875 | 7.98 | 1.4400 |
| 5 N | 23.8651 | 7.95 | 1.4794 |
| 15 N | 23.8738 | 7.95 | 1.4709 |
| 20 N | 23.8738 | 7.94 | 1.4790 |
| 30 N | 23.8694 | 7.94 | 1.4791 |
| 40 N | 23.8694 | 7.93 | 1.4793 |

The introduction of a second copper damping slot further modifies the fixture's dynamic characteristics by enhancing energy dissipation and increasing localized stiffness variations. The resonant frequency remains stable, ranging from 23.8651 Hz at 5N to 23.8694 Hz at 40N. A notable observation is the increase in FRF magnitude compared to the single copper slot damping case. The amplitude exhibits a significant reduction, with values ranging from 7.95 μm/N at 5N to 7.93 μm/N at 40N, which is considerably lower

than in the one-slot damping configuration (19.28 µm/N at 5N to 19.08 µm/N at 40N). This substantial reduction in amplitude confirms that the addition of a second copper slot further enhances fixture stiffness and restricts dynamic displacement, likely due to a cumulative eddy current damping effect, which more efficiently dissipates vibratory energy.

The damping percentage experiences an increase, reaching 1.44% under hammer impact and exceeding 1.48% at 40N, representing an improvement over the one-slot configuration. This increase can be attributed to the combined effects of material damping, contact interactions, and intensified eddy current dissipation, which collectively contribute to enhanced vibration suppression.

In summary, multiple damping slots primarily influence energy dissipation rather than altering mass-stiffness characteristics, further improving the fixture's ability to suppress vibrations. The next section investigates the influence of combining this configuration with a workpiece to assess additional modifications in fixture dynamics.

### Case 6: Two Copper Slot Damping with Workpiece

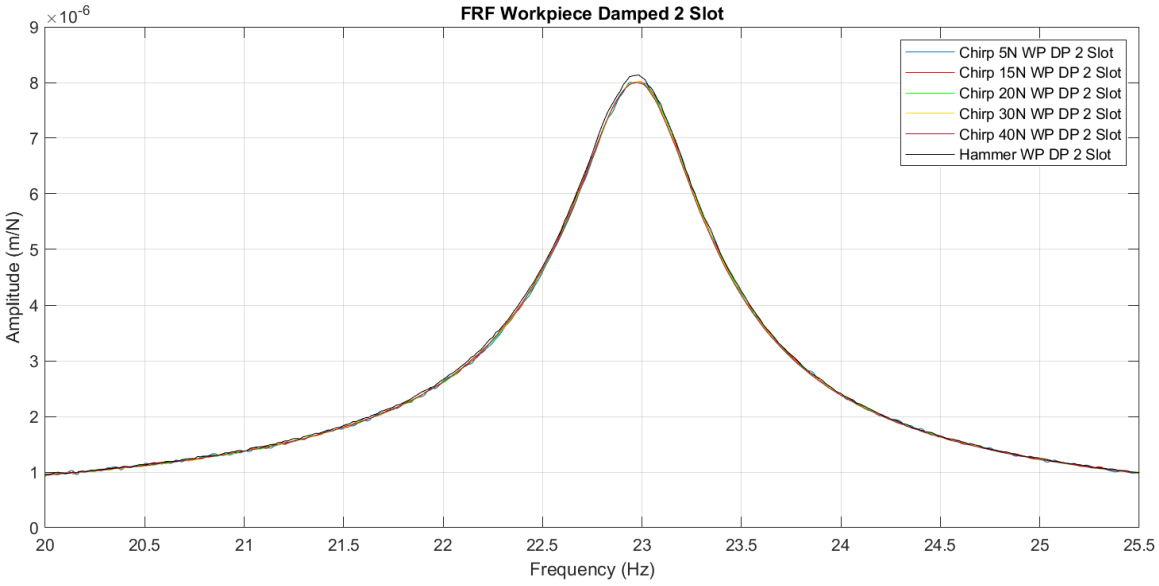


Figure 5.8 FRFs obtained by chirp excitation at different force levels with workpiece with 2 slot damping

Table 5.6 Resonance frequency, amplitude and damping values without workpiece with two slot damping

| STREGTH | FREQUENCY (Hz) | D/F (µm/N) | DAMPING (%) |
|---|---|---|---|
| Hammer | 22.9844 | 8.13 | 1.4399 |

| | | | |
|---|---|---|---|
| 5 N | 22.9834 | 8.01 | 1.4504 |
| 15 N | 22.9878 | 8.02 | 1.4693 |
| 20 N | 22.979 | 8.01 | 1.4696 |
| 30 N | 22.979 | 8.01 | 1.4698 |
| 40 N | 22.9702 | 8.00 | 1.4704 |

The integration of two copper slot damping with a workpiece further modifies the fixture's dynamic behavior. The resonant frequency exhibits a minor reduction, ranging from 22.98 Hz at 5N to 22.97 Hz at 40N, indicating that the increased effective mass of the workpiece further lowers the natural frequency while maintaining structural stability.

A significant observation is the continued decrease in the amplitude, with values ranging from 8.01 μm/N at 5N to 8.00 μm/N at 40N, reinforcing the trend observed in previous configurations. Moreover, the presence of the workpiece increases contact-induced frictional damping, which complements the eddy current effects of the copper slots, leading to improved attenuation of vibratory energy. The damping percentage demonstrates a further increase, reaching 1.44% under hammer impact and exceeding 1.47% at 40N.

In summary, the combination of two copper slot damping with a workpiece result in the most substantial FRF suppression and damping enhancement observed across all test conditions. These findings highlight the potential of integrating engineered damping solutions with mass-induced effects for optimizing machining stability.

This chapter explores the linear characteristics of a custom-designed fixture for robotic milling applications, focusing on the role of eddy current damping in enhancing dynamic stability. The experimental results confirm the critical importance of achieving single-mode dominance in fixture design, especially in low-frequency ranges relevant to robotic machining. Across all test conditions, varying damping configurations and the presence or absence of a workpiece, the fixture maintained primarily linear behavior, with minor nonlinearities observed at higher excitation forces.

# 6. VALIDATION WITH FIXTURE AND INDUSTRIAL ROBOT

## 6.1 Validation with Fixture

### 6.1.1 Flexure Experimental Setup

Because of the inherently variable and posture-dependent dynamics of robotic systems, validating stability models for robotic milling presents a significant challenge. To better understand the chatter phenomenon in this context, the polar stability plots shown in Section 3 were experimentally validated using a custom-designed flexure mounted on a machining center. The development of this flexure structure was explained in Section 4. This flexure featured a single dominant low-frequency mode, enabling consistent and controlled testing conditions.

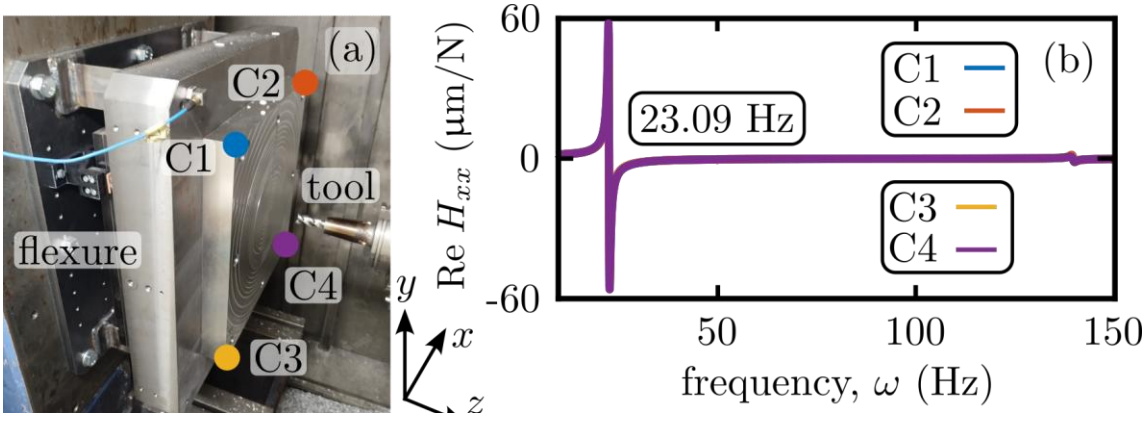


Figure 6.1 (a) Flexure with low frequency dominant bending mode. Receptance measurements (b) in the four corners of the workpiece.

To emulate the low structural rigidity characteristic of robotic systems, a custom-designed flexure structure (500 × 500 mm) was developed. This setup featured thin-walled welded

joints and an attached large mass to ensure a single dominant bending mode (Fig. 6.1(a)), creating a simplified system ideal for consistent and repeatable experimental validation.

The flexure was engineered to maintain uniform dynamic behavior throughout a 350 × 350 mm working area, as verified by impact (tap) tests at all four corners (Fig. 6.1(b)). While a secondary torsional mode was detected at 140 Hz, its considerably lower flexibility made its contribution to overall system stability negligible.

Although the flexure's dominant natural frequency is higher than that typically found in industrial robots (see Table 6.1), its dynamic stiffness $k_{d1}$ remains an order of magnitude lower, mainly due to its very low damping ratio. Notably, even compact milling machines offer far superior dynamic performance compared to robotic systems, highlighting the challenges of achieving chatter-free robotic milling.

Table 6.1Comparison of dynamic parameters of dominant modes between flexure, robot, and machining center.

| | **Flexure** | **Robot** | **Machine** |
|---|---|---|---|
| **Reference** | - | KUKA KR300 R2700 | DS630 |
| $\omega_{n,1}$ **(Hz)** | 23.09 | 10.7- | 69.6 |
| $\zeta_1$ **(%)** | 0.097 | 1.26 | 3.1 |
| $k_{d,1}$ **(N/µm)** | 0.0085 | 0.028 | 2.56 |

### 6.1.2 Milling Tests

To validate the theoretical polar stability structure illustrated in Section 3, circular and linear milling tests were conducted. The material AL7075-T6 was selected for its good machinability and consistent behavior under cutting conditions. A solid carbide end mill with three flutes (Z = 3), a diameter of 16 mm, and a 45° helix angle was used for all tests.

Cutting experiments were performed at five different spindle speeds: 2500, 5000, 7500, 10,000, and 12,000 rpm. These conditions yielded high tooth-passing frequency to natural frequency ratios of approximately 5.4, 10.8, 16.2, 21.6, and 26, respectively representing regimes where regenerative chatter is most likely to occur.

The cutting force coefficients required for the stability analysis were identified using the methodology outlined in (Altintas,1992). The resulting values were:

- Tangential cutting coefficient $K_{tc}$=774 MPa
- Relative radial coefficient $k_{rc}$=0.22

To directly validate the theoretical polar stability predictions (Fig.6.2(a–b)), a continuous variation of the feed direction θ was implemented through circular milling tests. This method allows for a comprehensive comparison between the theoretical stability map and the cutting response from a single tool pass, providing a holistic view of stability behavior across a full range of feed directions.

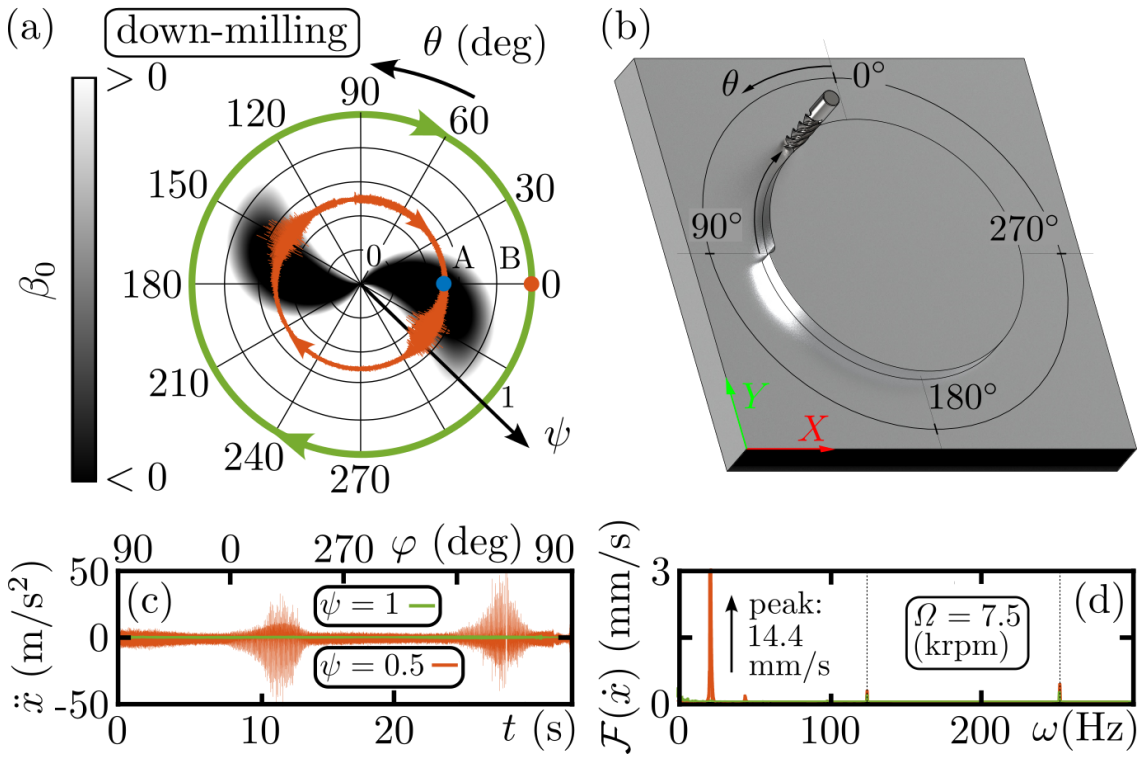


Figure 6.2 Validation of circular test at 10000 rpm: In (a) and (b) circular cutting tests with ψ = 0.5 DM and a= 0.4 (red path) and ψ = 1 and a=11mm (green path) are presented with overlayed circular vibration signals. (c) X direction vibration of the previous circular tests. (d) shows the frequency content of (c).

However, this approach also presents certain limitations, including a potential phase lag in the stability domains as reported in (Baer ,1998), as well as difficulties in detecting the onset of chatter in real time. To ensure effective testing while minimizing dynamic complications, a low feed per tooth of fz=0.1 mm/tooth was chosen.

In addition to the circular tests**,** straight-line cutting experiments were performed at selected feed directions and radial engagements. These tests targeted specific points (labeled A and B in Fig.6.3) on the polar plots, allowing for discrete validation of the predicted stability regions.

The experimental results confirmed the theoretical predictions, clearly demonstrating the onset of low-frequency chatter in feed directions corresponding to negative Minimum Directional Factors (MDFs) as indicated by the polar stability plots (Fig. 6.3).

The straight-line cutting tests showed strong alignment with the asymptotic predictions of the analytical model and revealed a pronounced dependency on spindle speed. Remarkably, chatter was observed even at a shallow axial depth of cut of just 0.4 mm, under conditions where the tooth-passing frequency exceeded 26 times the natural frequency of the flexure system (Fig. 6.3), highlighting the significance of regenerative effects even in high-speed cutting regimes.

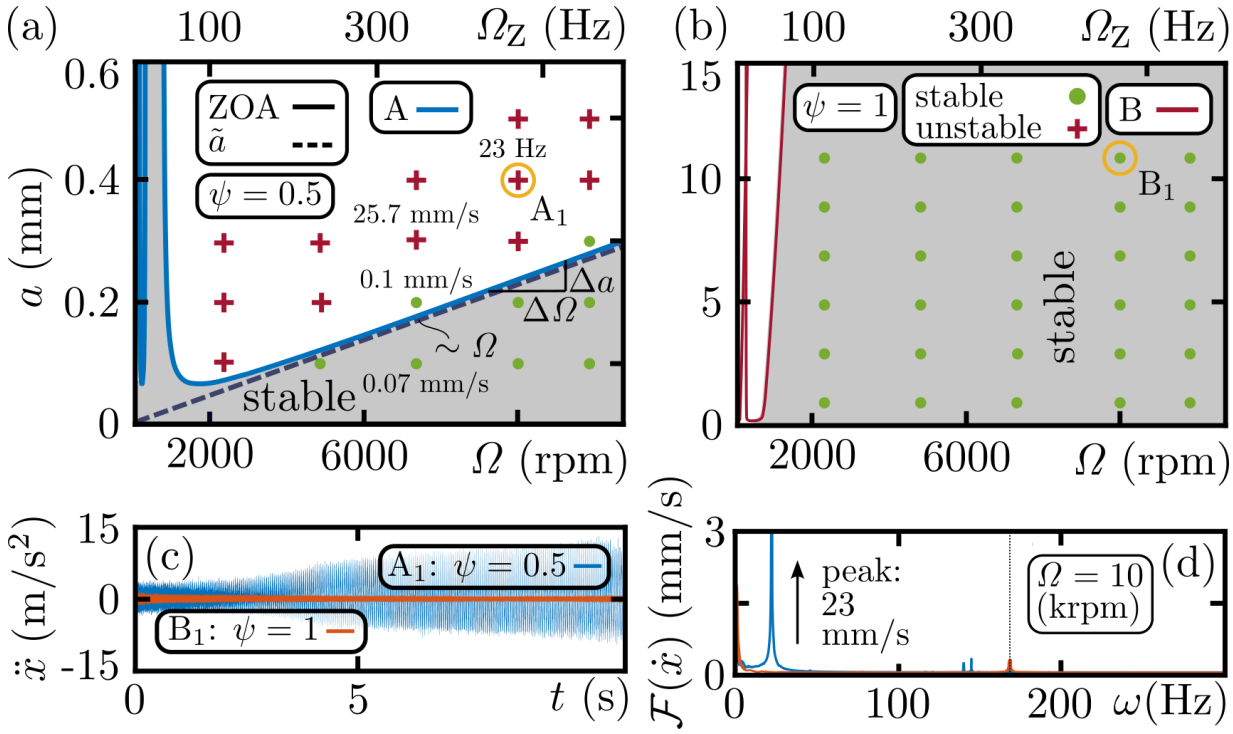


Figure 6.3 Validation by straight cutting tests: (a) SLD validation at point A of Fig. 5a (ψ = 0.5 DM, θ=0), (b) SLD at point B (ψ = 1, θ =0). Time domain signals (c) and the frequency content (d) of cutting test at 10000 rpm with a=0.4 mm for A and a=11 mm for B.

In contrast, all slotting tests conducted during the study exhibited stable behavior with consistently low vibration levels, as shown in Fig. 6.2 and Fig.6.3 The straight slotting operations delivered excellent performance and served to validate the predicted critical radial immersion threshold, a point beyond which the MDF remains positive, and chatter cannot occur. These results confirm that slotting is an effective and robust machining strategy for mitigating the adverse effects of low-frequency dominant modes. Its stability was maintained regardless of tool position, spindle speed, or feed direction, underscoring its suitability for ensuring chatter-free robotic milling in challenging dynamic conditions.

## 6.2 Validation with Industrial Robot

### 6.2.1 Experimental Setup

To validate theoretical stability predictions under realistic robotic machining conditions, a series of dynamic characterizations and milling tests were conducted using an industrial robotic system. The robotic platform used for experimentation was the Stäubli TX200, a six-degree-of-freedom serial manipulator designed for high-load, high-precision tasks. The Stäubli TX200 provides a wide workspace (reach up to ~2.6 m, payload up to 170 kg) but exhibits significantly lower stiffness than CNC machines particularly in extended positions.

Figure 6.4 The Stäubli TX 200 industrial robot with round fixture table

### 6.2.2 Frequency Response Function (FRF) Measurements

Dynamic characterization of the robot-tool-fixture system was carried out using experimental modal analysis to determine its structural compliance and modal properties. The tests employed three uniaxial velocimeters (model VO625B01), which were aligned

along the X, Y, and Z Cartesian directions. Each measurement was initially recorded as velocity per unit force (m/s/N) and subsequently integrated numerically to obtain the displacement-over-force response (m/N).

An instrumented modal hammer (PCB 086D20) was used to deliver impact excitation at four defined points (P1–P4) on the corners of the clamped workpiece. Each position was excited in three orthogonal directions, resulting in a total of 12 FRFs and only direct FRFs are plotted which are H-XX, H-YY, and H-ZZ measured at P1 through P4. The placement of the measurement points is shown in Figure 6.5 (a), with each corner distinctly labeled to enable traceability across FRF plots. Measured direct FRFs plotted into one plot to see the non-linearity behaviour of the robot.

a) b)

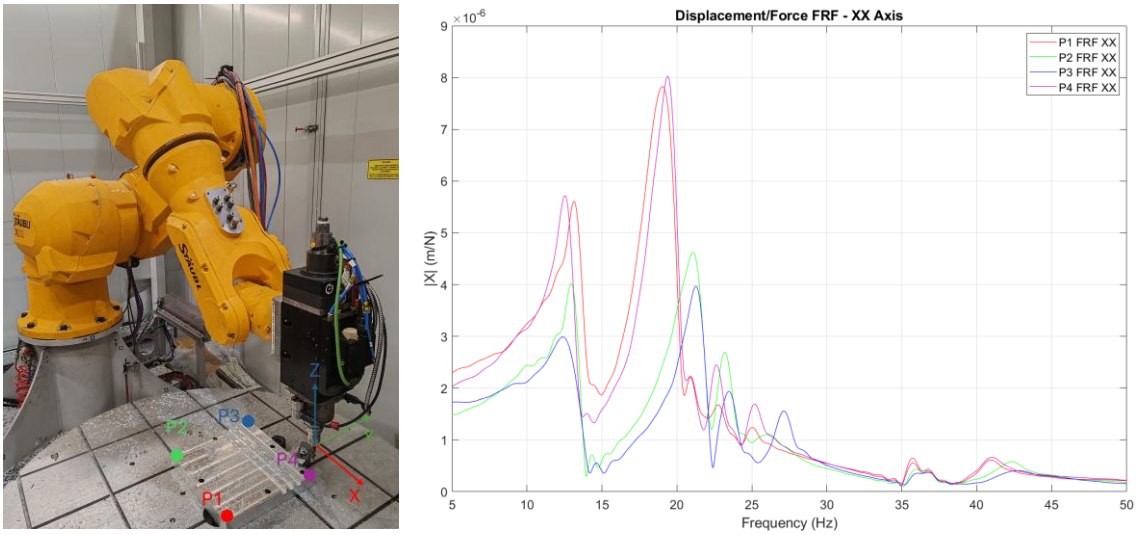


Figure 6.5 FRF measurements a) measured points on the robot b) FRF measurement of hit X velocimeter X in m/N

The measured displacement-over-force FRFs across the X, Y, and Z directions demonstrate a consistent and minor non-linear dynamic behaviour of the robot-tool system under low-energy excitation. Minor nonlinearity and localized variations are present but remain within acceptable limits for modal analysis. In the X-direction, dominant resonances were observed near 13 Hz and 20 Hz, with near frequency alignment across all four corner measurement points (P1–P4) as can be seen on figure 6.5 (b). Notably, P1 and P4, as well as P2 and P3, exhibit stronger pairwise similarity in FRF shape and amplitude. P2 and P3 show slightly higher natural frequencies and lower compliance, indicating greater local

stiffness. This is attributed to the robot's configuration: when the arm is stretched outward (as it is toward P1 and P4), the system experiences reduced structural stiffness, which accounts for the observed shift in dynamic response.

In the Y-direction, the primary mode appeared around 9–11 Hz in figure 6.6 (a), with moderate frequency differences and a slightly elevated amplitude at P4, suggesting marginally higher compliance at that location. This localized variation remains within the expected bounds of a serial robot's structure and does not indicate significant nonlinearity. In contrast, the Z-direction FRFs exhibited the most uniform characteristics, with a single dominant mode near 13–14 Hz in figure 6.6 (b) and nearly identical amplitude and shape across all measurement points.

Overall, the consistency in modal frequency and shape across directions confirms that the system behaves as a structurally nonlinear, but the non-linearity is minor. This makes it suitable for subsequent modal correlation and stability analysis in the context of posture-sensitive robotic machining applications.

a) b)

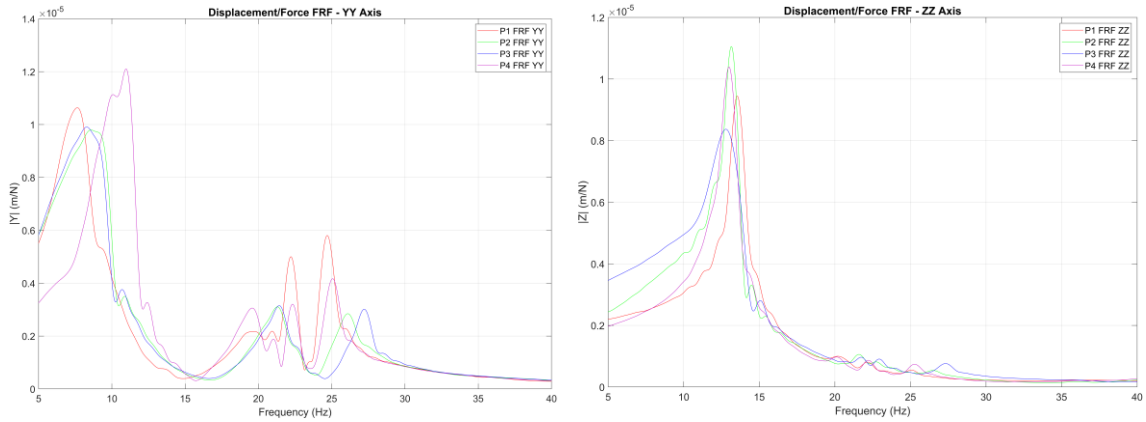


Figure 6.6 FRF measurements a) FRF hit Y velocimeter Y b) FRF hit Z velocimeter Z

### 6.2.3 Milling Conditions and Stability Analysis

Robotic milling experiments were conducted to evaluate dynamic stability under different tool-workpiece engagement strategies and validate the directional chatter model using real-

time measurements. A solid carbide end mill with a diameter of 16 mm, three flutes (Z = 3), and a 45° helix angle was used in all cutting tests. The feed direction was consistently aligned with the X-axis of the Cartesian coordinate system defined on the workpiece. Four cutting strategies were tested:

1. Slot Milling with feed in the +X direction, moving away from the robot base.
2. Up Milling with 50% radial engagement, feed in the +X direction.
3. Down Milling with 50% radial engagement, feed in the +X direction.
4. Reverse Up Milling, feed in the –X direction, moving toward the robot base.

Vibration data were acquired using Brüel & Kjær Type 3050-A-060 data acquisition hardware and the same set of velocimeters that used for FRF measurements employed for the capturing the time domain signals of milling processes. Signals were collected via BK Connect Pulse and analysed in the frequency domain using a custom MATLAB application developed for FFT computation.

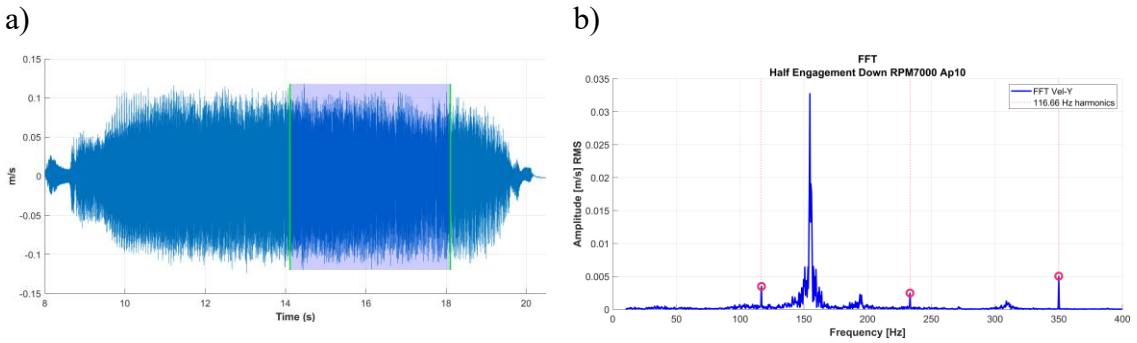


Figure 6.7 Half engagement down milling RPM 7000 Ap 10 mm a) time domain signal b) FFT analyses

Figure 6.7 (a),(b) shows the time-domain signal and corresponding FFT for the Down Milling case at 7000 RPM and ap = 10 mm. The signal exhibits high-amplitude, sustained oscillations with a modulated waveform, suggesting unstable cutting. The FFT spectrum reveals a dominant peak at approximately 154 Hz, which does not correspond to the tooth passing frequency (TPF = 350 Hz) or its harmonics. This indicates that the chatter is not regenerative in nature but rather associated with an uncharacterized structural resonance. Notably, this 150 Hz mode was not captured in the earlier FRF measurements, which primarily revealed dominant modes in the 10–40 Hz range. The emergence of this higher-frequency chatter mode under load suggests dynamic behaviour not observable during

modal testing, and it warrants further investigation, either through operational modal analysis or high-resolution FRF testing at extended frequency ranges.

a) b)

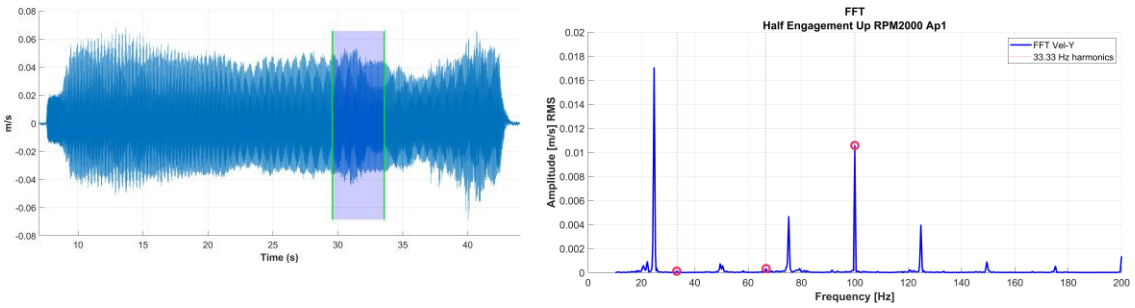


Figure 6.8 Half engagement up milling RPM 2000 Ap 1 mm a) time domain signal b) FFT analyses

In contrast, Up Milling at 2000 RPM with ap = 1 mm (Figures 6.8 (a), (b)) presents a relatively low-amplitude time-domain signal compared to higher-speed cases; however, the waveform reveals localized bursts of vibration around the 30-34 second mark, suggesting transient instability. This is further confirmed by the FFT spectrum, which shows a distinct and dominant peak at approximately 24 Hz a frequency that does not align with the fundamental tooth passing frequency (TPF = 100 Hz) or its harmonics. Instead, this frequency falls within the primary structural mode band identified in the FRF measurements (10–30 Hz), pointing to the presence of low-frequency structural chatter. This behaviour suggests that the cutting forces, aligned in the feed direction, excited the dominant low-frequency structural mode of the robot-fixture system. This interaction reflects the MDF-based mechanism described in earlier sections, where chatter arises not from regenerative feedback but from directional alignment between the applied cutting forces and the system's compliant vibration mode.

a) b)

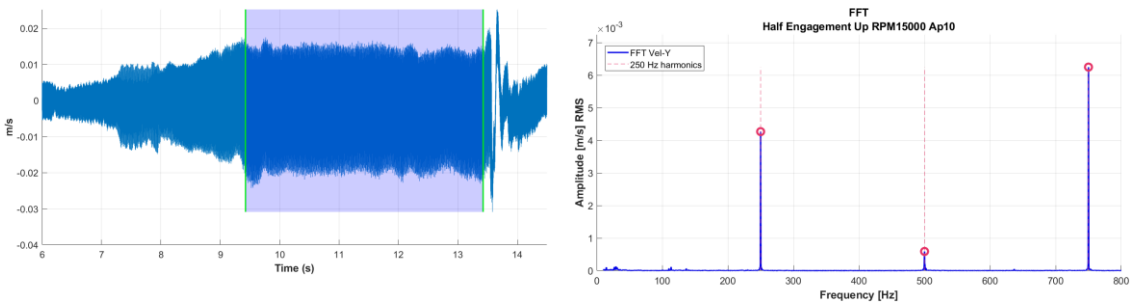


Figure 6.9 Half engagement up milling RPM 15000 Ap 10 mm a) time domain signal b) FFT analyses

The Up Milling case at 15000 RPM with ap = 10 mm (Figures 6.9 (a), (b)) exhibits sharp but controlled transients in the time-domain signal, without signs of self-excited growth. The corresponding FFT spectrum displays distinct peaks at 250 Hz and 750 Hz, the latter of which matches the tooth passing frequency (TPF = 15000 × 3 / 60 = 750 Hz). These peaks are attributed to the periodic excitation from the tool flutes rather than chatter. No broadband or low-frequency components typically associated with structural instability are observed. This indicates that the system remained in a stable cutting regime, despite the high spindle speed and high depth of cut. The stability is likely due to the favourable directional alignment of cutting forces with the structural stiffness of the robot in this configuration, as predicted by the positive MDF value along the +X feed direction.

### 6.2.4 Experimental Stability Diagram

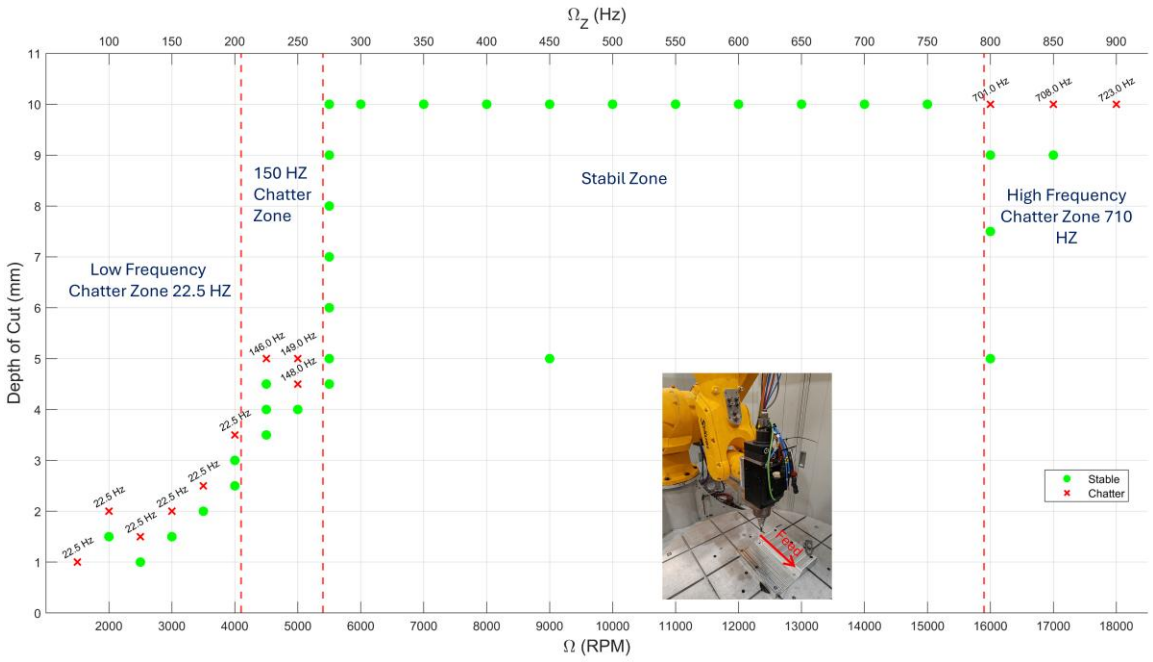


Figure 6.10 Experimental stability diagram of the slotting feed +X direction away from the robot base.

Figure 6.10 presents the experimental stability map for the Slot Milling configuration, in which the tool fully engages the workpiece while feeding in the +X direction, away from the robot base. This case was selected to examine the dynamic behavior under maximum radial immersion and force application along a direction with moderate posture-dependent stiffness. The stability diagram reveals four distinct behavioral zones:

- Zone A (RPM < 4000): In this low-speed range, low-frequency chatter (~22.5 Hz) was consistently observed at shallow depths of cut. These vibrations are attributed to the structural compliance of the robot, particularly the global bending modes of the arm, which are readily excited at low spindle speeds and result in unstable cutting. Notably, this chatter cannot be explained by conventional single-mode or regenerative theories, underscoring the importance of directional dynamic compliance and posture sensitivity.
- Zone B (4000–5500 RPM): Chatter persisted in this intermediate range but shifted to higher frequencies (~150 Hz). This behavior is not associated with the robot's primary structural modes identified in the FRF measurements. Instead, it likely

originates from local dynamics at the robot–spindle interface, such as a mechanical joint or coupling resonance. This highlights that different dynamic subsystems within the robotic machining chain can become dominant depending on spindle speed and excitation conditions.

- Zone C (5500–16000 RPM): This range represents the primary stable cutting window, where chatter was fully suppressed, and high-depth cuts up to 10 mm were achieved across the tested speeds. The absence of instability confirms the central hypothesis of this thesis: avoiding configurations with negative Mean Directional Factor (MDF) leads to effective suppression of low-frequency chatter, even under high radial and axial engagement.
- Zone D (>16000 RPM): While the system generally remained stable at very high spindle speeds, chatter re-emerged around 700–750 Hz during deep cuts. This high-frequency vibration does not correlate with the robot's measured FRF response and is presumed to result from spindle or tool-holder dynamics rather than robot compliance. Interestingly, this chatter was not repeatable under identical test conditions, suggesting a potential link to tool wear or temporary resonance amplification.

In summary, the slotting configuration demonstrates that robotic milling can achieve high material removal rates, provided that directionally unfavourable cutting postures and specific speed ranges are avoided. The observed chatter behaviour across the four zones reinforces the necessity of using direction-aware stability criteria, such as MDF, and suggests that future modelling efforts should move beyond single-mode approximations to

incorporate multi-source and posture-sensitive dynamic interactions.

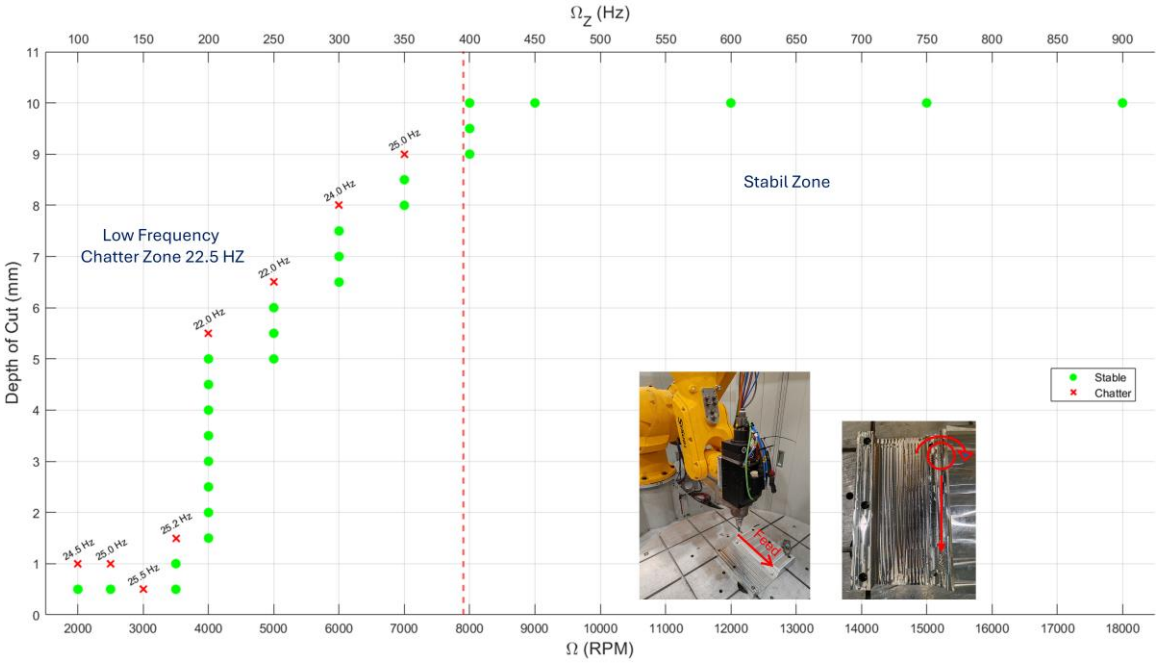


Figure 6.11 Experimental stability diagram of the half engagement up milling, feed +X direction away from the robot base.

Figure 6.11 presents the experimental stability diagram for the Up Milling configuration, where the feed direction is aligned with the +X axis, i.e., moving away from the robot base. The figure plots the cutting outcomes as a function of spindle speed (Ω, in RPM) and axial depth of cut (ap), using the same methodology as in the previous Slot Milling case. Green dots indicate stable cutting, while red crosses denote chatter occurrence. The corresponding chatter frequencies, identified from FFT analysis, are annotated next to the unstable points.

As seen in the figure, all instances of chatter occur within the low-frequency range of 22–25.5 Hz, which aligns closely with the dominant structural modes identified in the FRF measurements. The zone of instability spans from low spindle speeds (~2000 RPM) up to approximately 7000 RPM, after which no chatter is observed. Additionally, no signs of mid-frequency (~150 Hz) or high-frequency (~710 Hz) chatter previously observed in the Slot Milling tests were detected in the Up Milling configuration, further emphasizing the configuration-specific nature of structural excitation in robotic machining.

The absence of chatter beyond 7500 RPM defines a broad stable zone that extends up to the maximum tested speed of 18000 RPM. This high-speed stability is likely due to the

favourable alignment of the cutting force vector with the robot's stiffer structural directions in this specific feed configuration, as predicted by the positive mean directional factor (MDF) values for the +X direction in Up Milling posture.

Although slot milling involves full-width engagement and thus removes more material per pass, it reaches the stable cutting zone at a lower spindle speed (~5500 RPM) compared to up milling, which transitions to stable behaviour only above ~8000 RPM. This suggests that, despite its higher mechanical load, slotting provides a more favourable alignment between the cutting force direction and the dominant structural stiffness, as reflected by a more positive mean directional factor (MDF).

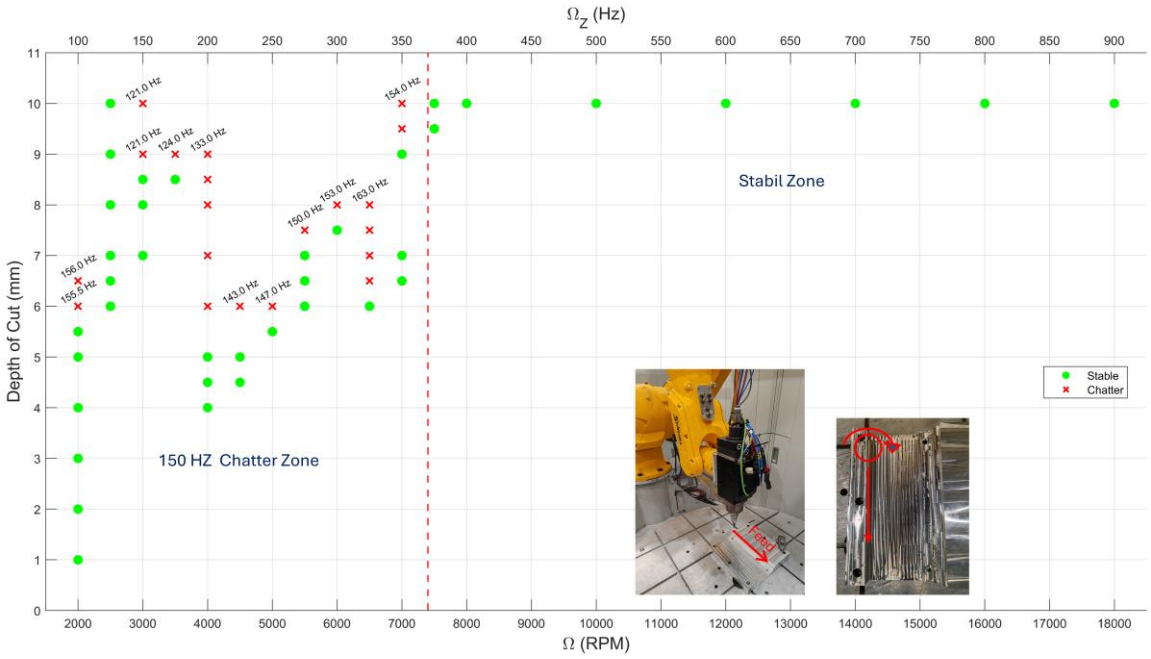


Figure 6.12 Experimental stability diagram of the half engagement down milling, feed +X direction away from the robot base.

Figure 6.12 presents the experimental stability diagram for the Down Milling configuration, where the feed direction is aligned with the +X axis, moving away from the robot base. This setup was examined to understand the influence of directional stiffness on process stability, particularly under the guidance of the Mean Directional Factor (MDF) framework.

Unlike the Slot Milling and Up Milling configurations, which exhibited low-frequency chatter (22–25 Hz) associated with structural bending modes, the Down Milling case showed no chatter in the low-frequency regime. Instead, all chatter occurrences were concentrated around a frequency range band between 120Hz to 160Hz, until spindle speed of 7000 RPM. This frequency was not observed in FRF measurements, suggesting the activation of an operational mode under cutting loads, potentially involving local spindle-tool-holder dynamics.

Importantly, the diagram shows that a maximum depth of cut of 10 mm was achieved at 2500 RPM without inducing chatter. This is notable given that the tooth passing frequency at 2500 RPM is 125 Hz, relatively close to the 150 Hz chatter band. The ability to sustain such engagement without instability suggests that this region lies within a local stability lobe.

From an MDF perspective, this configuration operates within a positive MDF zone, where the alignment between the cutting force direction and the system's dominant stiffness axis is beneficial. While MDF does not change the structural dynamics themselves, it defines how effectively the applied cutting forces interact with the system's directional compliance, shaping the likelihood of chatter. In this case, the alignment suppresses the excitation of lower-frequency bending modes and confines instability to a single, isolated high-frequency zone.

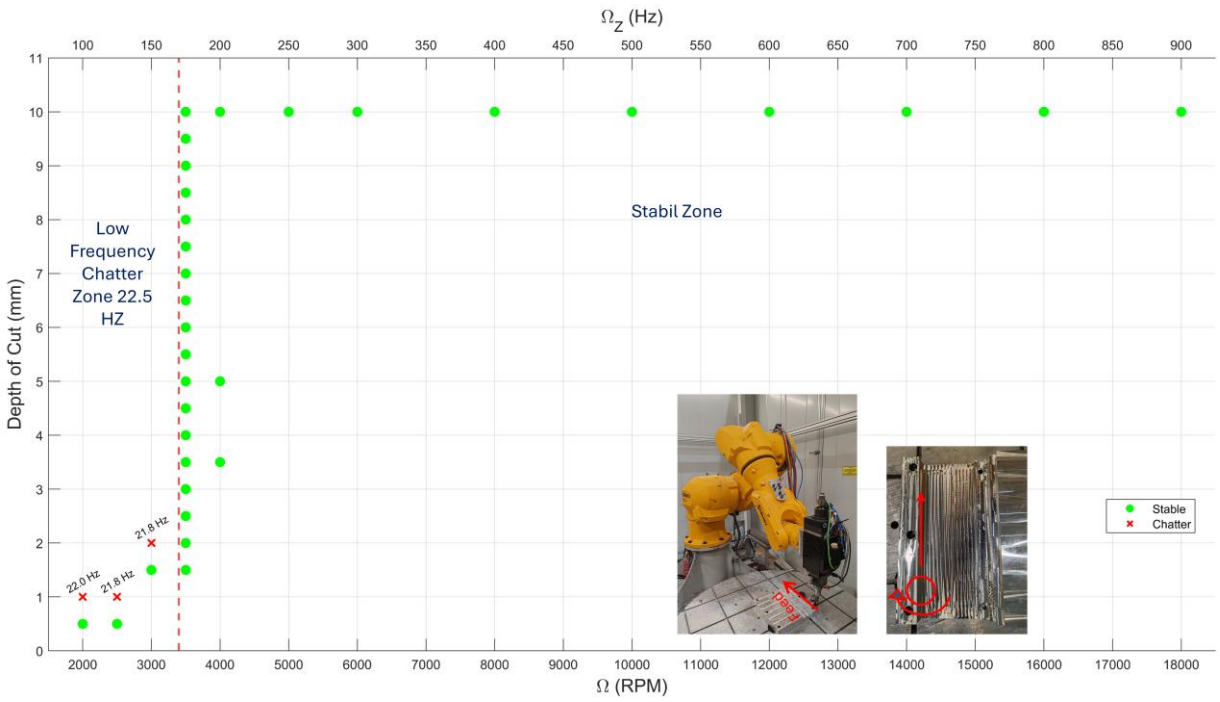


Figure 6.13 Experimental stability diagram of the half engagement up milling, feed -X direction away from the robot base.

Figure 6.13 displays the experimental stability diagram for the Up Milling configuration with feed direction along the –X axis, i.e., the tool moves toward the robot base. Among all tested configurations, this case exhibited the broadest and most robust stable region, indicating a highly favourable dynamic behaviour.

Chatter was only observed in a narrow region at low spindle speeds (2000–3000 RPM) and shallow depths of cut (<2 mm), where dominant vibration frequencies of around 22.0 Hz were recorded. These align with the low-frequency bending modes identified in the FRF measurements, suggesting that the system's structural flexibility is most vulnerable under low-speed, low-energy excitation.

Beyond 3000 RPM, the process remained fully stable up to 18000 RPM and 10 mm depth of cut, with no chatter detected across the entire tested envelope. Notably, no mid-frequency or high-frequency chatter zones were present in this configuration. This behaviour highlights that the robot-fixture system, in this particular posture and cutting direction, provides favourable alignment between the cutting force direction and the dominant stiffness axes, resulting in reduced susceptibility to vibration-induced instability.

These findings demonstrate that, despite the feed direction being oriented toward the robot base, which might intuitively be considered less stable the system exhibits excellent dynamic performance in this configuration. The results confirm that chatter onset is governed not only by structural flexibility, but more critically by the directional interaction between applied cutting forces and posture-dependent dynamic stiffness, as captured by the Mean Directional Factor (MDF). This configuration thus represents the most stable milling condition observed in this study.

# 7. CONCLUSION AND FUTURE WORK

This thesis introduced and validated the Mean Directional Factor (MDF) as a novel framework for predicting low-frequency chatter in robotic milling. Unlike traditional mode coupling theories, which rely on multi-mode interactions, MDF captures the directional alignment between cutting forces and a system's dominant vibration mode. The key contribution lies in showing that even in single-mode-dominant systems, chatter can occur when MDF is negative, challenging established assumptions in machining dynamics.

A custom-designed flexure-based fixture with a single dominant mode enabled controlled experiments to isolate and verify this effect. The findings confirmed that MDF more accurately predicts chatter onset than existing theories, as stability was consistently observed for positive MDF values and instability for negative ones. This demonstrates that directional effects alone without multi-modal coupling can govern chatter in flexible robotic structures.

MDF offers a unified, scalar measure that integrates both structural dynamics and toolpath orientation. This simplification allows for more efficient and accurate stability analysis, particularly in the posture-sensitive environment of robotic arms. Beyond theoretical insights, the MDF framework supports practical applications in toolpath planning, enabling engineers to select feed directions that avoid chatter, improve surface finish, and increase machining efficiency.

To further generalize the findings, the MDF framework should be tested on different robotic systems and under a variety of cutting conditions, including changes in tool geometry, material properties, and robot configurations. This would help validate the robustness and scalability of MDF as a universal chatter prediction tool.

Additionally, systematic polar plots of MDF versus feed direction should be developed to map stable and unstable regions across the robot's workspace. These maps would serve as practical guides for directionally optimized toolpath planning.

Finally, building on the identified role of damping, a dedicated damping mechanism either passive or active should be designed to target and suppress low-frequency chatter. This would enable real-time mitigation in MDF-critical regions and support the development of chatter-resistant robotic milling systems.

In summary, this work advances the understanding of robotic machining dynamics and provides a practical, posture-aware approach to enhance stability through directionally optimized cutting strategies.

# BIBLIOGRAPHY


A. Iglesias, J. Munoa, J. Ciurana, Z. Dombovari, G. Stepan, Analytical expressions for chatter analysis in milling operations with one dominant mode, Journal of Sound and Vibration, Volume 375, 2016, Pages 403-421, ISSN 0022-460X, https://doi.org/10.1016/j.jsv.2016.04.015.

Y. Altintaş, E. Budak, Analytical Prediction of Stability Lobes in Milling, CIRP Annals, Volume 44, Issue 1, 1995, Pages 357-362, ISSN 0007-8506, https://doi.org/10.1016/S0007-8506(07)62342-7.

Z. Dombovari, I. Laka, A. Bartfai, A. Karaca, E. Budak, G. Stepan, J. Munoa, Directional factor as the key factor for chatter-free robotic milling of light alloys, CIRP Annals - Manufacturing Technology, Accepted/In Press, 2025.

Hagele, Martin. (2016). Robots Conquer the World [Turning Point]. IEEE Robotics & Automation Magazine. 23. 120-118. 10.1109/MRA.2015.2512741.

Hazarika, Shyamanta & Dixit, Uday. (2018). Robotics: History, Trends, and Future Directions. 10.1007/978-3-319-78488-5_7.

Lutfi Taner Tunc, Bora Gonul, Effect of quasi-static motion on the dynamics and stability of robotic milling, CIRP Annals, Volume 70, Issue 1, 2021, Pages 305-308, ISSN 0007-8506, https://doi.org/10.1016/j.cirp.2021.04.077.

J. Munoa, X. Beudaert, Z. Dombovari, Y. Altintas, E. Budak, C. Brecher, G. Stepan, Chatter suppression techniques in metal cutting, CIRP Annals, Volume 65, Issue 2, 2016, Pages 785-808, ISSN 0007-8506, https://doi.org/10.1016/j.cirp.2016.06.004.

Gasparetto, A. (December 1, 1998). "A System Theory Approach to Mode Coupling Chatter in Machining." ASME. J. Dyn. Sys., Meas., Control. December 1998; 120(4): 545–547. https://doi.org/10.1115/1.2801501

Zengxi Pan, Hui Zhang, Zhenqi Zhu, Jianjun Wang, Chatter analysis of robotic machining process, Journal of Materials Processing Technology, Volume 173, Issue 3, 2006, Pages 301-309, ISSN 0924-0136, https://doi.org/10.1016/j.jmatprotec.2005.11.033.

Gurney JP. General Analysis of Two-Degree-of-Freedom Instability in Machine Tools. Journal of Mechanical Engineering Science. 1962;4(1):53-62. doi:10.1243/JMES_JOUR_1962_004_009_02

Lejun Cen, Shreyes N. Melkote, CCT-based mode coupling chatter avoidance in robotic milling, Journal of Manufacturing Processes, Volume 29, 2017, Pages 50-61, ISSN 1526-6125, https://doi.org/10.1016/j.jmapro.2017.06.010.

Badiola, X., Iturrospe, A., Abete, J.M. et al. State–space analysis of mode-coupling workpiece chatter. Int J Adv Manuf Technol 103, 2773–2781 (2019). https://doi.org/10.1007/s00170-019-03737-8

Huseyin Celikag, Erdem Ozturk, Neil D. Sims, Can mode coupling chatter happen in milling?, International Journal of Machine Tools and Manufacture, Volume 165, 2021, 103738, ISSN 0890-6955, https://doi.org/10.1016/j.ijmachtools.2021.103738.

Merritt, H. E. (November 1, 1965). "Theory of Self-Excited Machine-Tool Chatter: Contribution to Machine-Tool Chatter Research—1." ASME. J. Eng. Ind. November 1965; 87(4): 447–454. https://doi.org/10.1115/1.3670861

S. A. Tobias and W. Fishwick, 'Theory of regenerative machine tool chatter,' *The Engineer*, vol. 205, pp. 199–203, 1958.

Tlusty, J., and Ismail, F. (January 1, 1983). "Special Aspects of Chatter in Milling." ASME. J. Vib., Acoust., Stress, and Reliab. January 1983; 105(1): 24–32. https://doi.org/10.1115/1.3269061

Budak, E., and Altintas¸, Y. (March 1, 1998). "Analytical Prediction of Chatter Stability in Milling—Part I: General Formulation." ASME. J. Dyn. Sys., Meas., Control. March 1998; 120(1): 22–30. https://doi.org/10.1115/1.2801317

Budak, E., Altintas¸, Y., and Armarego, E. J. A. (May 1, 1996). "Prediction of Milling Force Coefficients From Orthogonal Cutting Data." ASME. J. Manuf. Sci. Eng. May 1996; 118(2): 216–224. https://doi.org/10.1115/1.2831014

Paccot, F., Andreff, N., & Martinet, P. (2009). A review on the dynamic control of parallel kinematic machines: Theory and experiments. The International Journal of Robotics Research, 28(3), 395-416.

Y. Altintas, Philip K. Chan, In-process detection and suppression of chatter in milling, International Journal of Machine Tools and Manufacture, Volume 32, Issue 3, 1992, Pages 329-347, ISSN 0890-6955, https://doi.org/10.1016/0890-6955(92)90006-3.

Markel Sanz-Calle, Jokin Munoa, Lorenzo Morelli, Alexander Iglesias, Luis Norberto López de Lacalle, Zoltan Dombovari, On the effect of radial engagement on the milling stability of modes perpendicular to the feed direction, CIRP Journal of Manufacturing Science and Technology, Volume 49, 2024, Pages 111-127, ISSN 1755-5817, https://doi.org/10.1016/j.cirpj.2024.01.006.

Honeycutt, A., & Schmitz, T. L. (2018). Milling bifurcations: a review of literature and experiment. *ASME J. Manuf. Sci. Eng.*, *140*(12), 120801.

Munoa, J., Dombovari, Z., Mancisidor, I., Yang, Y., & Zatarain, M. (2013). INTERACTION BETWEEN MULTIPLE MODES IN MILLING PROCESSES. Machining Science and Technology, 17(2), 165–180. https://doi.org/10.1080/10910344.2012.747935

Cordes, Marcel & Hintze, Wolfgang & Altintas, Yusuf. (2019). Chatter stability in robotic milling. Robotics and Computer-Integrated Manufacturing. 55. 11-18. 10.1016/j.rcim.2018.07.004.

Ozturk, Erdem & Budak, Erhan. (2007). Modeling of 5-axis milling processes. Machining Science and Technology - MACH SCI TECHNOL. 11. 287-311. 10.1080/10910340701554808.

N. J. M. van Dijk, N. van de Wouw, E. J. J. Doppenberg, H. A. J. Oosterling and H. Nijmeijer, "Robust Active Chatter Control in the High-Speed Milling Process," in IEEE Transactions on Control Systems Technology, vol. 20, no. 4, pp. 901-917, July 2012, doi: 10.1109/TCST.2011.2157160.

Eynian, M., and Altintas, Y. (July 8, 2009). "Chatter Stability of General Turning Operations With Process Damping." ASME. J. Manuf. Sci. Eng. August 2009; 131(4): 041005. https://doi.org/10.1115/1.3159047

Ismail, Firqi & Soliman, Essam. (1997). A new method for the identification of stability lobes in machining. International Journal of Machine Tools and Manufacture. 37. 763-774. 10.1016/S0890-6955(96)00032-6.

Munoa, Jokin & Beudaert, Xavier & Erkorkmaz, Kaan & Iglesias, Alex & Barrios, Asier & Zatarain, Mikel. (2015). Active suppression of structural chatter vibrations using machine drives and accelerometers. CIRP Annals - Manufacturing Technology. 64. 10.1016/j.cirp.2015.04.106.

Munoa, Jokin & Mancisidor, Iker & Loix, N. & Uriarte, L. & Bárcena, R. & Zatarain, Mikel. (2013). Chatter suppression in ram type travelling column milling machines using a biaxial inertial actuator. CIRP Annals-Manufacturing Technology. 62. 407-410. 10.1016/j.cirp.2013.03.143.

Munoa, J., Zatarain, M., Dombovari, Z., & Yang, Y. (2009, May). Effect of mode interaction on stability of milling processes. In 12th CIRP Conference on Modelling of Machining Operations, San Sebastian, Spain (pp. 927-933).

Altintas, Y., Stepan, G., Budak, E., Schmitz, T., and Kilic, Z. M. (August 11, 2020). "Chatter Stability of Machining Operations." ASME. J. Manuf. Sci. Eng. November 2020; 142(11): 110801. https://doi.org/10.1115/1.4047391

Alexander Verl, Anna Valente, Shreyes Melkote, Christian Brecher, Erdem Ozturk, Lutfi Taner Tunc, Robots in machining, CIRP Annals, Volume 68, Issue 2, 2019, Pages 799-822, ISSN 0007-8506, https://doi.org/10.1016/j.cirp.2019.05.009.

Alexander Iglesias, L. Taner Tunç, Orkun Özsahin, Oier Franco, Jokin Munoa, Erhan Budak, Alternative experimental methods for machine tool dynamics identification: A review, Mechanical Systems and Signal Processing, Volume 170, 2022, 108837, ISSN 0888-3270, https://doi.org/10.1016/j.ymssp.2022.108837.

Munoa, Jokin & Zatarain, Mikel & Bediaga, Iñigo & Peigne, Grégoire. (2006). Stability study of the milling process using an exponential force model in frequency domain.

Lutfi Taner Tunc, Sinem Kurnaz, Is process damping effective in the stability of robotic milling?, Journal of Manufacturing Processes, Volume 133, 2025, Pages 879-890, ISSN 1526-6125, https://doi.org/10.1016/j.jmapro.2024.11.084.

W. Hahn and G. Valery, "Eddy current damping for high-speed precision machining," *CIRP Ann. Manuf. Technol.*, vol. 51, no. 2, pp. 93–98, 2002.

J. Smith and B. Taylor, "Advancements in non-contact damping systems for machining stability," *Int. J. Adv. Manuf.*, vol. 47, no. 5-8, pp. 535–542, 2018.

L. Yuan, Z. Pan, D. Ding, S. Sun and W. Li, "A Review on Chatter in Robotic Machining Process Regarding Both Regenerative and Mode Coupling Mechanism," in IEEE/ASME Transactions on Mechatronics, vol. 23, no. 5, pp. 2240-2251, Oct. 2018, doi: 10.1109/TMECH.2018.2864652.

Gienke, O., Pan, Z., Yuan, L., Lepper, T., & Van Duin, S. (2019). Mode coupling chatter prediction and avoidance in robotic machining process. *The International Journal of Advanced Manufacturing Technology*, 104, 2103 - 2116. https://doi.org/10.1007/s00170-019-04053-x.

Wang, L., Liu, Y., Yu, Y., & He, F. (2022). Research on reliability of mode coupling chatter of orthopedic surgery robot. *Proceedings of the Institution of Mechanical Engineers, Part C: Journal of Mechanical Engineering Science*, 236, 8609 - 8620. https://doi.org/10.1177/09544062221085089.

Y. Altintas, *Manufacturing Automation: Metal Cutting Mechanics, Machine Tool Vibrations, and CNC Design*, 2nd ed. Cambridge, U.K.: Cambridge University Press, 2012.

T. Insperger, B. Mann, G. Stépán, and P. Bayly, “Stability of up-milling and down-milling, part 1: alternative analytical methods,” *Int. J. Mach. Tools Manuf.*, vol. 43, pp. 25–34, 2003. doi: 10.1016/S0890-6955(02)00159-1

Koegnisberger F, Tlusty J (1970) Machine tool structures. Pergamon Press, Oxford, UK.

Zatarain, Mikel, et al. "Analysis of directional factors in milling: importance of multi-frequency calculation and of the inclusion of the effect of the helix angle." The International Journal of Advanced Manufacturing Technology 47 (2010): 535-542.

Opitz, H. "Investigation and calculation of the chatter behavior of: Lathes and milling machines." Annals of the CIRP 18 (1979): 335-342.

Quintana, Guillem, and Joaquim Ciurana. "Chatter in machining processes: A review." International Journal of Machine Tools and Manufacture 51.5 (2011): 363-376.

Baer SM, Erneux T, Rinzel J (1998) The Slow Passage Through a Hopf Bifurcation: Delay, Memory Effects, and Resonance, SIAM Journal on Applied Mathematics, 49(1): 55–71.

E. Ozturk and E. Budak, “Dynamics and Stability of Five-Axis Ball-End Milling,” Journal of Manufacturing Science and Engineering, vol. 132, no. 2, p. 021003, Apr. 2010, doi: 10.1115/1.4001038.

E. Budak, E. Ozturk, and L. T. Tunc, “Modeling and simulation of 5-axis milling processes,” CIRP Annals - Manufacturing Technology, vol. 58, no. 1, pp. 347–350, 2009, doi: 10.1016/j.cirp.2009.03.044.